Snow Avalanche Impact Landform Geomorphology
in the Southern Canadian Cordillera

by

Alexis Leigh Johnson
B.Sc., University of Guelph, 2001

A Thesis Submitted in Partial Fulfillment of the
Requirements for the Degree of

MASTERS OF SCIENCE

In the Department of Geography

Supervisor: Dr. Dan Smith

ABSTRACT

Snow avalanche impact landforms (SAIL's) are typically elliptical-shaped depressions located at the base of avalanche tracks bounded by an arcuate crescent-shaped ridge. The purpose of this research was to determine the surface age and stability of SAIL's in the southern Canadian Cordillera. To achieve this, three sites were studied in detail: Blackhorn SAIL in the Central Coast Mountains, Spoon Lake SAIL in the Northern Cascade Mountains, and Peyto Lake SAIL in the southern Canadian Rocky Mountains. SAIL morphology is similar to other impact landforms, and in this study is compared with submarine plunge pools and meteorite impact craters.

The geomorphology of these features is controlled by variations in topography of the avalanche track, the availability of unconsolidated debris in the impact area, and the ability of the avalanche impact pressure forces to displace the available debris in the trajectory path of avalanche flow. Ground-based snow avalanches move debris by bulldozing, and airborne snow avalanches move sediment by explosion on impact. High-magnitude snow avalanche events that maintain the SAIL form are influenced by local weather conditions. Evidence of long-term SAIL development (e.g., well-developed ridge stratigraphy with buried organic layers, debris stratification) and present stability (e.g., well-vegetated, lichen abundance) was observed and supports the theory of formation through episodic, high-magnitude snow avalanche events.

Dendrochronology and lichenometry proved to be effective techniques for dating more recent high-magnitude snow avalanche events. Each site tells a distinct story. The avalanche track at Blackhorn SAIL has a gentle slope morphology that results in ground-based avalanches and suggests that it evolved from an avalanche boulder tongue. The most well-recorded avalanche year using dendrochronology was the winter of 1967-68. The oldest lichen present on the south side of the SAIL ridge date to the late 1930's and on the north side date to the mid-1960's. The lichen abundance and maturity on the SAIL ridge suggests the SAIL is presently stable.

The avalanche track at Spoon Lake SAIL has a jump morphology that promotes airborne snow avalanches. A resistant geologic feature restricts snow avalanche flow in the impact area and results in explosive excavation. The most well-recorded avalanche year using dendrochronology was 1989-90. Site conditions are not conducive to lichen colonization, however, the lichen present on the SAIL ridge supports the dendrochronological evidence. Dense vegetation cover on the SAIL ridge suggests present stability. Evidence of SAIL pool excavation was observed during data collection and implies long-term development of the present day SAIL.

The Peyto Lake SAIL avalanche track has chute and fall morphology that results in airborne snow avalanches that excavate sediment accumulated in the impact area. The most well-recorded avalanche year using dendrochronology was 1970-71. Lichen are not abundant on Peyto Lake SAIL as a result of site conditions, however, lichen present supports the dendrochronological evidence. Dense vegetation cover on the SAIL ridge suggests the landform is stable at the present time.

TABLE OF CONTENTS

Page

LIST OF TABLES

Page

LIST OF FIGURES

Page

ACKNOWLEDGEMENTS

I have a lot of people to thank after moving halfway across the country to do graduate work. Dan, thanks for scaring away the grizzly bear, not leaving town without me in the truck, all the adventures, and most of all supervising my graduate studies. Ian and Jim, thanks for all your thought provoking suggestions. Muchas gracias to all the members of the UVTRL for all the laughter, good times and for double-checking my questionable tree rings under the microscope. Ze'ev, thanks for the school supplies, fixing my computer and printer glitches, and holding onto my GPS. Colin, Laurel, and Sandy, thanks for hiking in precarious places to collect data for me. Sonya, thanks for teaching me the ropes in the lab. John, thanks for reminding me that CorelDRAW is not my fortЭ and for helping me put together my study site map. Mike King (White Saddle Air Service), thanks for flying us into Blackhorn SAIL, and unintentionally allowing me to take the controls. Thanks to the University of Victoria Fellowship, Geologic Society of America (GSA), Natural Science and Engineering Research Council (NSERC), and the Derrick Sewell Graduate Scholarship for funding my research.

Also, Aaron, Adam, Emmy, Keri, Kim, Shawna, and Sheri, thanks for all the distractions and friendships. Philbird, thanks for restarting your car as we sailed out of control down a steep mountain in the Rockies with a laden trailer in tow and a transport truck on our tail, and for being my practice audience before every presentation. Last but not least, I would like to thank my Mom, Cam, Sam, and Grandma and Grandpa Jones for all your love and support.

CHAPTER 1: INTRODUCTION

The geomorphic effects and significance of snow avalanche activity has been studied in alpine environments worldwide (Rapp 1959, Peev 1966, Gardner 1970, Luckman 1978, Carrara 1979, Corner 1980, Fitzharris and Owens 1984, Ward 1985, Ballantyne 1989, De Scally and Gardner 1989, Keylock 1997). Snow avalanche impact landforms (SAIL's) are geomorphic features that result from snow avalanche activity. SAIL's are typically circular bowl-shaped depressions bounded by a distal ridge, located at the base of avalanche tracks. Limited research has been conducted on SAIL's in Canada, New Zealand, Norway, Scotland, and the USA (Davis 1962, Liestøl 1974, Corner 1980, Fitzharris and Owens 1984, Ballantyne 1989, Butler 1989, Matthews and McCarroll 1994, Smith *et al.* 1994). To date, only one comprehensive paper by Smith *et al.* (1994) studied SAIL formation in North America, specifically in the southern Canadian Rocky Mountains.

SAIL development is controlled by avalanche track topography, availability of sediment in the impact area, and impact forces sufficient to move impacted debris. Track topography determines whether snow avalanches remain ground-based, moving available debris by bulldozing, or whether avalanches become airborne, moving available sediment by explosion on impact. Each of the SAIL's under study is distinct and tells a different story.

The purpose of this research is to determine the surface age and stability of three SAIL's in the southern Canadian Cordillera. The intention is to gain an understanding of the key processes involved in the formation of SAIL's. To further examine SAIL's in western Canada, study sites were chosen in the southern Canadian Cordillera. These sites are located in regions with different geologic and climatic settings. To achieve this, the following objectives were identified:

1) to describe the geomorphology at each snow avalanche impact landform site;
2) to document recent high-magnitude snow avalanches at each site and,
3) to describe the development of the snow avalanche impact landforms studied.

This thesis consists of 7 chapters. Chapter 2 provides a description of the study area, and reviews literature on snow avalanches (morphology, types, climatic effects), snow avalanche impact landforms, and describes similarities and differences between submarine plunge pools, meteorite impact craters and snow avalanche impact landforms. Chapter 3 outlines the methods used to map topography, dating techniques (dendrochronology and lichenometry) used to determine the frequency of high-magnitude avalanche events and SAIL stability, and grain-size analysis to determine size and mass of debris moved in excavation events. Chapter 4 provides site description, results and discussion of Blackhorn snow avalanche impact landform. Chapter 5 provides site description, results and discussion of Spoon Lake snow avalanche impact landform. Chapter 6 provides site description, results and discussion of Peyto Lake snow avalanche impact landform. Lastly, Chapter 7 provides a summary of the three sites under study, and concludes by discussing the significance of the results, limitations of the study and future directions.

CHAPTER 2: STUDY AREA AND RESEARCH BACKGROUND

The purpose of this chapter is to: 1) provide a description of the study area; 2) describe snow avalanche terrains, types and characteristics of snow avalanches, and the effects of climate on snow avalanche activity in the southern Canadian Cordillera; 3) gain an understanding of the processes involved in SAIL development; and, 4) describe and compare the common morphology of SAIL's, submarine plunge pools and meteorite impact craters.

2.1 STUDY AREA

The research was completed at three study sites in the southern Canadian Cordillera: 1) Blackhorn SAIL in the Nuit Range of the Coast Mountains of western British Columbia (51°36'40"N, 124°49'40"W); 2) Spoon Lake SAIL in the Skagit Range of the Northern Cascade Mountains of southwestern British Columbia (49°10'25'N, 121°40'45"W), and 3) Peyto Lake SAIL in the Waputik Range in the Canadian Rocky Mountains southwestern Alberta (51°43'08"N, 116°31'22'W) (Table 2.1, Figure 2.1). These sites were chosen based on location (different geologic and climatic regions) and relative ease of access.

The Canadian Cordillera covers 16% of Canada and consists of a series of mountain ranges, valleys, and plateaus (Bone 2002). The Cordillera extends along the west coast of Canada from the 49°N to the Beaufort Sea, just south of the 70°N (Bone 2002). This includes most of British Columbia and the Yukon, and the southwest corner of Alberta and the Northwest Territories. The southern Cordillera consists of five distinct geologic regions with a northwest-southeast trend (NRC 2000). This structure has changed little in the past 40 million years, although it has undergone several glaciations during this time. Approximately 18,000 years ago during the Wisconsinan glaciation the Cordillera ice sheet reached it maximum extent, flowing west into the Pacific Ocean, and east to the Laurentide ice sheet covering central Canada (Bone 2002). Glaciation in mountainous regions has eroded U-shaped valleys, resulting in large amounts of glacial

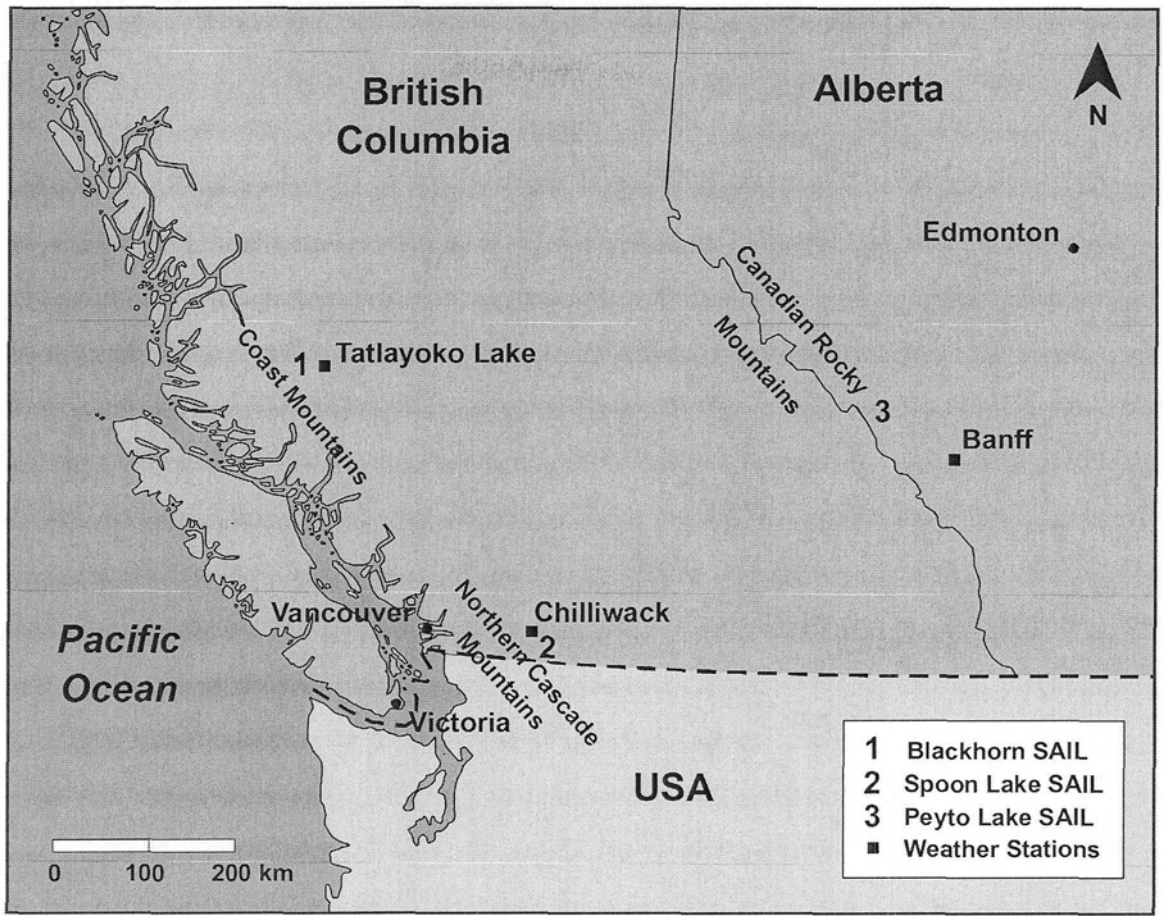

Figure 2.1 Study sites in the southern Canadian Cordillera.

Table 2.1 Locational characteristics of study sites.

No.	Site	Latitude	Longitude	Elevation of SAIL (m asl)	Slope Aspect	Map Sheet (1:50 000)
1	Blackhorn SAIL	51°36'40"N	124°49'40"W	1580	NW	92N/10
2	Spoon Lake SAIL	49°10'25"N	121°40'45"W	1470	WSW	92H/4
3	Peyto Lake SAIL	51°43'08"N	116°31'22"W	1860	E	82N/10

sediment carried and deposited to lower elevations, i.e., valley floors. More recently alpine valley glaciers and ice caps in the Cordillera have undergone Little Ice Age (LIA) advances between 1100 to 1900 A.D. (Luckman 2000).

The climate of the southwestern Canadian Cordillera is dominated by the cool, moist, unstable maritime polar (mP) air mass that originates over the Pacific Ocean (Ahrens 1994, Bone 2002). As this mP air mass moves inland from the Pacific Coast it is

forced to rise. As a result of orographic lifting, the windward side of the Coast and Northern Cascade Mountains receive large amounts of precipitation throughout the year, and the leeward side receives considerably less precipitation due to the drier air mass (CCEA 2002). Over the Interior Plateau of British Columbia the drier air converges with the cold, dry continental polar (cP) air mass from the north during the winter, as well as with the warm, moist maritime tropical (mT) air mass from the south in the summer (Bernhardt 2002). Similar to the Coast and Northern Cascade Mountains, the leeward side of the Canadian Rocky Mountains is drier than the windward side. Occasionally throughout the winter months the leeward side of the Canadian Rocky Mountains is quickly warmed by Chinook winds, resulting in rapid increases in air temperature by as much as 30°C and rapid snowmelt (Cameron 2002).

Vegetation in the southern Canadian Cordillera is extremely varied. This variability is due to the size of the region and the landforms that produce numerous microclimates. The Coast, Northern Cascade and Canadian Rocky Mountains are predominantly covered with coniferous forest interspersed with mixedwood forest (Lands Directorate 1986). As treeline is approached, conditions become harsher resulting in reduced or stunted tree growth (Bernhardt 2002).

2.2 SNOW AVALANCHES

Snow avalanches are frequently triggered when downslope shear stresses in a sloping snowpack exceed the resisting shear strength inherent to that snowpack. They occur most frequently on slopes ranging between 30-45° (Perla and Martinelli 1976, Daffern 1983), and occur in a variety of sizes ranging from small (10^0 m^3) to extremely large (10^5 m^3) (Schaerer 1967). The primary factors determining snow avalanche type and occurrence are topography and climate (Luckman 1977a, Armstrong 1986). Throughout this review, the term snow avalanche will be used interchangeably with avalanche.

Snow Avalanche Terrain

Avalanche paths consist of three parts: the starting zone, the track and the runout zone. Track morphology determines whether the avalanche remains ground-based or becomes airborne, which in turn affects avalanche flow behaviour in the runout zone (Luckman *et al.* 1994). Track morphology can be described as: i) confined or unconfined, ii) chute, jump, or fall, and iii) straight, concave, convex, or stepped longitudinal profile (Gardner 1970, Martinelli 1974, Martinelli 1986). Avalanches on tracks with a jump or fall morphology are likely to become airborne. Airborne avalanches have been observed traveling at velocities of up to 100 m/s (Schaerer 1981), which would produce high impact pressures upon contact with the ground.

Types of Snow Avalanches

Snow avalanches can be classified as: i) loose or slab, ii) wet or dry, iii) surface or full-depth avalanches, and iv) clean or dirty (Daffern 1983, Keylock 1997). *Loose* snow avalanches usually form when a small amount (e.g., 1 m^3) of fresh snow slides (point source origin), triggering the release of more snow downslope (Perla and Martinelli 1976, Daffern 1983). *Slab* snow avalanches, often larger and more dangerous than loose snow avalanches, form when a cohesive layer of snow (average thickness 1 m) slides downslope over a weak/failure layer in the snowpack (Perla and Martinelli 1976, Daffern 1983, Stethem *et al.* 2003).

Wet avalanches occur more frequently in the spring as higher temperatures produce meltwater and rain, which increases snowpack weight and/or creates a lubricated surface along which failure occurs (Daffern 1983, Gardner 1983, Keylock 1997). *Dry* avalanches occur throughout the season and often release as a result of snow loading. Depending on the types of snow in the starting zone, track and runout zone, snow avalanches can be a combination of *wet* and *dry* snow. *Wet* avalanches have higher densities, generally travel at lower velocities, and tend to follow the topography of the underlying surface (i.e., abrupt changes in direction) more closely (Table 2.2; Perla and Martinelli 1976). Gardner (1970) observed a wet spring snow avalanche deposit in the

Lake Louise area, Alberta that contained a boulder greater than 1 m^3 in size and more than 14 m^3 of rock debris.

Table 2.2 Velocity and density of dry and wet snow avalanches compared to clean ice and water.

Type	v (m/s) (Mears 1992)	v (m/s) (Schaerer 1981)	ρ (kg/m^3) (Schaerer 1981)
Dry	≤70	15-60	50-150
Wet	≤35	5-30	300-400
Ice (clean)	-	-	920
Water	-	-	1000 (at STP)

v = avalanche velocity, ρ = density

Surface avalanches develop when failure occurs along a weak layer in the snowpack; and *full-depth* avalanches extend to the underlying slope. Surface roughness of the starting zone is usually a key factor in determining the avalanche depth. Full-depth avalanches occur typically on smooth slopes (e.g., grass, bedrock), whereas surface avalanches are common on rougher surfaces (e.g., shrubs, saplings) (Luckman 1977a, Armstrong 1986).

An avalanche can also be classified as *clean* or *dirty* depending on the amount of sediment it moves (by pushing or entraining) (Gardner 1970, Luckman 1971). *Clean* avalanches erode little or no material and are more common than *dirty* avalanches, which are thought to be responsible for the erosion of material and the formation of landforms (both erosional and depositional). *Dirty* avalanches have been associated with wet, full-depth avalanches (Gardner 1970, 1983).

Snow Avalanche Impact Pressures

Schaerer and Salway (1980) calculated initial peak impact pressures (P) of snow avalanches on a surface perpendicular to flow using $P = c\ \rho\ v^2$, where c is a coefficient dependent on snow deformation and ranges from 0.5-2.0 (Hopfinger 1983), ρ is the density of avalanche snow (kg/m^3), and v is the avalanche velocity (m/s). Schaerer and Salway (1980) observed mean c-values of 1.5 for a light (or dry) avalanche and 1.7 for a

dense avalanche. Smith *et al.* (1994) used *c*-values of 1.5 and 2.0 when calculating snow avalanche impact pressures at SAIL sites. Impact pressures (*P*) were calculated using maximum predicted velocities and densities of dry and wet snow avalanches from Table 2.2, and 100 m/s velocity for airborne avalanches (Table 2.3). Fitzharris and Owens (1984) modified this equation to determine snow avalanche impact pressures on surfaces not perpendicular to flow using $P \sin \theta$, where θ is the angle of snow avalanche flow upon contact at the base of the track (runout zone). In the past, theoretical impact pressures of highly destructive snow avalanches have ranged from 0.01-0.6 MPa (Kotyakov 1974, Mellor 1978, Lang and Brown 1980), 1.0 MPa (Kuriowa 1974, Kotyakov *et al.* 1977), to 0.5-1.4 MPa (Shimizu *et al.* 1980).

Table 2.3 Maximum impact pressures (*P*) of snow avalanches (calculated using maximum density and velocity values).

Type	ρ (kg/m^3)	*c*	N (m/s)	*P* (MPa)
Dry	150	1.5	70	1.1
			100	2.3
		2	70	1.5
			100	3.0
Wet	400	1.7	35	0.8
			100	6.8
		2	35	1.0
			100	8.0

ρ = density of avalanche snow, *c* = coefficient dependent on snow deformation, v = avalanche velocity

Snow Avalanche Climatology in the southern Canadian Cordillera

The attributes of regional climates result in different snow avalanche conditions (Table 2.4; LaChapelle 1966, Armstrong and Armstrong 1987, De Quervain and Meister 1987, Keylock 1997). Warm, moist *maritime* air masses encountering the Coast and Cascade Mountains bring moderate winter temperatures, and heavy, frequent snow and rainfalls (LaChapelle 1966, Fitzharris 1987, Keylock 1997). Snow avalanches in these regions are typically wet, and release during or soon after storms (Keylock 1997).

Table 2.4 Weather characteristics observed from November to April from mountain regions in the Pacific Northwest USA (Armstrong and Armstrong 1987).

Weather Factor	Maritime	Intermountain	Continental
Mean air temp (°C)	-1.3	-4.7	-7.3
Mean total ppt. (mm)	1290	850	540

Cooler, drier *continental* air masses characterize climate conditions in the Canadian Rocky Mountains and bring low winter temperatures, and light, less frequent snowfalls (LaChapelle 1966, Fitzharris 1987, Keylock 1997). Snow avalanches in continental regions are typically dry, and are generally related to snowpack conditions making their release less predictable (Keylock 1997). Snowpack instability leading to snow avalanche release in continental regions often arises from the development and collapse of depth hoar at the base of the snowpack. Depth hoar development favours cold, thin snowpacks and forms when basal snow recrystallizes into a cohesionless form (Daffern 1983, Armstrong 1986).

Fitzharris (1987) identified major snow avalanche winters in the last century in western Canada using data collected from Roger's Pass. Roger's Pass is located in the intermountain region (transition between maritime and continental air masses). The winters of 1919-20, 1932-33, 1934-35, and 1971-72 were identified as major snow avalanche seasons.

2.3 GEOMORPHOLOGY OF SNOW AVALANCHE IMPACT LANDFORMS

Snow avalanches can create new landforms and/or modify existing landforms (Luckman 1977a). Snow avalanches form both small- and large-scale erosional landforms such as debris tails to chutes, and depositional landforms such as perched boulders to boulder tongues (Gardner 1970, Luckman 1977a). These landforms are a consequence of available unconsolidated sediment at the base of the track, ability of avalanche to move sediment, and the deceleration of the flow in the runout zone (Luckman 1978, Ward 1985). SAIL's are relatively rare and do not occur at the base of all avalanche tracks. Previous to this study, 66 SAIL's had been identified and studied in Canada, New Zealand, Norway, Scotland, and the USA (Table 2.5).

Table 2.5 Catalogue of snow avalanche impact landforms identified / studied. (*) identifies the New Zealand (NZMS 1) reference system. Italics identify information not provided by the author, but calculated from the information provided. In addition to this compilation, Smith (1947), Serbenko (1954), Reite (1976), Hole (1981), Carlson *et al.* (1983), and Blikra *et al.* (1989) identified snow avalanche impact landforms; however, these references were inaccessible.

Snow Avalanche Impact Landforms				Locational Characteristics			Pool Dimensions				Ridge Dimensions				Track Dimensions			
No.	Site	Source	Country	UTM reference	Elevation of SAIL (m asl)	Aspect	Corner's Class.	Length (m)	Width (m)	Depth (m)	Height (m)	Width (m)	Proximal Slope < (°)	Distal Slope < (°)	Track Slope (°)	Runout Zone Slope (°)	Max. Fall (m)	Start Zone (m asl)
1	1 Burstall Lake SAIL	Smith *et al.* 1994	AB, Canada	174273	1974	SW	pit	50	45	9	17	-	-	-	27-36	-	580	-
2	2 Tombstone Lake SAIL		AB, Canada	428165	2170	NE	pit	45	25	7	9	-	-	-	21-45	-	750	-
3	3 Geikie Creek SAIL	(McCarthy 1985)	AB, Canada	093338	1675	NW	pit	55	22	5	4	-	-	-	26-51	-	1,000	-
4	1 Sprongdalen	Matthews and	S. Norway	-	900	S-SE	tongue	-	-	-	5	26	22	13	-	28	560	1460
5	2 Sprongdalen	McCarroll 1994	S. Norway	-	860	S-SE	tongue	-	-	-	7	14	34	18	-	22	480	1340
6	3 Sprongdalen		S. Norway	-	700	N	tongue	-	-	-	7	26	28	14	-	25	680	1380
7	4 Sprongdalen		S. Norway	-	670	N	tongue	-	-	-	3	15	29	5	-	25	790	1460
8	5 Sprongdalen		S. Norway	-	620	N	tongue	-	-	-	20	41	34	7	-	28	860	1480
9	6 Sprongdalen		S. Norway	-	610	N	tongue	-	-	-	18	14	28	16	-	<36	870	1480
10	7 Sprongdalen		S. Norway	-	600	N-NW	tongue	-	-	-	19	13	42	21	-	27	880	1480
11	8 Sprongdalen		S. Norway	-	590	N-NW	tongue	-	-	-	15	16	34	8	-	29	890	1480
12	9 Sprongdalen		S. Norway	-	580	N-NW	tongue	-	-	-	13	15	31	13	-	28	880	1460
13	10 Jostedalen		S. Norway	-	450	N-NW	tongue	-	-	-	9	14	42	35	-	35	650	1100
14	11 Jostedalen		S. Norway	-	420	E	tongue	-	-	-	35	58	18	11	-	20	980	1400
15	12 Jostedalen		S. Norway	-	390	E	tongue	-	-	-	19	20	35	15	-	21	1050	1440
16	1 Coire na Cista	Ballentyne 1989	Scotland	-	910	NE	pit	30	15	3	3	-	25-35	15	*35*	-	*300*	*1210*
17	1 Waterton-Glacier Park	Butler 1989	MT, USA	-	-	SE	pool	-	-	-	-	-	-	-	-	-	-	-
18	2 Waterton-Glacier Park		MT, USA	-	-	SE	pool	-	-	-	-	-	-	-	-	-	-	-
19	1 W. Clinton	Fitzharris and	New Zealand	S121 823878*	330	NE	pit	-	-	-	-	-	-	-	51	-	*1350*	1680
20	2 W. Clinton	Owens 1984	New Zealand	S121 814890*	335	NE	pit	-	-	-	-	-	-	-	46	-	*1405*	1740
21	3 W. Clinton		New Zealand	S121 831931*	460	SW	pit	-	-	-	-	-	-	-	38	-	*1065*	1525
22	4 W. Clinton		New Zealand	S121 812497*	525	NW	pit	-	-	-	-	-	-	-	53	-	*1155*	1680
23	5 Joes		New Zealand	S121 823988*	550	SW	pit	-	-	-	-	-	-	-	48	-	*820*	1370
24	6 Diamond		New Zealand	S121 765031*	180	W	pit	-	-	-	-	-	-	-	44	-	*1405*	1585
25	7 Staircase		New Zealand	S121 730973*	305	SW	pit	300	150	-	-	-	-	-	59	-	*1125*	1430
26	8 Prospect		New Zealand	S121 731877*	610	S	pit	-	-	-	-	-	-	-	53	-	*1220*	1830
27	9 Hollyford		New Zealand	S122 985972*	730	E	pit	-	-	-	-	-	-	-	47	-	*1100*	1830
28	10 Hollyford		New Zealand	S122 978985*	760	NE	pit	-	-	-	-	-	-	-	45	-	*980*	1740
29	11 Joes		New Zealand	S122 858019*	150	NE	pit	-	-	-	-	-	-	-	48	-	*1280*	1430
30	12 Cleddau		New Zealand	S122 908044*	300	W	pit	-	-	-	-	-	-	-	57	-	*1530*	1830
31	13 Cleddau		New Zealand	S113 927109*	30	SE	pit	-	-	-	-	-	-	-	49	-	*1525*	1555
32	14 Cozette		New Zealand	S139 350363*	530	SE	pit	-	-	-	-	-	-	-	47	-	*930*	1460
33	15 Freeman		New Zealand	S140 432280*	730	W	pit	-	-	-	-	-	-	-	40	-	*730*	1460
34	16 W. Clinton		New Zealand	S121 786934*	520	E	pit	20	10	-	-	-	-	-	54	-	*1005*	1525
35	1 Tytebærdalen, Lyngen	Corner 1980	N. Norway	605223	160	S	tongue	-	-	-	-	-	-	-	20-35	-	750	-
36	2 Reindalen, Lyngen		N. Norway	716389	120	S	tongue	-	-	-	-	-	-	-	30-40	-	450	-
37	3 Reindalen, Lyngen		N. Norway	721388	90	NE	tongue	-	-	-	-	-	-	-	15-40	-	700	-
38	4 Pfastdalen, Lyngen		N. Norway	675275	240	SE	tongue	-	-	-	-	-	-	-	10-20	-	150	-
39	5 Lysvassdalen, Lyngen		N. Norway	477853	460	S	tongue	-	-	-	-	-	-	-	20-45	-	550	-
40	6 Lysvassdalen, Lyngen		N. Norway	478853	460	SW	pit	-	-	-	-	-	-	-	25-35	-	350	-
41	7 Hessfjord, Ringvassøy		N. Norway	414600	32	E	pit	35	20	-	6	-	-	-	30-40	-	250	-
42	8 Rundvatnet, Andersdalen	(and Leistøl 1974)	N. Norway	263063	145	SW	pit	100	80	14-22	-	-	-	-	15-35	-	1,200	-
43	9 Finnkjeila, Laukøy		N. Norway	952738	15	SE	pit	-	-	-	-	-	-	-	40	-	>200	-
44	10 Vassnes, Laukøy		N. Norway	965755	30	SE	pit	-	-	-	-	-	-	-	30-35	-	700	-
45	11 Ersfjorden, Kvaløya		N. Norway	980362	0	SE	pool	-	-	-	-	-	-	-	30-35	20-35	800	-
46	12 Ersfjorden, Kvaløya		N. Norway	983363	0	S	pool	-	-	-	-	-	-	-	20-35	20-35	700	-
47	13 Ersfjorden, Kvaløya		N. Norway	986362	0	S	pool	-	-	5	-	-	-	-	25-40	20-35	800	-
48	14 Ersfjorden, Kvaløya		N. Norway	000361	0	S	pool	-	-	-	-	-	-	-	28-35	20-35	850	-
49	15 Ersfjorden, Kvaløya		N. Norway	006361	0	S	pool	-	-	-	-	-	-	-	30-35	20-35	800	-
50	16 Ersfjorden, Kvaløya		N. Norway	012360	0	S	pool	-	-	5	-	-	-	-	35	150 m cliff	800	-
51	17 Ersfjorden, Kvaløya		N. Norway	036356	0	S	pool	-	-	-	-	-	-	-	30-40	20-35	800	-
52	18 Ersfjorden, Kvaløya		N. Norway	038356	0	S	pool	-	-	-	-	-	-	-	30-40	20-35	800	-
53	19 Skredholet, Lyngen		N. Norway	726364	0	E	pool	-	-	-	-	-	-	-	30-45	-	800	-
54	20 N. of Skredholet, Lyngen		N. Norway	727370	0	E	pool	-	-	-	-	-	-	-	35	-	900	-
55	21 Laddo, Lyngen		N. Norway	734403	0	E	pool	-	-	-	-	-	-	-	35-45	-	900	-
56	22 Bjørneskorra, Lyngen		N. Norway	744443	0	E	pool	-	-	-	-	-	-	-	35-45	-	1,000	-
57	23 Mittelegga, Lyngen		N. Norway	745449	0	E	pool	-	-	-	-	-	-	-	35-40	-	1,100	-
58	24 Goddeskorra, Lyngen		N. Norway	751461	0	E	pool	-	-	-	-	-	-	-	30-45	-	1,200	-
59	25 Holsteinen, Lyngen		N. Norway	753483	0	E	pool	-	-	-	-	-	-	-	35-40	-	700	-
60	26 Urdbukta, Lyngen		N. Norway	505092	0	W	pool	-	-	-	-	-	-	-	25-35	-	850	-
61	27 Brevatnet, Lyngen		N. Norway	621252	542	N	pool	-	-	-	-	-	-	-	20-35	-	800	-
62	28 Sandbakken, Laukøy		N. Norway	954739	0	SE	pool	-	-	-	-	-	-	-	22-38	-	600	-
63	1 Leirdalen, Jotunheimen	Leistøl 1974	N. Norway	-	-	-	pit	-	-	-	-	-	-	-	-	-	-	-
64	2 Valldal, Trollstigen		N. Norway	-	-	-	pit	-	-	-	-	-	-	-	-	-	-	-
65	3 Valldal, Trollstigen		N. Norway	-	-	-	pit	-	-	-	-	-	-	-	-	-	-	-
66	1 Grouse Meadow	Davis 1962	CA, USA	-	2590	-	pit	18	8	3	-	-	-	-	-	-	-	-

SAIL's have been referred to as scour pits (Davis 1962), avalanche mounds (Peev 1966), avalanche-plunge pools (Liestøl 1974), avalanche tarns (Fitzharris and Owens 1984), avalanche impact tongues (Corner 1980), avalanche impact pits (Peev 1966, Corner 1980, McCarthy 1985), avalanche impact pools (Corner 1980, Butler 1989, Smith *et al.* 1994), avalanche boulder ramparts (Ballantyne 1989, Matthews and McCarroll 1994), and avalanche impact landforms (Corner 1980, Ballantyne 1989, Matthews and McCarroll 1994, Luckman *et al.* 1994). In this thesis all of these features will be referred to as SAIL's (snow avalanche impact landforms), since this term encompasses all previous terminology.

SAIL characteristics

SAIL's typically do not result from a single catastrophic avalanche event (Liestøl 1974, Corner 1980, Smith *et al.* 1994). Repeated snow avalanche events are usually required in order for a sufficient amount of debris to accumulate, and episodic, high-magnitude avalanche events are necessary to create and maintain a SAIL form (Liestøl 1974, Corner 1980). High-magnitude refers to snow avalanche events that excavate debris/sediment from the impact area at the base of the track.

Snow avalanche impact landforms are variable in size and appearance. Corner (1980) identified three distinct SAIL morphologies, which included avalanche impact *tongues*, avalanche impact *pits*, and avalanche impact *pools*. Avalanche impact *tongues* are arcuate crescent- or tongue-shaped ridges located on the distal bank of a stream or river. Avalanche impact *pits* are elliptical or bowl-shaped depressions that are often water-filled, bound by arcuate crescent-shaped ridges (Figure 2.2). Avalanche impact *pools* differ from *pits* in that the ridges are partially or entirely submerged. As water levels fluctuate and/or the impact feature further develops, avalanche impact *pool*s may transform into *pits* and vise versa. Elliptical-shaped water-filled depressions (*pits* and *pools*) have been recorded in varying sizes from 10-20 m across to 200-300 m across (Corner 1980, Fitzharris and Owens 1984).

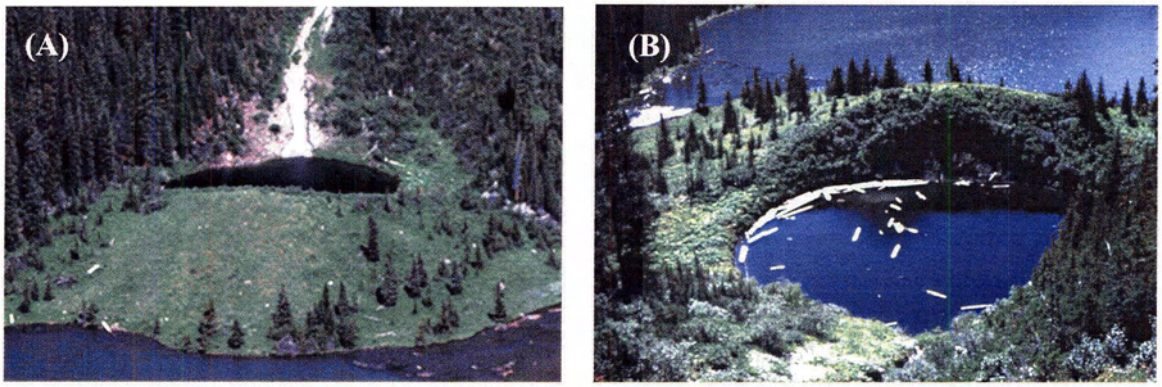

Figure 2.2 (A) Burstall Lake SAIL located in Peter Lougheed Provincial Park, Alberta, Canada (Smith *et al.* 1994). (B) Oblique view of Burstall Lake SAIL.

The characteristic raised arcuate, crescent-shaped ridge of a SAIL typically projects several metres above the impact depression, and tends to be positioned obliquely to the avalanche track (Corner 1980, Ballantyne 1989, Smith *et al.* 1994). The ridges are composed of a mixture of rock and/or soil and/or organic debris ranging in size from micrometres to metres (Smith *et al.* 1994). Ridge dimensions (length, width, and height) and the rate of development are site-specific, and are a reflection of high-magnitude snow avalanche characteristics (type, size, frequency, impact pressures), availability of unconsolidated debris, local topography and the size of the target impact area (Corner 1980, Matthews and McCarroll 1994). Maximum development of the width and height of the ridge forms opposite the avalanche track where the largest impact pressures are assumed to develop (Luckman *et al.* 1994).

When snow avalanches excavate the impact area, unconsolidated debris is moved from the proximal side of the impact landform and is deposited on the distal slope (Liestøl 1974, Corner 1980, Smith *et al.* 1994). Debris is moved along the trajectory path of the avalanche flow by means of lifting, bulldozing and/or entraining debris (Smith *et al.* 1994). Due to the erosional processes involved, the gradient of the proximal slope of the ridge is typically steeper than that of the depositional distal slope (Peev 1966, Corner 1980). Water-filled SAIL's may enhance development, as the impact of the rapidly moving snow avalanche would initially drive the water downwards, and then subsequently deflect water upwards and outwards increasing erosional and depositional processes (Liestøl 1974, Smith *et al.* 1994). After the SAIL has developed, high-magnitude avalanches are necessary in order for the SAIL shape to be maintained,

otherwise smaller avalanches will slowly infill the landform with debris (Liestøl 1974, Smith *et al.* 1994).

Mechanisms of SAIL formation

Three mechanisms have been proposed to explain the formation of SAIL's. The first is that SAIL development occurs at the base of steep avalanche tracks that terminate abruptly in unconsolidated debris (Schytt 1965, Peev 1966, Liestøl 1974, Corner 1980, Fitzharris and Owens 1984, Ballentyne 1989, Matthews and McCarroll 1994, Smith *et al.* 1994). The SAIL results when an explosive avalanche impact force moves debris radially from the impact area, primarily in the trajectory path of the avalanche flow (Liestøl 1974). The second is that SAIL development occurs at the base of gentle slopes that terminate in unconsolidated debris, resulting in ground-based avalanches that bulldoze or shovel debris in the direction of the avalanche flow (Davis 1962, Nyberg 1985, 1989, Smith *et al.* 1994). Fitzharris and Owens (1984) suggest a third explanation that requires an abrupt change in track topography (i.e., protrusion on the track, convexity in slope) causing snow avalanches to become airborne prior to plunging to the base of the track. This explanation, like the first, would also result in an explosive impact force upon contact with the debris at the base of the track.

Previous researchers note SAIL's have formed at the base of avalanche tracks with varied morphology, ranging from unconfined (open) to confined (gully, depression), short (e.g., 150 m) to long vertical fall distances (e.g., 1530 m), gradual (e.g., 10-20°) to steep slopes (e.g., 59°), and ground-based (bulldoze) to airborne (explosive) profiles (Corner 1980, Fitzharris and Owens 1984, Smith *et al.* 1994). Based on these assessments it would seem that the impact pressures needed to create and maintain SAIL's develop on a wide range of slope morphologies. Fitzharris and Owens (1984) and Smith *et al.* (1994) predicted theoretical snow avalanche impact pressures at SAIL sites to be ≥ 0.7 MPa, and 0.3 to 3.3 MPa, respectively (using the impact pressure equation in section 2.1). Smith *et al.* (1994) concluded that the snow avalanche impact pressures necessary to create and maintain SAIL's likely exceed 1 MPa (based on theoretical calculations), and may only occur only once every 50 to 150 years.

Based on these assessments, it is suggested that SAIL's are most likely a function of the variation in topography of the avalanche path (i.e., slope, maximum fall distance, abrupt changes in slope), the availability of unconsolidated debris in the impact area, and avalanche impact pressures competent to move available debris in the trajectory path of avalanche flow. Liestøl (1974) suggested that the presence of water at the base of the track (i.e., river, lake) is a fundamental ingredient for snow avalanche impact landform development, as it would accentuate the impact by snow avalanches. SAIL's have been, however, observed where standing water is not present at the base of the avalanche track, thus water does not play a vital role in SAIL formation (Corner 1980, Ballantyne 1989, Smith *et al.* 1994).

Evidence of long-term SAIL development

The frequency of high-magnitude snow avalanche events at SAIL sites has previously been described using dendrogeomorphic evidence (Leistøl 1974, Smith *et al.* 1994), lichenometric dating (Ballantyne 1989, Matthews and McCarroll 1994), ^{14}C-dating of organic material buried in the ridge (Corner 1980, Smith *et al.* 1994), historical photographic evidence, observation of ridge stratification, contemporary activity building the ridge (Smith *et al.* 1994), and debris infill in the pool (Corner 1980).

It is suspected that most SAIL's have been developed within the last few thousand years, and have possibly been maintained throughout the Holocene (Corner 1980, Fitzharris and Owens 1984, Matthews and McCarroll 1994, Smith *et al.* 1994). Matthews and McCarroll (1994) were able to date SAIL development in South Norway to the LIA deglaciation in the nineteenth century using lichen simulation modeling. Corner (1980) used ^{14}C-dating to date SAIL development in North Norway as far back as 13,000 years B.P.

2.4 GEOMORPHOLOGY OF SUBMARINE PLUNGE POOLS

Submarine plunge pools are impact landforms that typically form entirely underwater. These impact features share many characteristics with SAIL's making a review of their morphogenesis useful. They have been studied in Norwegian fjords (Aarseth *et al.* 1989), the Great Bahama Bank (Wilber, *et al.* 1990), along the continental margin of New Jersey, USA (Farre and Ryan 1985), and along the continental margin of California, USA (Lee *et al.* 2002) using high-resolution bathymetric data.

Landform Similarities

Submarine plunge pools are elliptical-shaped depressions typically bounded by a subdued ridge or mound (Figure 2.3). Like SAIL's, no relationship exists between the plunge pool diameter ratio and pool depth (Lee *et al.* 2002). The adjacent ridge is composed of sediment, eroded upslope of the depression and/or excavated from the depression; it is poorly sorted and ranges in size from fines to boulders (Farre and Ryan 1985, Lee *et al.* 2002).

Submarine plunge pools are well developed where there is an abrupt break (>15°) in the slope (Lee *et al.* 2002). Lee *et al.* (2002) proposed that sediment-laden density flows (SLDF) are the agent forming submarine plunge pools. Although SLDF's are not well understood because they are difficult to study (transient and inaccessible), it is believed that the events forming submarine plunge pools are episodic (Aarseth *et al.* 1989, Lee *et al.* 2002).

Mechanisms of Submarine Plunge Pool Formation

Lee *et al.* (2002) describe two possible SLDF mechanisms, *hydraulic jumps* and *impact events*. Hydraulic jumps arise when an abrupt change in slope causes supercritical flows (fast, shallow flow with a Froude number >1) to change to subcritical flows (slow, deep flow with a Froude number <1). Modeling suggests that the length of the hydraulic jump influences the size of the resultant depression. Theoretically, the decrease in bed

shear stress downstream of the hydraulic jump deposits the entrained sediment (i.e., ridge). Alternatively, impact events of high-momentum SLDF's can excavate a depression upon an abrupt slope change. The eroded and ejected sediment is subsequently deposited adjacent to the depression in the form of a distally bound ridge. Both mechanisms may play a role in the formation and development of submarine plunge pools throughout their existence.

Farre and Ryan (1985) suggested three possible mechanisms that might be responsible for the formation of a submarine plunge pool bounded by a low-relief ridge. First, the depression/ridge complex was a resultant slump scar caused by mass wasting initiated by erosional undercutting/downcutting and/or numerous debris flow processes. Second, turbidity currents that scoured away material at the base of the slope created the depression. Third, similar to the Lee *et al.* (2002) impact event theory, the depression/ridge complex may represent an impact crater caused by high-energy submarine slope avalanche event(s).

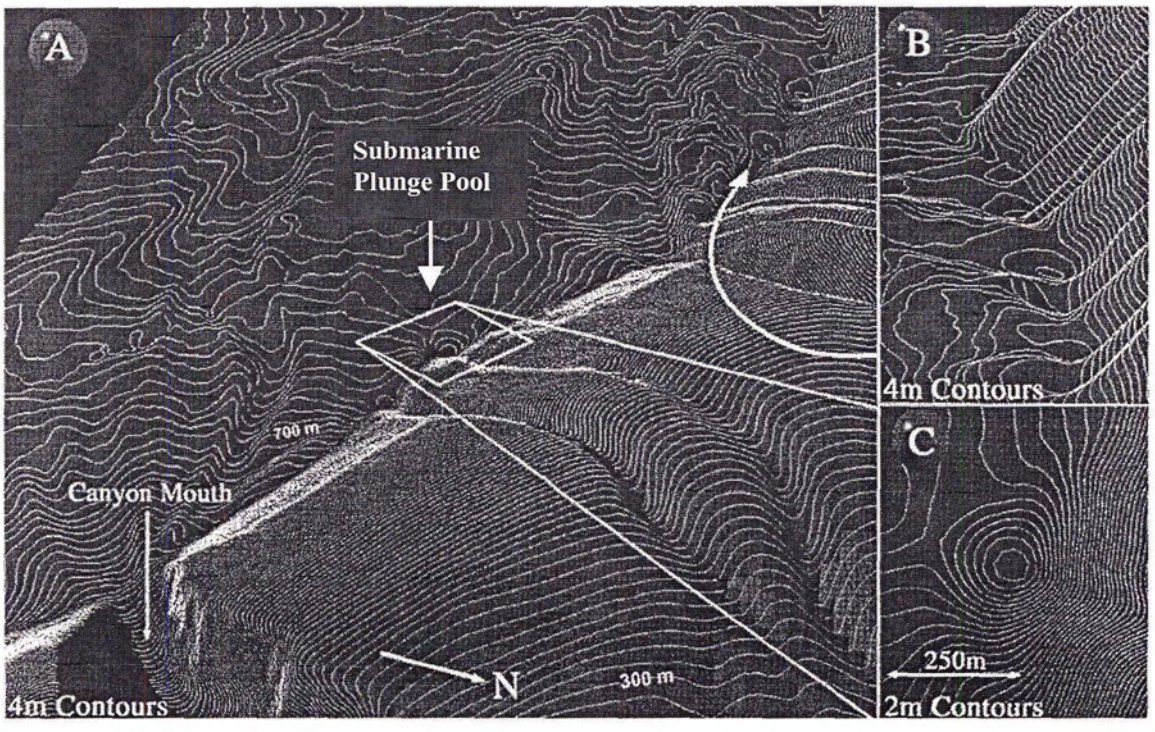

Figure 2.3 (A) Digital elevation model of submarine plunge pools on the Californian continental margin. (B) Profile of submarine plunge pools at base of the continental slope. (C) Overview of a submarine plunge pool (modified from Lee *et al.* 2002).

Landform Differences

Any differences between submarine plunge pool and SAIL formation appears to be primarily the result of differing physical properties of the flows, mediums, and environments (Table 2.6). Submarine plunge pools are features that form underwater and are 1-135 times the size of subaerial SAIL's. Unlike SAIL's, submarine plunge pools can be situated both normal and parallel to the local base of the slope, with a raised crescent or elliptical-shaped ridge (Lee *et al.* 2002).

Submarine plunge pools are most likely a result of sediment-laden density flows (SLDF); whereas, SAIL's are formed by snow avalanches. Although SLDF's are 5-40 times denser than snow avalanches, they only have an effective density 2.5-20 times that of snow avalanches as a result of density differences between snow-air, and SLDF-water. Flow velocities of snow avalanches are approximately 3-4.5 times faster than SLDF's. The impact pressures of SLDF's range between 0.14-2 times the impact pressures of snow avalanches; snow avalanches are on the order of kPa-MPa.

Table 2.6 Differences between submarine plunge pools created by SLDF's and snow avalanche impact landforms (source Lee *et al.* 2002).

Attribute	Submarine Plunge Pool	SAIL
Location	submarine	subarerial
Depression Size	diameter = 300 (Aarseth *et el.* 1989) to 2700 m (Farre and Ryan 1985) depth (maximum) = 75 m	diameter = 20 to 300 m (Fitzharris and Owens 1984) depth (maximum) = 22 m (Corner 1980)
Flow Type	sediment-laden density flow (SLDF)	snow avalanche
Density of Flow (kg/m^3)	~ 2000 (upper limit) (Elverhøi *et al.* 1997)	50-400 (Hopfinger 1983)
Fluid Medium	seawater	air
Density of Fluid Medium (kg/m^3)	~ 1028	1.29 (expense negligible resistance)
Effective Density (kg/m^3)	~ 972 (upper limit)	50-400
Flow Velocities (m/s)	~ 20 (on 5° slope) (Piper *et al.* 1988)	60-85 (Smith et al. 1994)
Impact Pressures	0.14 to 2 times the impact pressure of snow avalanches	order of kPa-MPa

2.5 GEOMORPHOLOGY OF METEORITE IMPACT CRATERS

Corner (1973, 1975) and Pettersen (1973) misidentified the origin of Rundvatnet SAIL in Norway and thought it to be a product of a meteorite impact. Although this origin was later refuted (Liestøl 1975), SAIL's do share morphological similarities with meteorite impact craters, making a review of their morphogenesis (Figure 2.4).

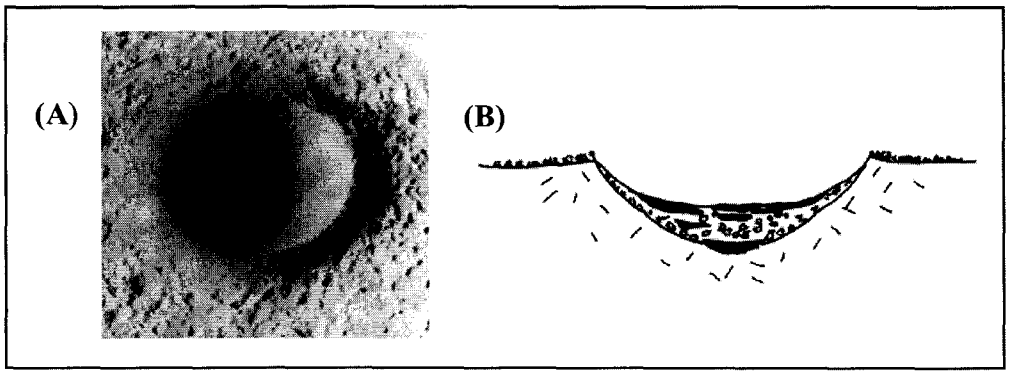

Figure 2.4 (A) Meteorite impact crater on the moon (B) Profile of a meteorite impact crater (Melosh 1989).

Meteorite Impact Crater Formation

Gault *et al.* (1968) classified the event sequence of meteorite impact cratering into three stages: compression, excavation, and modification. During the *compression stage* the meteorite makes contact with the impact surface. Upon contact the impact velocity of the meteorite decelerates as the impact area resists deformation (Melosh 1989). Simultaneously the surface directly below the meteorite is compressed in a downward direction, and adjacent surfaces are predominantly moved in the horizontal direction. (Gault *et al.* 1968). The shockwaves produced upon impact propagate into both the impact area and the meteorite.

During the *excavation stage* the shockwave propagating the impact area, semi-circular in shape, weakens the material in the impact area. Excavation occurs when the initially downward compressed and then weakened impact material is set into motion.

The excavated material is deflected upwards and outwards prior to deposition adjacent to the impact area in the form of a lip or ridge.

The result of the excavation stage is a circular depression bounded by a raised lip or ridge (Roberts 1968, Melosh 1989). Over a much longer time period (e.g., years, decades, centuries), processes such as erosion and infill slowly modify the appearance of the impact crater.

Landform Similarities

Meteorite impact craters, like SAIL's, can be circular depressions bounded by a raised ridge. The three-stage event sequence (compression, excavation, and modification) is similar to the theorized formation and development sequence of SAIL's. The proximal slope of the crater ridge is characteristically steeper than the distal slope, unless modification has occurred (Roberts 1968). The ejecta range in size from micrometres to metres and are deposited up to a distance equivalent to the crater diameter (Roberts 1968, Melosh 1989). Typically both ejecta size and deposit thickness decrease with increasing distance from the crater (Gault *et al.* 1968, Roberts 1968). The ejected material forming the ridge sometimes preserves the underlying surface (e.g., evidence of flora) and stratigraphy and/or soil horizons (Roberts 1968). This evidence is useful for dating the impact event.

Landform Differences

Differences between meteorite impact cratering and SAIL formation appear to be mainly a result of scale (e.g., size of meteorite, impact velocity, etc.) (Table 2.7). The impact velocity and pressure associated with meteorite impacts are predicted to be in km/s and GPa (Melosh 1989), compared to m/s and MPa for SAIL's (Smith *et al.* 1994). Meteorite impacts have the ability to form craters in any substrate, are formed during one-time catastrophic impact events, and are many times larger than the size of the meteorite (Melosh 1989). The much larger impact velocities and pressures of meteorite impacts result in a more complex morphology and formative processes. For instance,

approximately half the height of the lip or ridge encircling impact craters is a result of structural uplift of the substrate adjacent to the impact area, and the remaining half is deposited ejecta (Melosh 1989). Meteorite impact crater modification can include slumping and isostatic rebound processes. The size of the meteorite impact crater is a function of meteorite size, substrate in impact area, planet, and age (Gault *et al.* 1968, Melosh 1989); whereas, SAIL size is thought to be a function of snow avalanche and impact area size, topography of the track and impact area, availability of unconsolidated debris in the impact area, and large avalanche impact pressures. Due to the variability in SAIL formation, shape, and differences in magnitude of formative processes (i.e., impact velocity, momentum of impacting agent, etc.) equations used to determine and/or predict meteorite crater attributes are not interchangeable.

Table 2.7 Differences between meteorite craters and SAIL's (Melosh 1989).

Attribute	Meteorite Crater	SAIL
Event	1 catastrophic event	epsodic high-magnitude events
Impact Velocity	km/s	m/s
Impact Pressure	GPa	MPa
Impact Area Material	any material	unconsolidated debris
Crater / Depression Size	10's m – km	m to 100s m
Impact Agent	many times smaller than crater size	similar to depression size

CHAPTER 3: METHODS

This chapter describes the methodology used in this study. The intention was:

1) To describe the geomorphology at each snow avalanche impact landform site;
   - Topography of the SAIL's and avalanche tracks were described using geomorphic and bathymetric mapping techniques;
2) To document recent high-magnitude snow avalanches at each site and,
   - Frequency of high-magnitude snow avalanches were identified using absolute dating (dendrochronology) and relative dating (dendrochronology and lichenometry) techniques;
   - SAIL ridge composition described using grain-size analysis.
3) To describe the development of the snow avalanche impact landforms studied.
   - Used insight gained by the analysis of objectives 1 and 2 to make inferences regarding SAIL development.

3.1 MAPPING

3.1.1 Geomorphic Mapping

Geomorphic and bathymetric mapping were used to survey the snow avalanche tracks and SAIL's. Geomorphic mapping entailed surveying the SAIL above the water level, and the avalanche track. At each site a grid was created by running transects (10 m apart) from a perpendicular baseline. The number of measurements taken was defined by the changes in slope. An abney level was used to measure changes in slope and a tape measure was used to measure slope length. Trigonometry was used to calculate the change in elevation, and in turn the topography.

3.1.2 Bathymetric Mapping

Bathymetric mapping was used to determine the bottom topography of the water-filled SAIL's, and the submerged portion of the distal slope of the mound (Smith *et al.* 1994). Depth measurements were recorded at 5 m intervals along transects by lowering a weighted tape measure over the side of a raft.

Using the x, y, and z points calculated from the geomorphic and bathymetric mapping, schematic contour maps and avalanche track profiles were created for each site. The morphology of the track (Gardner 1970, Martinelli 1974), and the dimensions of the avalanche track, pool and ridge (Matthews and McCarroll 1994, Smith *et al.* 1994) were recorded as follows:

1. Track morphology: longitudinal profile (i.e., straight concave, convex, stepped), morphology of path (i.e., chute, jump, fall), path is confined or unconfined;
2. Track dimensions: slope of track (°), length of track (m), maximum fall (m), width of track (m);
3. Pool dimensions: length (m), width (m), width to length ratio, maximum depth (m), approximate volume (m^3);
4. Ridge dimensions: maximum height (m), maximum width (m), mean proximal and distal slope angles (°), volume above water (m^3), entire volume (m^3).

3.2 DATING TECHNIQUES

3.2.1 Dendrochronology Background

Dendrochronology is the science of using annual tree rings to date events (Fritts 1976, Shroder 1980). Trees living in temperate and subarctic climates experience changing seasons, producing distinct annual growth ring boundaries. These growth rings vary in width from year to year, depending on both environmental and physiological conditions, and provide a useful dating tool (Burrows and Burrows 1976).

Dendrogeomorphology has been employed to date slope movement (e.g., landslides, snow avalanches and rockfalls), glacier and lake level fluctuations, floods and

volcanic activity (e.g., Burrows and Burrows 1976, Schweingruber 1988). Trees that can adapt to disturbances are useful in dating geomorphic events, such as the frequency and magnitude of snow avalanches (Burrows and Burrows 1976).

A historic record of disturbance events can be established using both the *age of trees* and the *disturbance response of trees* (Shroder and Butler 1987, Butler *et al.* 1987). Using the age of the oldest trees on an avalanche slope is a relative dating method, as an ecesis date is added to the age of the tree (Figure 3.1; Shroder and Butler 1987). An ecesis date is an estimate of time between when the surface was created or denuded to the time of establishment of the trees. Problems may arise when using this method because trees that have reforested avalanche tracks can be protected by the snowpack (if the avalanche is not full-depth), and the stems of the smaller trees are flexible and are less likely to break. Stem breakage is a function of tree size, and the transition between flexibility and breakage occurs at approximately 10 cm stem diameter (Pattern and Knight 1994). Trees living on avalanche paths are generally stunted due to stress and can, therefore, live to an older age before they are killed (Carrara 1979, Pattern and Knight 1994). Slopes that avalanche frequently tend to have little or no vegetation colonizing the track; however, one major avalanche event can result in the same appearance until colonization and stabilization take place (Burrows and Burrows 1976). Due to the uncertainty of this dating method, it should be used in conjunction with *tree disturbance responses*.

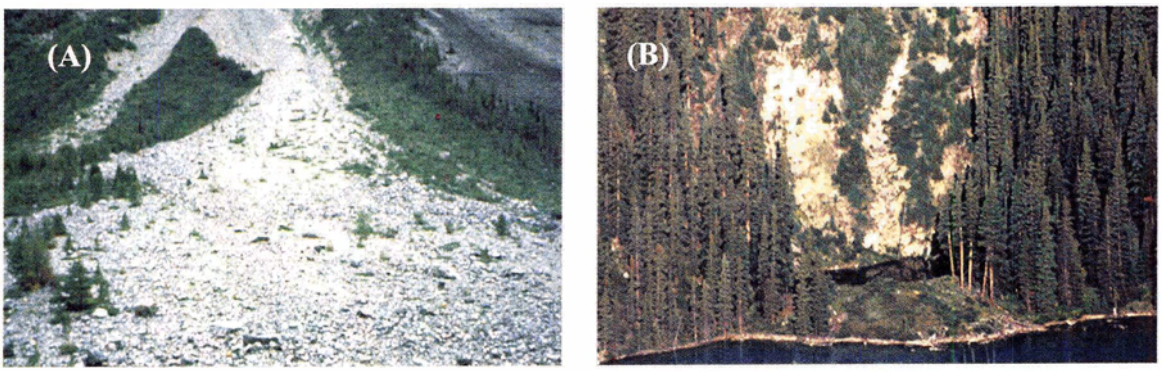

Figure 3.1 Using the age of trees growing on an avalanche track is a relative dating technique to determine when the surface was last denuded. (A) Relatively denuded avalanche track with the establishment of a few saplings. (B) Vegetated avalanche track. Track (A) denuded more recently than track (B).

The *disturbance response of trees* to snow avalanche events can be dated using the following evidence: (1) scars on trees; (2) initiation of abrupt reaction wood; (3) abrupt changes in ring-width, and (4) kill dates of trees (Potter 1969, Smith 1973, Glenn 1974, Burrows and Burrows 1976, Carrara 1979, Shroder 1980). According to Potter (1969), Smith (1973), and Shroder (1978) the first two methods are the most reliable for establishing the frequency and magnitude of avalanche events. Scarring is a very precise method of determining snow avalanche event dates. The snow, ice, and/or rock debris carried in avalanches may damage the bark and the underlying perimeter rings (Figure 3.2; Carrara 1979). Scar tissue forms around the wound and can be used to date the event (Butler *et al.* 1987). Scars can be difficult to detect once scar tissue completely covers the wound and normal growth resumes (Shroder 1980). Rockfalls, frost damage, and fires can also cause scarring, but are usually distinguishable from those caused by snow avalanches since there is evidence that snow avalanches occur at the site (Burrows and Burrows 1976, Carrara 1979).

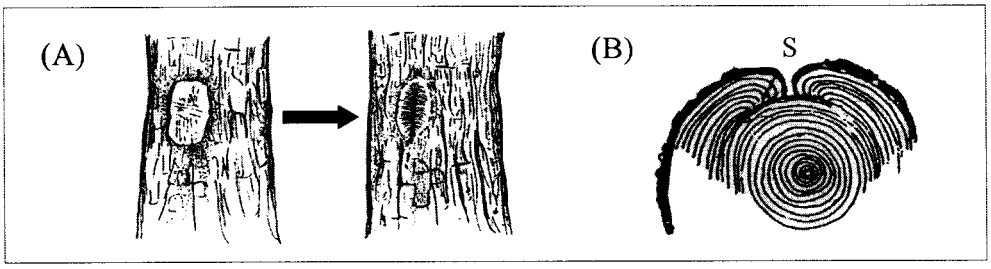

Figure 3.2 (A) Tree scarred by snow avalanche and slowly healing over, years after the event. (B) Cross section of an avalanche scarred tree, where S is the scar healing over (modified from Burrows and Burrows 1976).

Trees that have been tilted produce a distinct yellowish to reddish brown coloured reaction wood, as the tree attempts to return its stem to an upright position. Reaction wood in conifers tends to result in eccentric growth, since wider annual rings are produced on the downslope side of the tree (Figure 3.3; Burrows and Burrows 1976, Shroder 1980). Tilting can also result from events such as snowpack loading, strong winds, and creep. Tilting caused by snow avalanching can, however, be distinguished from that caused by other disturbances by its abrupt initiation and because it is produced in the direction of avalanche flow (Burrows and Burrow 1976).

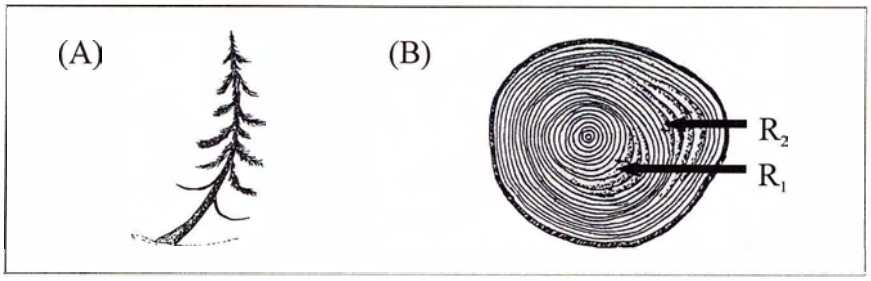

Figure 3.3 (A) Profile of a tilted tree recovering by straightening. (B) Cross-section of the tree illustrating two tilting episodes (R_1 and R_2), where R is reaction wood after the tilting has occurred (modified from Burrows and Burrows 1976).

Abrupt changes in ring-width are characterized by either suppression or release of the growth rings (Figure 3.4; Burrows and Burrows 1976). Suppression causes unusually narrow growth rings and can be a result of drought, insect infestation, and/or geomorphic events (e.g., snow avalanche event) (Burrows and Burrows 1976, Shroder 1980). Damaged trees usually produce several years of narrow growth rings before normal growth is resumed (Burrows and Burrows 1976). Only the first narrow ring is important for dating snow avalanche events, as it identifies the growing season immediately after the snow avalanche event. Growth release results in the production of unusually large annual tree rings and is not to be confused with reaction wood production. Release can result from the removal of some vegetation by an avalanche event, thus opening up the canopy (Potter 1969).

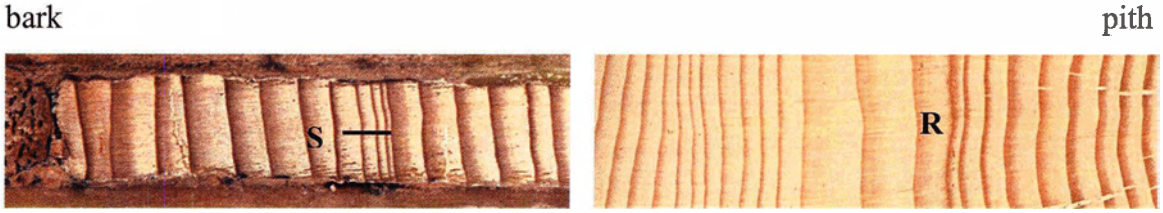

Figure 3.4 Snow avalanche events can result in abrupt changes in annual trees rings. S is ring suppression and R is ring release.

Trees that have been killed by an avalanche event are useful in determining large destructive avalanches; however, they can be problematic to cross-date if they contain any of the other previously discussed responses to avalanche events. Broken trees are

found on, along the margins of or at the base of the track, preferably *in situ*. Determining kill dates of trees is an absolute method if the perimeter wood and/or bark is present, and is a relative method if perimeter rings are missing (Figure 3.5; Burrows and Burrows 1976).

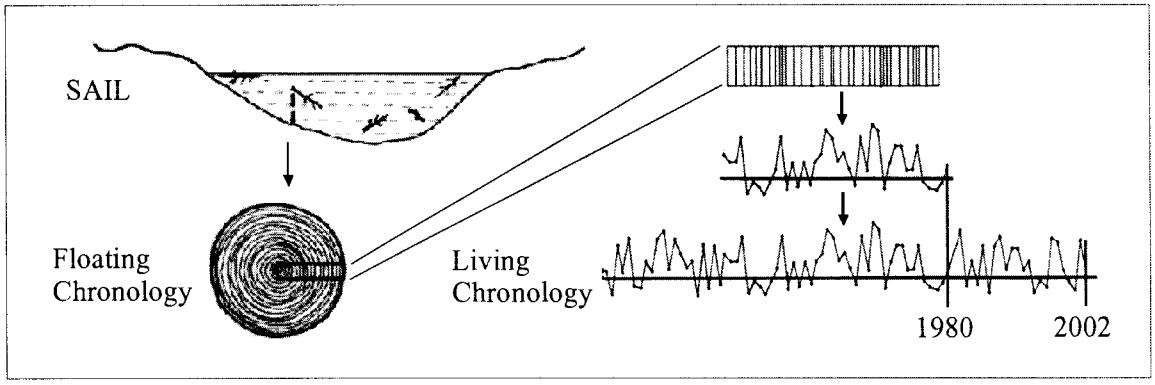

Figure 3.5 Samples collected from snow avalanche killed trees are 'floating chronologies'. A floating chronology is cross-dated to local living chronology of the same species. Absolute kill dates of trees of a floating chronology can be determined if perimeter wood and bark are present, otherwise a minimum kill date can be determined (modified from Schwiengruber 1988).

Event Response Indexes (ERI), created by snow avalanche activity can be created by plotting the *response of trees* to physical disturbance (e.g., frequency of high-magnitude events). Schweingruber (1988) calculated an ERI = (total number of events / number of trees sampled) * 100. There is no definitive ERI value for determining the magnitude of snow avalanche events. Butler and Malanson (1985) concluded ERI's greater than 40% corresponded with high-magnitude snow avalanches. Marion *et al.* (1995) and Larocque *et al.* (2001) used a 1% ERI cut-off to determine debris slope and slushflow events, suggesting that values < 10% could be a result of smaller events and/or other physical/biological disturbances. Lower than expected ERI values sometimes arise for large-scale avalanche events that happened many years ago and/or where the evidence has not survived. Butler *et al.* (1987) suggested that the minimum ERI value used to determine geomorphic activity should be user-defined based on the site(s) under study. They also note that at snow avalanche sites the sample size and location of trees sampled must be representative of the extent of the high-magnitude events. ERI's can be

compared with local climate data, such as temperature and precipitation, to determine whether a relationship exists between events and weather (Schwiengruber 1988).

3.2.2 Dendrochronology Techniques Applied

Dendrochronology was used to determine the frequency of high-magnitude snow avalanches at each study site. Handsaws and chainsaws were used to cut cross-sections and wedges from dead and living trees on and along the perimeter of the avalanche track and SAIL (Burrows and Burrows 1976, Cararra 1979). Increment cores extracted at ground level from living trees were used to determine the age of the tree, and in turn the date of stabilization (i.e., avalanche slope denudation, landform ridge). Living chronologies were used to determine kill dates of floating cross-sections. Two cores (at approximately 90°) were extracted at breast height from 20 living trees per species in a given area.

The samples collected were left to air dry. The cores were glued onto notched wooden boards, and brittle cross-sections were coated with paraffin wax. The cores and cross-sections were sanded using six grades of progressively finer sandpaper, until a high polish was achieved. The samples were scanned using a high-resolution flat bed scanner, and the annual tree rings were measured to the nearest 0.01 mm using WinDENDRO (Regent Instruments Inc., Version 6.5A-C, 2002a). A 40 times microscope was used to check and clarify any uncertainties in the annual tree rings.

Living chronologies were visually cross-dated. Quality control and accuracy of cross-dating was completed by the software program COFECHA (Holmes 1983). Series correlations (R) were measured at 99% confidence, where $R \geq 0.328$ at 50 lag 25 years is significant (Holmes 1999). A cubic smoothing spline (50% frequency cutoff of 32 years) was fit to each measured path. Paths measured in each floating chronology (A, B, C) were internally cross-dated using this method to generate the following standardized tree-ring statistics (Fritts 1976):

- Mean series correlation is a measure of the degree to which a series responds to common external factors (low = low correlation, high = high correlation).

- Mean sensitivity is an index that measures the relative difference between ring-width from one year to the next (0 = complacent rings, 2 = missing ring).
- Mean first-order autocorrelation is a measure of the correlation of a year's growth to the preceding and following year's growth (low = low correlation, high = high correlation).

Floating chronologies (killed trees) were cross-dated to a living chronology of the same species using one of two methods. First, the paths measured on each cross-section were compared to a local living chronology using COFECHA. Cross-dating was considered successful when the paths cross-dated at the same place, with the highest R-values above the critical level of series correlation (R_{CR}). The R_{CR} at 99% confidence level is 0.328 at 50 lag 25 years, or is 0.462 at 25 lag 12 years. If paths did not cross-date at the same place, cross-dating was determined by the path(s) with the least number of avalanche disturbances.

In the second instance, the International Tree-Ring Viewer (ITRviewer; Varem-Sanders 1996) was used to date floating chronologies that failed to cross-date using the COFECHA. This was done either by using:

1) the software program ARSTAN (Cook 1985) was used to create a standard index for each living and floating chronology. Double detrending first fitted a negative exponential curve to the chronology to remove the growth trend, and then fitted a cubic smoothing spline (50% frequency cutoff 128 years) to remove any non-climatic growth trends. Each floating chronology ARSTAN index was cross-dated to the living chronology ARSTAN index in ITRviewer.
2) the measured ring-widths (mm) were cross-dated to the living chronology ARSTAN index in ITRviewer. In either case, cross-dating was considered to be achieved when the floating index cross-dated with the highest R-values above the critical level of series correlation (R_{CR}).

Cross-sections and cores (living and cross-dated) were used to determine dates of initiation of reaction wood, initiation of abrupt ring changes, establishment year and age of the trees growing on the track and ridge, and the kill dates of trees. Wedges and cross-sections were used to determine impact scars dates. High-magnitude snow avalanche

events were identified using the Larocque *et al.* (2002) cut-off of 10% and observing clusters of kill dates of trees.

3.2.3 Lichenometry Background

Lichenometry is a biological dating technique that has proven to be a useful tool in determining relative surface age and stability of exposed rock surfaces (Gellatly 1982, Innes 1985, McCarroll 1994). It is based on the principle that the largest crustose lichen thallus present on an exposed rock surface is directly proportional to the age of the exposure (Gellatly 1982, Innes 1985, McCarthy 1999). The technique is useful for dating surfaces that are less than 500 years of age, after which the lichen curve becomes less reliable (Innes 1985).

The most commonly used lichen is *Rhizocarpon geographicum*, due to its slow radial growth pattern (approximately 0.02-2.00 mm/yr diameter increase), longevity and abundance (Innes 1985, McCarthy 1999). Applications of lichenometry can be grouped into geomorphic (natural depositional events) and non-geomorphic (anthropogenic structures). Geomorphic applications include dating moraine sequences (Beschel 1973, Smith and Desloges 2000), snow/slush avalanche fans (Matthews and McCarroll 1994, Bull *et al.* 1995), talus landforms (Gray 1973), debris flows (Rapp and Nyberg 1981) and rockfalls (Orombelli and Porter 1981). Non-geomorphic applications date stone structures such as stone walls (Benedict 1967), bridges, buildings, gravestones (Calkin *et al.* 1998, Smith and Desloges 2000) and cairns (Beschel and Weidick 1973, Larocque and Smith *submitted*). Natural landforms can be broken down further into single event surfaces, (e.g., moraines), and diachronous surfaces in which repeated depositional events have occurred, (e.g., rockfalls, avalanche deposits; Innes 1985, McCarroll 1994).

Several attempts have been made to standardize lichenometric-dating techniques (Webber and Andrews 1973, Lock *et al.* 1979, Innes 1985), but no one technique has been adopted. Three methods of measuring lichen thalli are currently used: i) measuring the longest diameter (a-axis) (Figure 3.6, Karlén 1973, Proctor 1983), ii) measuring the shortest diameter (b-axis), otherwise known as the largest inscribed circle method (Lock *et al.* 1979, Gellatly 1982), and iii) averaging measurements of the longest and shortest

diameters (Pitman 1973, Smith and Desloges 2000). The number of lichen thallus measured on a deposit or substrate is variable, and ranges from measuring the single largest thallus present on a deposit (Webber and Andrews 1973, Gordon and Sharp 1983), to measuring all the lichen present in a given area (Lock *et al.* 1979). A commonly used technique to determine the surface age of a single event surface is to measure and compute an average diameter of the five largest thalli (Matthews 1974, Innes 1985, McCarroll 1994).

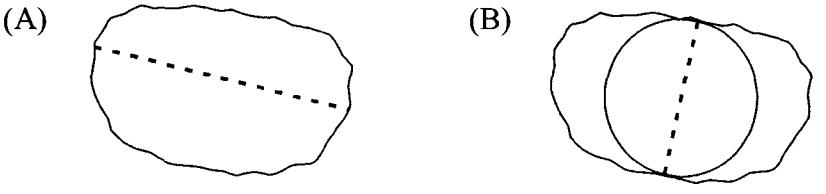

Figure 3.6 Methods of measuring lichen thalli include (A) measuring the longest diameter, (B) measuring the shortest diameter (largest inscribed circle; modified from Innes 1985).

Size- and age-frequency diagrams of the largest lichen are useful in determining the geomorphic event history of a surface that is exposed to intermittent periods of accretion (Beschel 1973, Benedict 1985, McCarroll 1994). According to Bull *et al.* (1995), size-frequency distributions for diachronous surfaces are a function of the size of the geomorphic event, rock size and accumulation per event, length of time substrate is exposed, and the local lichen growth rate. Diachronous surfaces produce lichen distributions with peaks and troughs illustrating periods of stability and disturbance; whereas, stable single event surfaces typically show a near normal distribution (Cook-Talbot 1991, McCarroll 1994). The accuracy of event history typically increases with an increase in sample size (Bull and Brandon 1998). Farrar (1974) suggested that a minimum of 100 thalli per deposit be measured. When using lichen size-frequency diagrams for diachronous surfaces it is important to remember that intermittent accretion can bury older surfaces (McCarroll 1994).

When using any of these methods, it is important that the lichen is carefully examined prior to measuring to ensure that it is a single thallus, especially on older substrates where lichen become increasingly more irregular in shape (Innes 1985). It is

uncertain if anomalously large lichen are growing at their optimum rate, are coalesced thalli, or whether they established on the substrate prior to deposition or redeposition (Innes 1985, McCarroll 1994). The largest lichen is sometimes rejected if the diameter is greater than 10 mm larger (Rapp and Nyberg 1981), 10% larger (Hodgson 1978), or 20% larger (Calkin and Ellis 1980) than the second largest lichen on the substrate. Since the risk of measuring anomalously large lichen proportionally decreases as the number of lichen measured increases, a sample size of at least the largest five thalli is recommended (Innes 1985).

Lichen diameter measurements can be used to establish lichen growth curves, or can be plotted on existing lichen growth curves to determine minimum surface age in years (Gellatly 1982, Innes 1985). Lichen growth curves provide minimum dates, and are created *directly* by using lichen diameters measured on rock surfaces over a known period of time, and/or *indirectly* by using lichen measurements on previously dated rock natural or anthropogenic surfaces (Innes 1985). Published lichen growth curves have been both linear (Porter 1981, Reynolds 2001, Wiles *et al.* 2002), and curvilinear (Luckman 1977b, Porter 1981, Larocque and Smith *submitted*).

Curvilinear-trending growth curves indicate that lichen growth occurs in three different phases (Beschel 1973, Innes 1985). During the initial phase the growth rate is slow since the lichen are colonizing. The ecesis date of lichen establishment is variable depending on the locality of the curve; for example, 10 to 50 years in the Arctic (Calkin and Ellis 1984), 17 years in Alaska, USA (Calkin *et al.* 1998), approximately 7 years in Bella Coola, British Columbia (Smith and Desloges 2000), and approximately 9 years in the Mount Waddington area of the Coast Mountains, British Columbia (Larocque and Smith *submitted*). In the second phase lichen growth occurs at a rapid rate, and was termed the *great period* by Beschel (1973). During the final phase, the lichen growth rate gradually decreases uniformly through time (Proctor 1977, Aplin and Hill 1979).

Many factors, including both physiological and environmental, affect the rate at which lichen growth occurs (Beschel 1973, Innes 1985, Benedict 1990). Physiological factors can result in a discrepancy of growth rates of individual lichen within a population of the same species (Hill 1981); whereas, environmental factors can affect entire populations of lichen resulting in more variable growth rates over a given area (local and

regional) (Luckmann 1977b). Environmental factors include components such as temperature, moisture availability, substrate lithology, duration of the growing season, vegetation presence/extent, wind exposure, aspect, stability, texture, and stone size. Gellatly (1982) and Innes (1985) observed that lichens were sometimes larger and more abundant on the distal slope than on the proximal slope of a moraine sequence, and concluded that this was a result of stability, microclimate, and age of the deposit. Little is understood about the optimum growing conditions for lichen. Lichen may respond differently to variables in different environments, therefore, it is important that a local lichen growth curve is used, and calibrated prior to use if possible, to ensure minimal error is produced (Gellatly 1982, McCarthy 1999).

3.2.4 Lichenometry Techniques Applied

The lichen measurement procedures were consistent between the three study sites, but the number of lichen measured varied (from 5-360). The a- and b-axes of circular lichen were measured to the nearest 0.1 mm using digital calipers. The largest lichen thallus at the site was assumed anomalous and removed from the dataset if it was 10 mm larger than the second largest lichen (Rapp and Nyberg 1981). The 10 mm cut-off value, the least discriminative method, was chosen to detect anomalous lichen since some of the lichen sample sizes were small. The *longest diameter method* was used to determine surface age, so the a-axis was plotted on local lichen growth curves, lichen diameter (mm) versus age of surface deposit (in years) (Karlén 1973, Proctor 1983).

3.3 GRAIN-SIZE ANALYSIS

At all three sites the mass of the largest boulders were estimated using $m = D * v$. Where m is the mass calculated in kg, D is the average rock density of 2650 kg/m^3, and v volume of the boulder (m^3), which was estimated by measuring length, width, and height. Mass was calculated to determine the competency of avalanches at the site.

At one site (Blackhorn SAIL) the size of the rock debris on the surface of the landform was estimated to describe relative changes in size and placement of rock debris

deposited by snow avalanches. Using the same transects created for mapping, the landform was divided into eleven sections of equal width (10 m) and varied length. The orientations of the sections were parallel to the avalanche track.

Wentworth's grain-size classification was simplified to five categories since time was a constraint and because relative comparisons were being observed (Wentworth 1922). At each section the percentage of fines, small pebbles, large pebbles, cobbles and boulders was estimated. The fines included clay, silt, sand; pebbles were broken down further into small pebbles and large pebbles; and cobbles and boulders sizes remained the same (Table 3.1).

Table 3.1 Wentworth grain-size classes.

Wentworth size-class	grain-size (mm)	grain-size (ϕ)
fines	0-2	10 to -1
coarse	2-64	-1 to -6
clay	0 - 0.004	10 to 8
silt	0.004 - 0.625	8 to 4
sand	0.625 - 2	4 to -1
small pebbles	2-16	-1 to - 4
large pebbles	16-64	-4 to -6
cobbles	64-250	-6 to -8
boulders	250-1000	-8 to -10

At the other two sites, grain-size analyses of bulk sediment samples from the ridges were completed by sieving into fine and coarse fractions (Table 3.1). Pits were dug on the proximal and distal slopes of the ridges. Samples collected were placed in crucibles, labeled, weighed, and then dried at 110°C for 24 hr to remove moisture. Samples were dry-sieved using a mechanical shaker for 12 minutes with a 2 mm mesh size. Subsequently the fine and coarse sediment was weighed.

CHAPTER 4: BLACKHORN SAIL

4.1 SITE DESCRIPTION AND GEOMORPHOLOGY

Blackhorn SAIL is located in the Nuit Range on the leeward side of the Pacific Coast Mountains (Table 2.1, Figure 4.1). The local mountains are composed of fine-grained volcanic andesite and diorite (igneous rock), with a mixture of metamorphosed sedimentary rocks and intrusive rocks. Monthly air temperatures at the nearest weather station 30 km east at Tatlayoko Lake (830 m asl; Meteorological Service of Canada 2001) average (1930-1997) 3.9°C (monthly maximum 26.5°C and minimum –29.9°C). The average total annual precipitation is 457.2 mm/yr (monthly maximum 175.8 mm), and average total annual snowfall snow water equivalent (SWE) is 125.1 mm/yr (monthly maximum 132.7 mm).

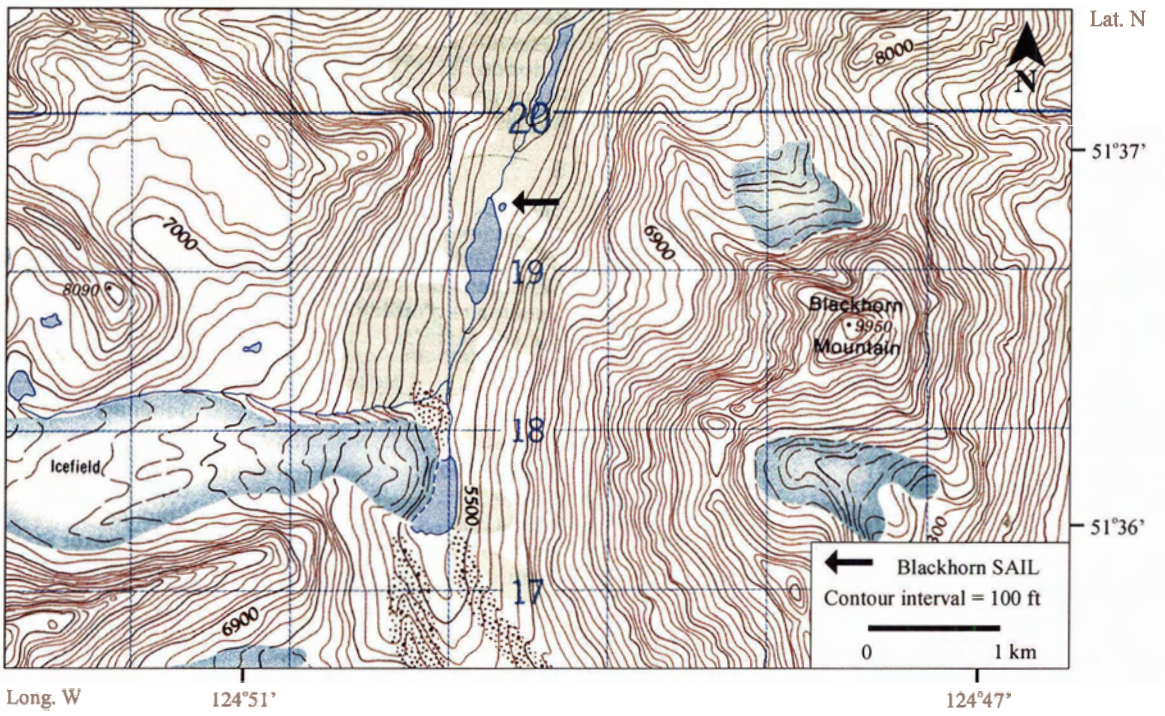

Figure 4.1 Blackhorn study site location (NTS map sheet 92N/10, 1:50,000).

The SAIL is positioned obliquely to the avalanche track at the northwest base of Blackhorn Mountain (3033 m asl), located 1.5 km downvalley of the outermost LIA

terminal moraine of White Saddle Glacier (Figure 4.2; Larocque and Smith 2003). The elliptical-shaped pool is 85 m long by 43 m wide, giving it a width:length ratio of 1:2 (Table 4.1, Figure 4.3). The pool has a maximum depth of 6 m, and an estimated water volume of 9,000 m^3.

Figure 4.2 Blackhorn SAIL positioned obliquely at the base of the avalanche path. (Photograph taken July 15, 2001)

Table 4.1 Blackhorn SAIL site geomorphology summary. *Italics* represent estimated measurements.

Track Morphology	
Longitudinal profile	concave
Morphology of track	Chute
Confined / unconfined	Both
Track Dimensions	
Slope of track (°)	14-37
Length of track (m)	825
Maximum fall (m)	350
Width of track (m)	60-120
Pool Dimensions	
Length (m)	85
Width (m)	43
Width to length ratio	2.0
Maximum depth (m)	6
Approximate volume (m^3)	*9,000*
Ridge Dimensions	
Maximum proximal slope height (m)	4.5
Maximum distal slope height (m)	3
Maximum width (m)	20
Mean proximal slope angle (°)	36
Mean distal slope angle (°)	23
Volume above water (m^3)	*4,000*
Entire volume (m^3)	*10,000*

The SAIL ridge is 10-20 m wide, rises 4.5 m above the pool surface, and 1.5 m above the water level of the adjacent lake (Table 4.1). The ridge is composed of a rocky matrix of unconsolidated sediments with numerous cobbles (cm) and boulders (m). At its highest point, the proximal slope angle is 36° and the distal slope angle is 23° (Figure 4.4). The estimated volume of debris in the SAIL ridge protruding above the pool and lake is 4,000 m^3; whereas, the estimated volume of debris in the entire SAIL above and below the water level was 10,000 m^3.

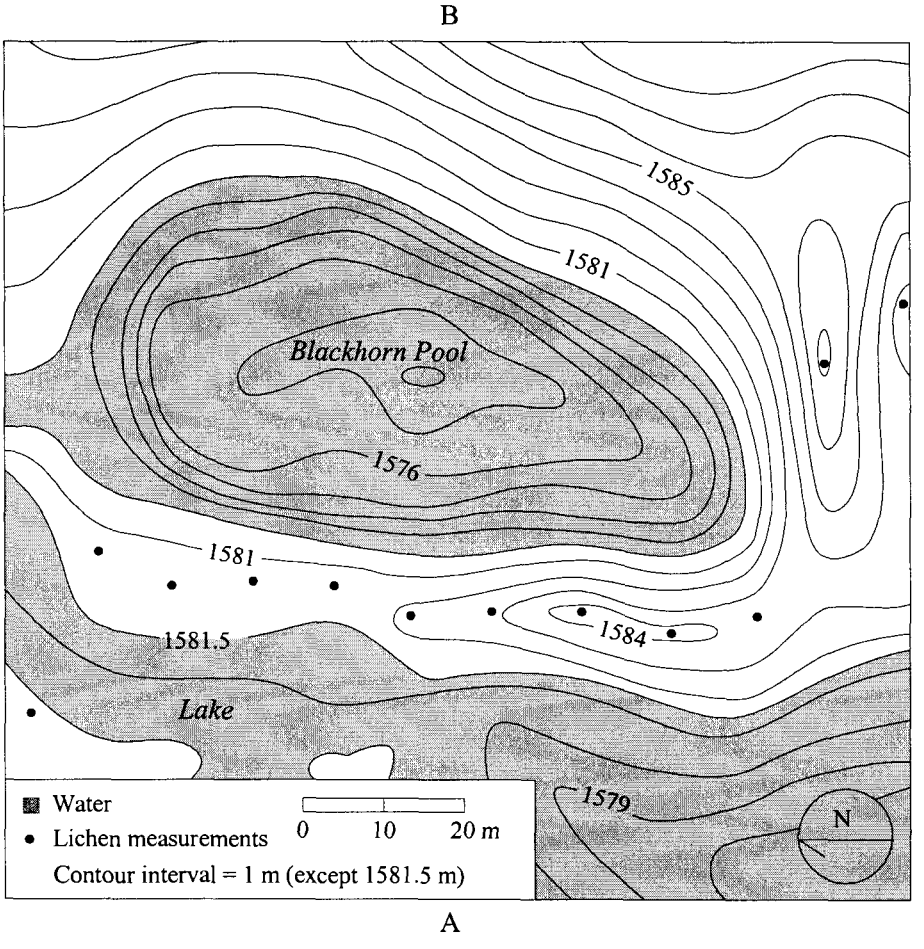

Figure 4.3 Contour map of Blackhorn SAIL. A-B illustrate transect shown in Figure 4.4.

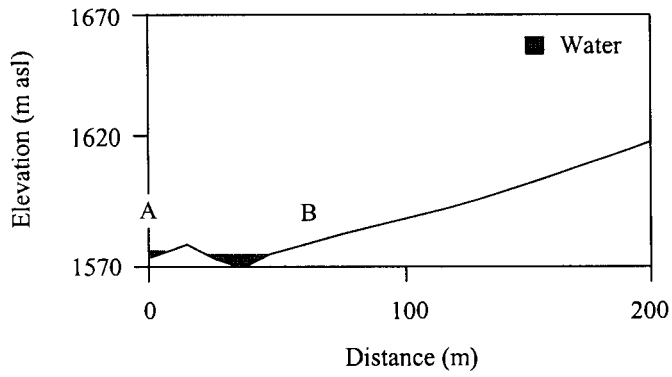

Figure 4.4 Close-up profile of Blackhorn SAIL and lower portion of the avalanche track. A-B illustrate transect shown in Figure 4.3.

The water level in the pool is maintained as water flows from the adjacent lake through the coarse rock matrix of the ridge (Figure 4.5), and drains by an outlet at the northeast end of the landform. Avalanche-killed trees are scattered along the shores of the pool near the outlet. The ridge is sparsely vegetated with juniper (*Juniperus communis*), subalpine fir saplings (*Abies lasiocarpa*), whitebark pine saplings (*Pinus albicaulis*), and willow (*Salix sp.*) Lichen are abundant on the distal slope of the landform. *Melanelia stygia* (black lichen) are the most common, with *R. geographicum* and *Xanthoria elegans* present in fewer numbers.

The slope above the site has a northwest aspect, and is comprised of two abutting concave snow avalanche pathways that originate in semi-circular, bowl-shaped catchments *approximately* 350 vertical m above the valley bottom (Table 4.1, Figure 4.6). The cirque located directly above the bowl-shaped catchments is covered with rock debris ranging in size from cobbles to boulders (Figure 4.7). One avalanche path terminates at the SAIL, and the second path deposits snow and sediment downvalley of the SAIL. The SAIL avalanche path has a gentle concave latitudinal profile steepening from 14 to 37°, from the runout zone to the starting zone (Figure 4.8). The upper shallowly confined portion of the track has a chute morphology that terminates in a mid-slope bottleneck (1770 m asl). The lower unconfined portion of the track is an accumulation zone for rock debris, and has a slightly convex profile.

Although, the track is primarily unvegetated, whitebark pine and subalpine fir seedlings are encroaching on the track margins (Figure 4.6). Avalanche scarred trees are evident along the track margin, on the island west of the SAIL, and on the mountain slope opposite the SAIL. Surrounding undisturbed valley slopes are colonized by mixed stands of mature whitebark pine and subalpine fir.

Figure 4.5 Blackhorn SAIL ridge coarse rock matrix. Note water level of the adjacent lake is higher than the water level in the pool. (Photograph taken July 16, 2001)

Figure 4.6 Two adjacent snow avalanche paths. The path on the right terminates at the SAIL. (Photograph taken July 15, 2001)

Figure 4.7 Cirque above the starting zone of Blackhorn SAIL is covered with rock debris. (Photograph taken July 15, 2001)

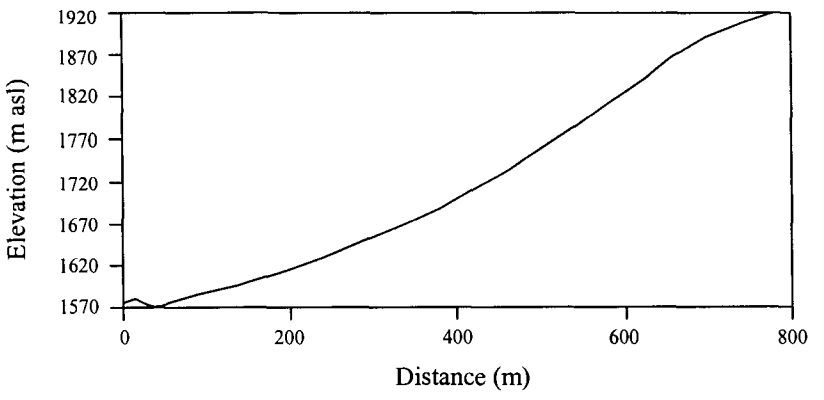

Figure 4.8 Blackhorn SAIL avalanche track profile.

4.2 DENDROCHRONOLOGY

Wood samples collected from Blackhorn SAIL were a mixture of subalpine fir, and whitebark pine. The samples collected included 59 cross-sections and 10 cores, from a total of 68 trees (Table 4.2). Of these samples, 14 were collected from the avalanche track, 10 were collected from the periphery of the avalanche track, 32 were collected from the SAIL pool and ridge, 6 were collected from the island, and 7 were collected across the lake.

Table 4.2 Wood samples collected at Blackhorn SAIL.

No.	Sample No.	Species	Sample Type	Living	Duration (yrs)	Range
Track						
1	BH01-824	whitebark pine	cross section	N	24	1966-1989
2	BH01-825	whitebark pine	cross section	N	23	1967-1989
3	BH01-826	whitebark pine	cross section	N	48	-
4	BH01-827	whitebark pine	cross section	Y	43	1959-2001
5	BH01-828	whitebark pine	cross section	Y	37	1965-2001
6	BH01-830	whitebark pine	cross section	N	23	1955-1977
7	BH01-831	subalpine fir	cross section	Y	22	1980-2001
8	BH01-832	subalpine fir	cross section	Y	25	1977-2001
9	BH01-833	subalpine fir	cross section	Y	40	1962-2001
10	BH01-834	subalpine fir	cross section	Y	32	1970-2001
11	BH01-835	subalpine fir	cross section	Y	20	1982-2001
12	BH01-400	subalpine fir	core	Y	>33	1969-2001
13	BH01-401	subalpine fir	core	Y	>25	1977-2001
14	BH01-600	whitebark pine	core	Y	>40	1962-2001

Continued...

Table 4.2 Continued...

Track Periphery						
1	BH01-823	whitebark pine	cross section	N	40	1920-1959
2	BH01-829	subalpine fir	cross section	N	46	1884-1929
3	BH01-836	whitebark pine	cross section	N	66	1898-1963
4	BH01-837	whitebark pine	cross section	N	60	-
5	BH01-838	whitebark pine	cross section	N	62	1897-1958
6	BH01-839	whitebark pine	cross section	N	52	1913-1964
7	BH01-840	whitebark pine	cross section	N	53	1895-1947
8	BH01-841	whitebark pine	cross section	N	63	-
9	BH02-401	subalpine fir	core	Y	>201	1802-2002
10	BH02-402	subalpine fir	core	Y	>295	1708-2002
Pool / Ridge						
1	BH01-800	whitebark pine	cross section	N	58	1901-1958
2	BH01-801	whitebark pine	cross section	N	59	1912-1970
3	BH01-802	whitebark pine	cross section	N	38	1924-1961
4	BH01-803	whitebark pine	cross section	N	98	1874-1971
5	BH01-804	whitebark pine	cross section	N	41	1915-1955
6	BH01-805	whitebark pine	cross section	N	37	1919-1955
7	BH01-806	whitebark pine	cross section	N	29	1922-1950
8	BH01-807	whitebark pine	cross section	N	41	1915-1955
9	BH01-808	subalpine fir	cross section	N	40	-
10	BH01-809	whitebark pine	cross section	N	42	1915-1956
11	BH01-810	whitebark pine	cross section	N	66	-
12	BH01-811	whitebark pine	cross section	N	96	-
13	BH01-812	whitebark pine	cross section	N	-	-
14	BH01-813	subalpine fir	cross section	N	63	-
15	BH01-814	subalpine fir	cross section	N	107	1858-1964
16	BH01-815	whitebark pine	cross section	N	56	1913-1968
17	BH01-816	whitebark pine	cross section	N	35	1921-1955
18	BH01-817	whitebark pine	cross section	N	58	-
19	BH01-818	whitebark pine	cross section	N	49	1916-1964
20	BH01-819	subalpine fir	cross section	N	55	-
21	BH01-820	whitebark pine	cross section	N	68	1901-1968
22	BH01-821	whitebark pine	cross section	N	43	1920-1962
23	BH01-822	whitebark pine	cross section	N	59	1910-1968
24	BH02-848	whitebark pine	cross section	N	39	1929-1967
25	BH02-849	whitebark pine	cross section	N	51	1907-1957
26	BH02-850	whitebark pine	cross section	N	58	1899-1956
27	BH02-851	whitebark pine	cross section	N	53	1905-1957
28	BH02-852	whitebark pine	cross section	N	46	1912-1957
29	BH01-402	subalpine fir	core	Y	>29	1973-2001
30	BH01-601	whitebark pine	core	Y	-	-
31	BH01-602	whitebark pine	core	Y	>23	1979-2001
32	BH01-603	whitebark pine	core	Y	>18	1984-2001
Island						
1	BH01-842	whitebark pine	cross section	N	56	1911-1966
2	BH01-843	whitebark pine	cross section	N	60	1906-1965
3	BH01-844	subalpine fir	cross section	Y	51	1951-2001
4	BH01-845	subalpine fir	cross section	Y	73	1929-2001
5	BH01-846	whitebark pine	cross section	N	47	1914-1960
6	BH01-847	whitebark pine	cross section	N	61	1905-1965

Continued...

Table 4.2 Continued...

Across the Lake						
1	BH02-853	subalpine fir	cross section	N	92	1892-1989
2	BH02-854	subalpine fir	cross section	N	104	-
3	BH02-855	subalpine fir	cross section	N	92	1889-1980
4	BH02-856	subalpine fir	cross section	Y	125	1878-2002
5	BH02-857	subalpine fir	cross section	Y	86	1920-2002
6	BH02-858	subalpine fir	cross section	Y	68	1935-2002
7	BH02-601	whitebark pine	core	Y	>215	1788-2002

Cross-sections and cores were collected from dead and living trees on the *avalanche track*. A lobate terminus, an irregular line of rock debris, formed by a ground-based snow avalanche was located 90 m upslope of the SAIL. Living trees (BH01-827 and BH01-828) above the terminus were scarred during the winter of 1985-86. The oldest of 4 living seedlings (BH01-831 to BH01-834) on the terminus established themselves in 1962. Two of four detrital *in situ* boles (BH01-824, BH01-825, BH01-826 and BH01-830) sampled below the terminus were trapped under boulders in 1989-90 (Figure 4.9). Seedlings sampled (BH01-835 and BH01-401) below the terminus were scarred in the winter of 1998-99. The oldest living tree sampled (BH01-400 and BH01-600) below the terminus established prior to 1962.

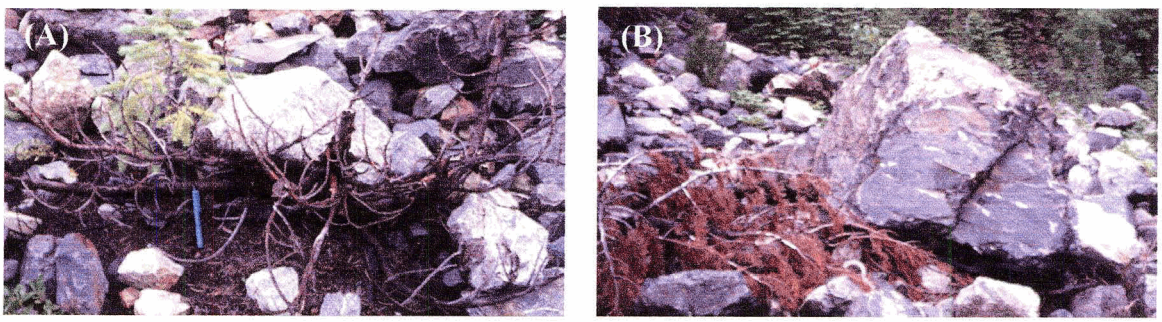

Figure 4.9 *In situ* boles trapped under (A) boulder approximately 0.02 m^3, and (B) boulder approximately 1.5 m^3. (Photographs taken July 10, 2002)

Cross-sections and cores were collected from living and detrital trees on the lower portion of *avalanche track periphery*. Eight detrital *in situ* boles (BH01-823, BH01-829, BH01-836 to BH01-841) were sampled. The oldest core (BH02-401 and BH02-402) sampled established before 1708.

Cross-sections were collected from 28 detrital trees (BH01-800 to BH01-811, BH01-815 to BH01-822, and BH02-848 to BH02-852) scattered on the *SAIL ridge* near the outlet. Cross-sections BH01-812 to BH01-815 were collected from remnant boles partially buried by soil and/or cobbles, situated on the west side of the pool near the mouth of the river. The cross-sections were predominantly from whitebark pine (86%) boles, and were missing both bark and perimeter wood. The outermost dates of these cross-sections ranged between 1950 and 1971. Cores were collected from 4 living trees (BH01-402, BH01-601, BH01-602, and BH01-603) on the SAIL ridge. The oldest tree was >29 years.

Cross-sections were sampled from living and detrital trees on the *island located behind SAIL* (14 m northwest). Scars on the living trees (BH01-844 and BH01-845) dated to 1967-68, and were aligned with the avalanche track. The 4 cross-sections sampled were from remnant *in situ* stumps (BH01-842, BH01-843, BH01-846, and BH01-847).

Cross-sections and cores were collected from living and avalanche-killed trees *across the lake*, 30 m upslope. The slope sampled was in direct alignment with the avalanche track, 100 m west of the SAIL. Cross-sections sampled from 3 avalanche-killed trees (BH02-853, BH02-854, BH02-855) were pointed upslope in the direction of avalanche flow. Reaction wood present in these trees was on the upslope side. Living trees BH02-856 and BH02-857 were scarred on the downslope side in 1921-22 and 1989-90, respectively. Cross-section BH02-858 was sampled from a leader (68 years old) growing immediately in front of detrital boles pointing upslope. A increment core taken from the largest tree on this slope (BH02-601) protected by a 64 m^3 boulder showed that it was >215 years old.

Cross-Dating Avalanche-Killed Trees

Living whitebark pine and subalpine fir tree chronologies were collected 2 km up valley of the Blackhorn site (Table 4.3, 4.4). Of the detrital cross-sections collected, 11 of the 47 (23.4%) did not cross-date to either chronology.

Table 4.3 Living tree-ring chronologies used to cross-date detritus wood from Blackhorn SAIL.

Attribute	Chronology 1	Chronology 2
Source	this study	this study
Species	Subalpine fir	Whitebark pine
Site Characteristics		
Location	Liberty Glacier	Liberty Glacier
Latitude	51°35'45"N	51°35'45"N
Longitude	124°49'40"W	124°49'40"W
Elevation	1730	1730
Series Statistics		
Number of Cores	38	32
Series Correlation	0.566	0.501
Mean Sensitivity	0.189	0.184
Autocorrelation	0.805	0.894
Length (years)	296	364
Range	1705-2001	1637-2000

Table 4.4 Detrital wood cross-dating statistics (rw = reaction wood).

Sample No.	Species	Cross-Dated Interval (yrs)	Bark	Cross-Dated with (arstan files)	Correlation of Path			
					Arstan	A	B	C
BH01-800	whitebark pine	1901-1958	N	whitebark pine	0.432	0.391	0.345	-
BH01-801	whitebark pine	1912-1970	N	whitebark pine	0.601	0.290	0.528	-
BH01-802	whitebark pine	1924-1961	N	whitebark pine	0.414	0.531	0.580	-
BH01-803	whitebark pine	1874-1971	N	whitebark pine	0.294	0.409	0.309	-
		1964-1913	N	BH01-801	0.528	0.620	0.440	-
BH01-804	whitebark pine	1915-1955	N	whitebark pine	0.580	0.460	0.457	-
BH01-805	whitebark pine	1919-1955	N	whitebark pine	0.608	0.541	0.573	-
BH01-806	whitebark pine	1922-1950	N	whitebark pine	0.637	0.466	0.585	-
BH01-807	whitebark pine	1915-1955	N	whitebark pine	0.410	0.433	0.212	-
BH01-809	whitebark pine	1915-1956	N	whitebark pine	0.626	0.487	0.452	-
BH01-814	subalpine fir	1858-1964	N	subalpine fir	0.416	0.505	0.482	0.504
BH01-815	whitebark pine	1913-1968	N	whitebark pine	0.581	0.620	0.312	-
		1916-1955	N	BH01-804	0.557	-	-	-
BH01-816	whitebark pine	1921-1955	N	whitebark pine	0.467	0.316	0.503	-
BH01-818	whitebark pine	1916-1964	N	whitebark pine	0.573	0.620	0.445	0.549
BH01-820	whitebark pine	1901-1968	N	whitebark pine	0.489	0.405	0.471	-
		1916-1955	N	BH01-804	0.559	-	-	-
BH01-821	whitebark pine	1920-1962	N	whitebark pine	0.608	0.522	0.600	-

Continued...

Table 4.4 Continued...

BH01-822	whitebark pine	1910-1968	N	whitebark pine	0.489	0.619	0.319	-
BH01-823	whitebark pine	1920-1959	N	whitebark pine	0.587	0.572	0.508	-
BH01-824	whitebark pine	1966-1989	Y	whitebark pine	0.415	0.698	0.589	-
BH01-825	whitebark pine	1967-1989	Y	whitebark pine	0.110	0.606	0.473	-
BH01-829	subalpine fir	1884-1929	N	subalpine fir	0.590	0.439	0.433	-
BH01-830	whitebark pine	1955-1977	Y	used rw and kill date	-	-	-	-
BH01-836	whitebark pine	1898-1963	N	whitebark pine	0.417	0.403	0.409	-
BH01-838	whitebark pine	1897-1958	N	whitebark pine	0.514	0.480	0.410	-
BH01-839	whitebark pine	1913-1964	N	whitebark pine	0.578	0.521	0.354	-
BH01-840	whitebark pine	1895-1947	N	whitebark pine	0.307	0.489	0.393	-
BH01-842	whitebark pine	1911-1966	N	whitebark pine	0.601	0.598	0.557	0.573
BH01-843	whitebark pine	1906-1962	Y	whitebark pine	0.448	0.469	0.268	0.260
BH01-846	whitebark pine	1914-1960	N	whitebark pine	0.558	0.295	0.291	-
BH01-847	whitebark pine	1902-1962	N	whitebark pine	0.562	0.309	0.281	-
BH02-848	whitebark pine	1926-1964	N	whitebark pine	0.393	0.691	0.777	0.799
BH02-849	whitebark pine	1907-1957	N	whitebark pine	0.500	0.513	0.473	0.525
BH02-850	whitebark pine	1899-1956	N	whitebark pine	0.468	0.436	0.411	0.510
BH02-851	whitebark pine	1905-1957	N	whitebark pine	0.368	0.414	0.435	0.261
		1907-1956	N	BH02-850	0.674	0.648	0.618	0.690
BH02-852	whitebark pine	1912-1957	N	whitebark pine	0.400	0.285	0.419	0.006
		1917-1956	N	BH02-850	0.847	0.839	0.854	0.667
BH02-853	subalpine fir	1892-1989	N	subalpine fir	0.095	0.581	0.459	-
BH02-855	subalpine fir	1889-1980	Y	subalpine fir	0.360	0.598	0.596	0.437

Disturbance Results

High-magnitude snow avalanche events at Blackhorn SAIL were identified using the ERI of the scars, reaction wood, and abrupt ring changes, along with the age of the trees established on the track and ridge, and dates of the avalanche-killed trees (Figure 4.10 and 11). No snow avalanche events had ERI's greater than 10% for all three categories. The most well-recorded snow avalanche event in the ERI occurred in 1939-40. The second, third and fourth most well-recorded snow avalanche events based on the ERI's were in 1924-25, 1917-18, 1967-68.

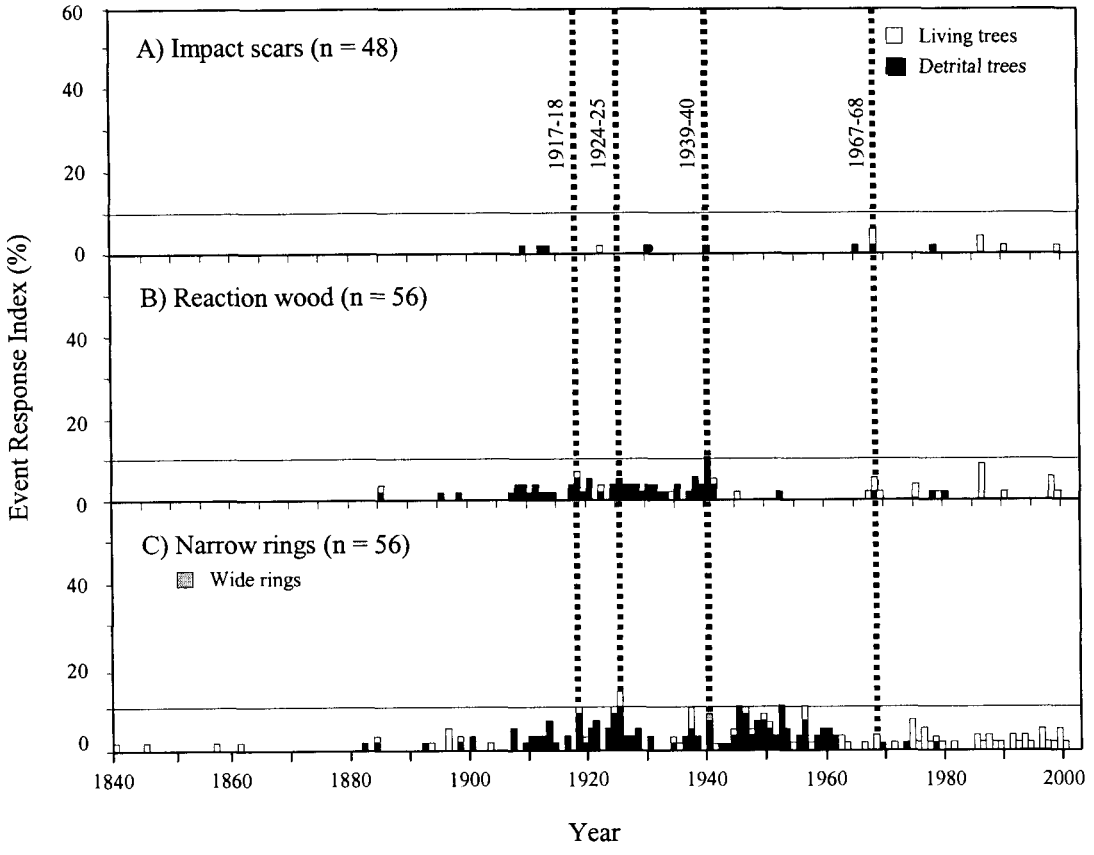

Figure 4.10 Tree event response index at Blackhorn SAIL (A) impact scars, (B) reaction wood, and (C) narrow rings. Vertical lines illustrate well-recorded snow avalanche events identified using dendrochronology.

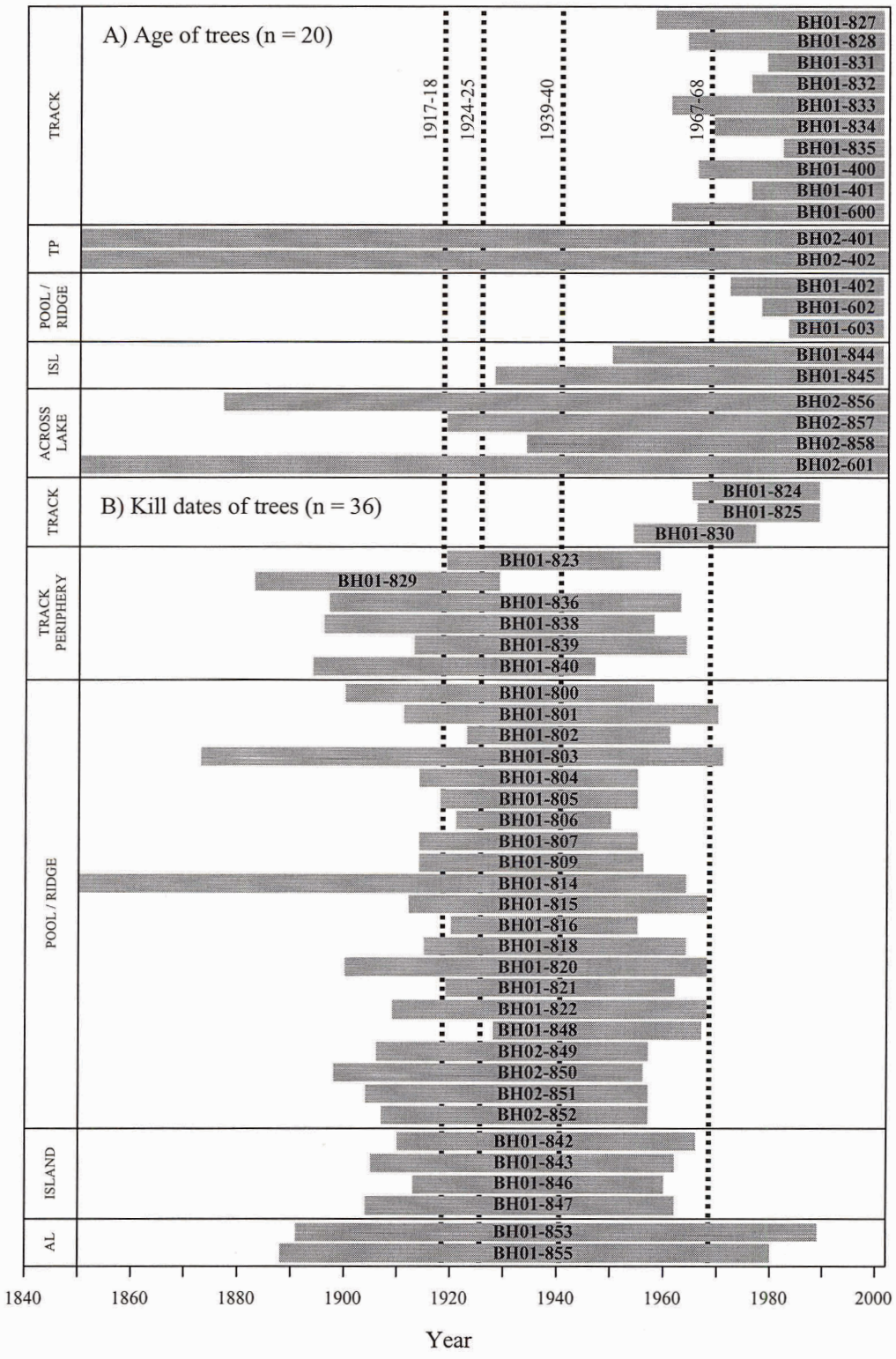

Figure 4.11 (A) age of trees and (B) kill dates of trees at Blackhorn SAIL (TP = track periphery, ISL = island behind SAIL, AL = across lake). Vertical lines illustrate well-recorded snow avalanche events identified using dendrochronology.

The oldest tree growing on the ridge (BH01-402) established prior to 1973, and may relate to either the 1967-68 or the 1939-40 event. The oldest tree growing on the avalanche track (established above the terminus in 1959) may date to the 1939-40 event. Of the 36 avalanche-killed trees, 28 trees missing bark and perimeter wood were killed after the 1939-40 event and prior to 1967. Since detrital wood (n = 36) was included in calculating the ERI's, and 29 were killed prior to 1967-68, this event was not well-recorded.

The recurrence interval of avalanche events having an ERI greater than 10% and of high-magnitude events that form and maintain the SAIL could not be calculated at this site using the data collected. However, the ERI's suggest that lower-magnitude avalanche events occur often at this site. The age of the detrital wood and living trees at this site implies some stability of the SAIL and avalanche track.

4.3 LICHENOMETRY

The 30-largest *R. geographicum* were measured at eleven points along the crest of the landform and one point on the island situated 14 m northwest of the SAIL (n = 360) (Table 4.5, Figure 4.7). Lichen age was determined using the *R. geographicum* curve developed for the Mount Waddington area in the Coast Mountains of British Columbia (Larocque and Smith 2003). Using this curve, the largest lichen measured on the SAIL ridge was estimated to be 211 years old. However, this lichen was omitted from the dataset because it was > 10 mm larger than the second largest lichen.

The lichen age-frequency distribution has a similar shape to snow avalanche lichen size-frequency distributions produced by McCarroll (1993; Figure 4.12). The establishment of *R. geographicum* was continuous from the 1960's through to the late 1980's (cutoff of large lichen measured), and the distribution increased in an exponential fashion and peaked in 1980. The distribution shows little evidence of well-defined peaks and troughs that would indicate periods of stability and large disturbance. Relatively few lichen were established on the proximal slope of the ridge, while the distal slope was well covered. The size and abundance of lichen (*R. geographicum* and *M. stygia*) on the SAIL ridge suggests stability of the landform since the 1960's.

Table 4.5 *R. geographicum* measurements from Blackhorn SAIL ridge and island. Measurements in bold are the largest lichen measured (A = A-axis, B = B-axis, and ALD = Age of Largest Diameter).

ISLAND				B			C			D			E			F		
No.	A (mm)	B (mm)	ALD (yrs)	A (mm)	B (mm)	ALD (yrs)	A (mm)	B (mm)	ALD (yrs)	A (mm)	B (mm)	ALD (yrs)	A (mm)	B (mm)	ALD (yrs)	A (mm)	B (mm)	ALD (yrs)
1	18.8	15.8	36.7	13.7	11.5	25.1	10.2	10.1	19.3	12.9	12.8	23.6	15.4	14.8	28.5	10.5	8.5	19.8
2	14.2	13.3	26.0	10.8	7.5	20.2	11.1	10.3	20.7	8.1	7.6	16.5	19.2	17.0	37.8	7.9	6.0	16.3
3	13.6	10.1	24.9	21.8	18.4	45.9	8.2	7.5	16.7	8.8	8.3	17.4	14.5	12.9	26.6	15.9	13.4	29.6
4	14.6	12.8	26.8	18.4	14.6	35.6	10.5	9.5	19.8	13.5	11.1	24.7	13.8	12.7	25.3	10.8	9.9	20.2
5	11.2	11.2	20.8	16.0	16.0	29.8	11.2	10.2	20.8	9.5	9.4	18.3	13.0	12.7	23.8	7.3	6.5	15.6
6	9.6	9.4	18.5	15.0	13.0	27.6	8.9	9.5	17.5	6.6	5.1	14.8	11.3	10.3	21.0	11.9	11.9	21.9
7	13.3	10.7	24.4	13.7	12.4	25.1	10.1	8.2	19.2	10.4	8.4	19.6	11.7	9.2	21.6	5.4	4.7	13.5
8	12.3	9.7	22.6	16.7	16.7	31.4	9.3	8.9	18.1	8.3	7.7	16.8	12.4	11.0	22.8	17.9	15.9	34.3
9	12.5	12.0	22.9	13.4	11.8	24.5	9.9	8.9	18.9	13.2	12.8	24.2	13.1	11.8	24.0	16.7	16.6	31.4
10	11.4	10.6	21.1	12.9	11.7	23.6	11.2	10.9	20.8	9.8	8.9	18.8	9.3	7.4	18.1	14.5	14.1	26.6
11	12.0	11.8	22.1	13.0	10.9	23.8	9.8	9.4	18.8	9.1	8.5	17.8	10.1	9.1	19.2	16.6	16.6	31.2
12	13.1	9.9	24.0	13.8	12.2	25.3	11.2	10.1	20.8	8.1	7.8	16.5	12.2	9.1	22.4	15.9	14.6	29.6
13	10.8	9.7	20.2	11.1	9.7	20.7	14.9	13.2	27.4	6.8	6.6	15.0	11.0	10.1	20.5	11.1	9.6	20.7
14	13.2	9.4	24.2	12.2	12.1	22.4	7.8	7.7	16.2	5.7	5.7	13.8	11.0	9.4	20.5	16.1	13.8	30.0
15	11.2	8.7	20.8	11.4	10.2	21.1	10.2	9.8	19.3	10.6	10.3	19.9	11.1	9.4	20.7	11.4	11.4	21.1
16	12.7	11.6	23.3	7.9	7.4	16.3	8.6	8.1	17.2	11.7	9.8	21.6	10.6	7.9	19.9	10.4	8.2	19.6
17	10.4	8.4	19.6	12.3	11.7	22.6	8.7	8.6	17.3	10.3	8.8	19.5	7.9	7.7	16.3	10.4	9.8	19.6
18	12.1	12.1	22.3	11.6	11.3	21.5	6.8	6.6	15.0	7.9	7.5	16.3	7.6	7.6	15.9	11.8	10.3	21.8
19	9.6	9.5	18.5	9.9	9.5	18.9	9.9	9.9	18.9	10.4	10.3	19.6	13.9	11.7	25.5	23.4	14.3	51.7
20	12.3	9.2	22.6	15.2	15.2	28.1	9.6	7.3	18.5	9.4	8.4	18.2	15.4	13.0	28.5	16.5	13.4	30.9
21	8.9	6.4	17.5	18.1	11.6	34.8	12.3	10.6	22.6	7.5	7.0	15.8	17.1	12.5	32.3	18.0	14.9	34.6
22	12.3	7.8	22.6	12.3	11.4	22.6	11.2	11.1	20.8	8.0	7.9	16.4	15.9	11.8	29.6	12.0	11.7	22.1
23	12.1	8.2	22.3	11.4	10.4	21.1	7.8	7.0	16.2	9.2	7.2	17.9	11.7	11.6	21.6	15.8	15.7	29.3
24	12.3	9.9	22.6	10.5	10.1	19.8	16.2	15.9	30.2	9.2	9.2	17.9	10.1	8.6	19.2	16.9	15.8	31.9
25	11.5	10.1	21.3	15.7	13.8	29.1	12.3	12.3	22.6	7.4	7.4	15.7	14.2	12.6	26.0	10.0	9.7	19.0
26	11.5	10.2	21.3	14.6	13.1	26.8	9.7	9.7	18.6	11.6	11.1	21.5	13.7	13.7	25.1	7.9	9.6	16.3
27	12.0	11.7	22.1	9.4	9.4	18.2	10.1	10.1	19.2	10.7	10.5	20.1	9.6	8.4	18.5	12.4	12.1	22.8
28	11.6	8.9	21.5	11.2	9.0	20.8	11.5	11.0	21.3	9.2	8.9	17.9	10.1	9.0	19.2	9.7	8.2	18.6
29	11.2	11.2	20.8	11.8	11.2	21.8	9.7	9.3	18.6	9.1	9.1	17.8	11.2	10.1	20.8	12.0	11.6	22.1
30	12.8	12.7	23.5	10.6	8.5	19.9	16.3	14.8	30.5	8.8	8.7	17.4	7.9	6.7	16.3	16.5	14.5	30.9
G				H			I			J			K			L		
No.	A (mm)	B (mm)	ALD (yrs)	A (mm)	B (mm)	ALD (yrs)	A (mm)	B (mm)	ALD (yrs)	A (mm)	B (mm)	ALD (yrs)	A (mm)	B (mm)	ALD (yrs)	A (mm)	B (mm)	ALD (yrs)
1	16.4	15.7	30.7	19.2	15.2	37.8	8.2	8.0	16.7	18.9	18.6	37.0	**32.0**	**31.1**	**98.2**	20.3	14.7	41.1
2	17.0	16.3	32.1	20.5	18.5	41.7	8.3	7.6	16.8	13.1	13.0	24.0	25.9	22.7	62.3	11.9	11.3	21.9
3	15.7	13.5	29.1	18.7	12.6	36.4	14.2	12.7	26.0	7.2	5.6	15.5	25.4	15.9	60.0	16.7	12.7	31.4
4	12.8	10.8	23.5	25.7	24.5	61.4	11.9	7.6	21.9	10.4	8.3	19.6	11.4	9.4	21.1	12.1	10.4	22.3
5	14.2	13.1	26.0	25.8	20.4	61.9	10.3	9.8	19.5	7.1	7.1	15.3	23.0	20.3	50.2	24.2	23.1	54.9
6	11.1	9.6	20.7	17.3	15.6	32.8	14.0	10.7	25.7	7.3	7.2	15.6	13.1	11.3	24.0	9.5	7.4	18.3
7	15.5	13.6	28.7	26.9	24.4	67.2	9.8	9.0	18.8	11.5	11.5	21.3	12.1	10.9	22.3	7.6	6.6	15.9
8	17.9	15.9	34.3	21.2	16.7	43.9	21.3	17.9	44.2	5.5	5.2	13.6	13.2	13.2	24.2	13.8	12.5	25.3
9	20.8	15.5	42.6	25.1	20.8	58.7	13.9	11.2	25.5	6.9	6.4	15.1	15.4	12.2	28.5	9.8	8.7	18.8
10	15.6	13.6	28.9	23.3	17.5	51.3	9.3	8.7	18.1	8.9	8.7	17.5	10.9	9.6	20.4	15.7	15.2	29.1
11	15.7	11.8	29.1	31.8	23.5	96.8	17.8	14.7	34.1	12.8	12.7	23.5	10.9	9.3	20.4	12.7	12.4	23.3
12	11.5	11.5	21.3	20.5	19.5	41.7	15.6	14.8	28.9	14.0	12.1	25.7	17.8	17.7	34.1	6.4	6.4	14.6
13	13.7	11.8	25.1	24.5	21.2	56.1	16.8	16.5	31.6	8.9	7.8	17.5	**42.4**	**32.9**	**211.1**	11.9	11.2	21.9
14	20.8	16.2	42.6	21.0	18.8	43.3	17.5	14.4	33.3	11.0	11.3	20.5	16.5	16.3	30.9	11.8	9.9	21.8
15	19.5	15.6	38.7	25.5	24.5	60.5	17.3	16.3	32.8	8.7	7.9	17.3	15.0	13.2	27.6	14.6	12.7	26.8
16	13.1	12.4	24.0	27.6	26.1	70.8	13.5	12.7	24.7	12.0	11.0	22.1	23.4	18.8	51.7	16.8	16.7	31.6
17	15.7	12.1	29.1	24.4	20.8	55.7	15.8	13.5	29.3	12.4	11.0	22.8	25.3	20.6	59.6	19.6	14.5	39.0
18	14.6	14.6	26.8	14.9	13.6	27.4	10.0	9.4	19.0	6.6	4.8	14.8	17.7	13.3	33.8	9.4	7.7	18.2
19	15.2	13.8	28.1	13.1	11.5	24.0	15.1	12.3	27.9	6.8	6.5	15.0	12.5	11.4	22.9	24.3	22.4	55.3
20	19.4	15.5	38.4	19.8	16.9	39.5	12.5	10.7	22.9	7.0	7.0	15.2	10.6	10.6	19.9	15.3	13.0	28.3
21	17.9	16.9	34.3	13.4	11.6	24.5	12.6	10.1	23.1	10.5	10.1	19.8	16.6	16.3	31.2	16.5	14.2	30.9
22	18.6	14.0	36.2	19.1	16.2	37.5	21.6	19.3	45.2	11.9	9.7	21.9	22.9	20.9	49.8	14.5	13.0	26.6
23	31.2	25.0	92.5	9.6	9.6	18.5	17.2	14.1	32.6	24.2	17.6	54.9	16.1	14.8	30.0	17.2	15.3	32.6
24	15.5	12.0	28.7	14.7	12.4	27.0	16.6	12.3	31.2	16.0	15.1	29.8	17.4	14.9	33.1	17.4	16.7	33.1
25	25.0	19.2	58.3	12.4	7.0	22.8	14.3	10.8	26.2	18.8	14.9	36.7	19.4	18.2	38.4	10.9	9.7	20.4
26	22.0	18.3	46.6	19.0	16.8	37.3	13.3	12.5	24.4	11.7	9.8	21.6	13.7	11.8	25.1	14.9	11.6	27.4
27	9.4	8.4	18.2	18.5	14.0	35.9	14.8	14.1	27.2	13.1	12.0	24.0	9.9	9.8	18.9	14.8	13.1	27.2
28	13.8	11.7	25.3	16.7	15.4	31.4	13.0	12.0	23.8	11.0	10.8	20.5	12.7	12.3	23.3	10.0	9.5	19.0
29	10.5	7.8	19.8	14.1	11.4	25.9	13.0	10.9	23.8	15.8	15.7	29.3	11.0	9.6	20.5	13.5	13.3	24.7
30	12.6	11.9	23.1	12.3	11.4	22.6	9.8	9.9	18.8	18.2	18.2	35.1	11.6	11.6	21.5	15.0	12.5	27.6

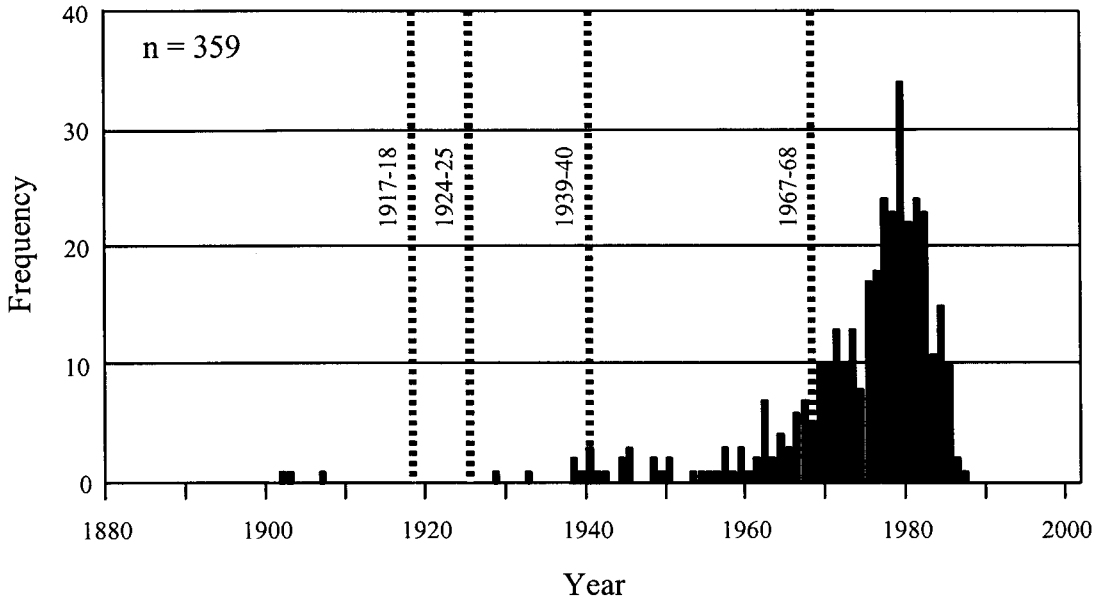

Figure 4.12 Age-frequency diagram of the establishment of *R. geographicum* on Blackhorn SAIL. Vertical lines illustrate well-recorded snow avalanche events using dendrochronology.

The lichen data was divided into two groups illustrating lichen age-frequency distribution on the north and south side of the SAIL ridge. Distribution of the north side included lichen ISLAND-F (Figure 4.13). The oldest lichen measured on the north side established in 1949 (23 mm). Establishment of *R. geographicum* was essentially continuous between the mid-1960's and late 1980's.

Distribution of the south side included lichen G-L (Figure 4.13). The oldest lichen measured on the south side was omitted because it was > 10 mm larger than the second largest lichen. The second oldest lichen measured established in 1903 (32 mm). Figure 4.13 illustrates a positive correlation between SAIL ridge topography and lichen age. The oldest and age range of the measured lichen suggests greater the south side of the SAIL ridge experienced greater disturbance. Establishment of *R. geographicum* was essentially continuous between the late-1930's and late 1980's.

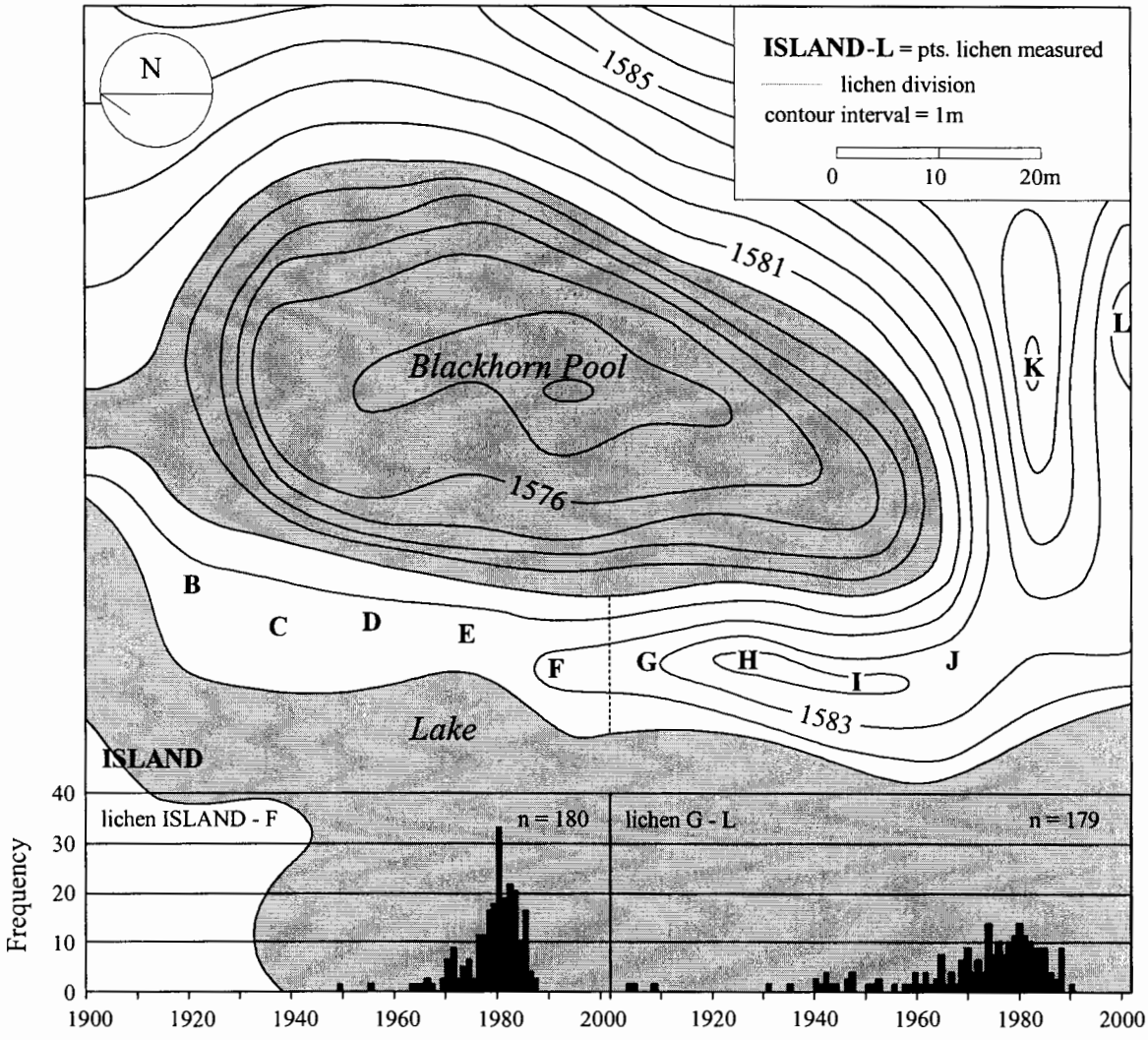

Figure 4.13 Age-frequency diagrams of *R. geographicum* establishment on the north and south sides of Blackhorn SAIL.

4.4 GRAIN-SIZE ANALYSIS

Relative changes in grain-size around the landform were observed at the Blackhorn SAIL. Grain-size was estimated for eleven sections on the exposed surface of the ridge (Figure 4.14). Grain-sizes estimated were fines, small pebbles, large pebbles, cobbles and boulders. The highest part of the ridge (section 11) was composed of 50% boulders (Figure 4.14). The second highest part of the ridge (sections 7 and 8) was composed of 40% boulders. Areas of low relief (sections 1-5) located at the north end of the ridge had the least boulders.

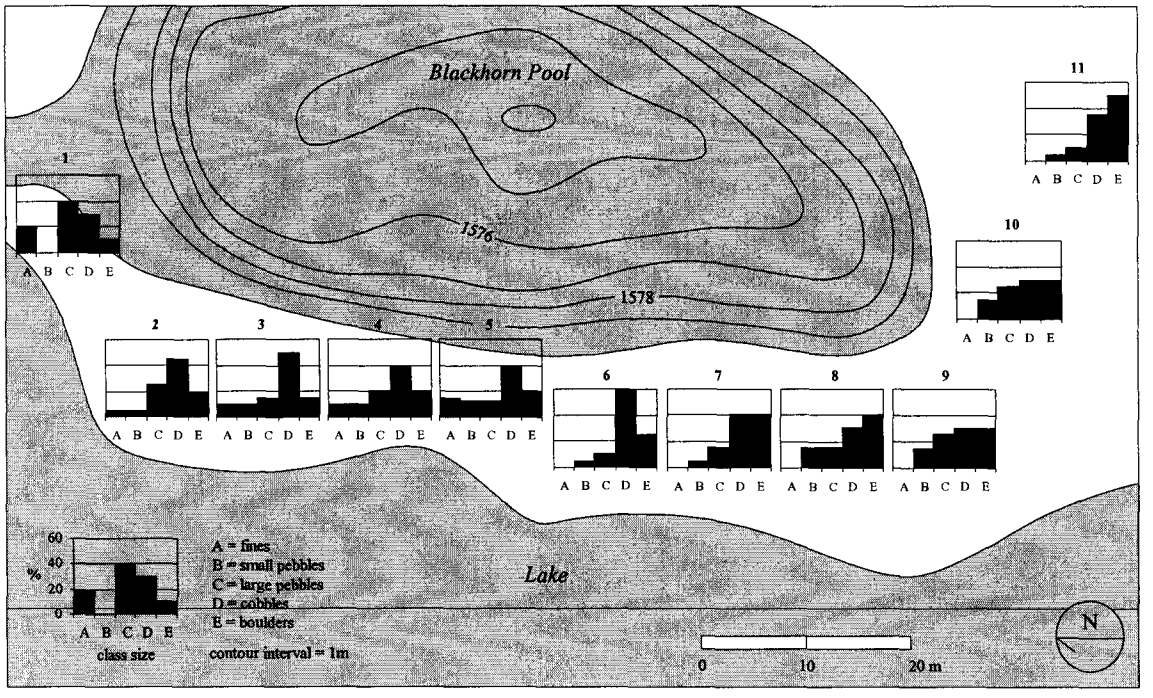

Figure 4.14 Estimated grain-size distributions on Blackhorn SAIL ridge.

The dimensions of the largest boulder in each of the eleven sections is presented in Table 4.6. The estimated mass of the three largest boulders was 10,971 kg (section 7; Figure 4.15A), 6,797 kg (section 9; Figure 4.15B), and 5,936 kg (section 6). Due to uncertainty in the origin of these exceptionally large boulders, the second largest boulder in these sections was measured. The estimated weight of the next three largest boulders measured was 4,325 kg (section 9), 2,703 kg (section 6), and 2,343 kg (section 7). The largest boulders on the ridge correspond with high topographic relief on the ridge.

Table 4.6 Measurements and locations of boulders situated on the SAIL ridge. Highlighted boulders depict exceptionally large boulders on SAIL margin (P = proximal, C = crest, D = distal).

No.	A-axis (m)	B-axis (m)	C-axis (m)	Vol. (m^3)	Mass (kg)	Location
1-1	1.3	0.6	0.4	0.31	827	C
2-1	0.6	1.0	0.6	0.36	954	P
3-1	1.0	0.6	0.5	0.30	795	D
4-1	0.9	0.3	0.8	0.22	572	P
5-1	0.6	1.1	0.5	0.33	875	P
6-1	2.0	1.6	0.7	2.24	5936	P
6-2	1.0	1.7	0.6	1.02	2703	D
7-1	1.5	2.3	1.2	4.14	10971	D
7-2	1.7	1.3	0.4	0.88	2343	C
8-1	1.0	1.0	0.4	0.35	928	C
9-1	2.7	1.9	0.5	2.57	6797	D
9-2	1.7	1.2	0.8	1.63	4325	D
10-1	0.9	1.8	0.4	0.65	1717	P
11-1	1.4	0.8	0.5	0.47	1252	C

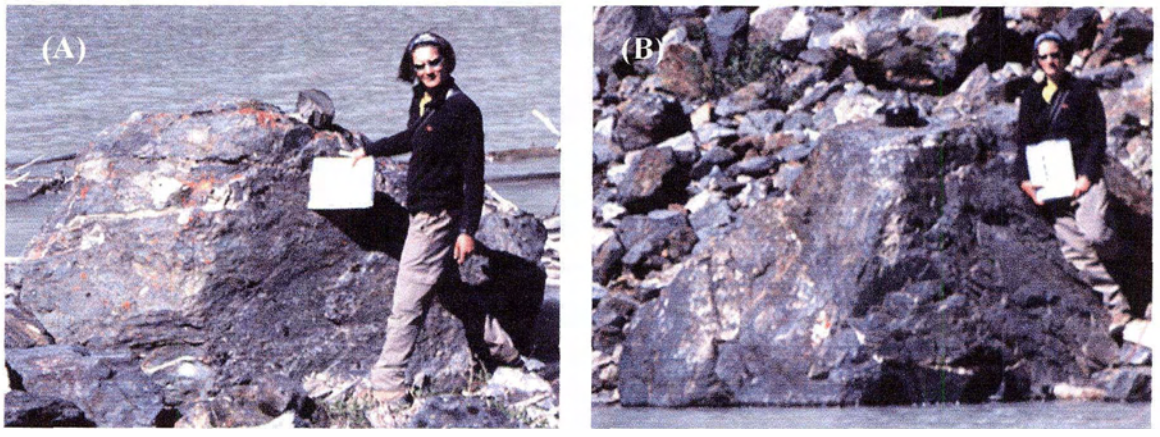

Figure 4.15 (A) Boulder 7-1 (B) Boulder 6-1. (Photographs taken July 10, 2002)

4.5 DISCUSSION

The most well-recorded snow avalanche event identified by dendrochronology occurred in the winter of 1967-68. The presence of the lobate terminus on the avalanche track (90 m upslope of the SAIL), and the establishment dates on the trees above the terminus, imply that no full-depth avalanches have occurred beyond the terminus since prior to 1962. At least twice in the past century (1921-22 and 1989-90) snow avalanches

have scarred and killed trees on the other side of the lake (100 m distance). Although the 1989-90 avalanche event traveled a considerable distance, the presence of the lobate terminus on the track suggests little or no erosion and deposition took place on the SAIL.

The lichen age-frequency distribution along the *north* side of the ridge suggest this area has been stable since the mid-1960's. The lichen age-frequency distribution along the topographically high *south* side of the ridge suggests stability since the late-1930's. The discrepancy in stability between the north and south sides is likely a result of late-lying snowpack and/or flooding on the topographically low *north* side of the ridge. Absence of lichen on the proximal slope, and abundance of lichen on the distal slope suggests excavation and/or late-lying snowpack. Overall, lichen size and abundance suggests both little deposition (few dirty avalanches), and stability at this SAIL over the past 60 years. The dendrochronology and lichenometry evidence corroborate each other, suggesting that this SAIL develops through high-magnitude low-frequency events.

4.5.1 Weather in Winter of 1967-68

The weather data used to gain an understanding of the temperature and snowfall conditions at Blackhorn SAIL during the winter of 1967-68 was measured at the Tatlayoko Lake weather station located 30 km east of Blackhorn SAIL. Although there is a 750 m difference in elevation between the sites, the data are used to illustrate trends in the local weather conditions. Monthly snowfall (SWE), rainfall and maximum monthly temperature (°C) from July 1967 to June 1968 were graphed with mean monthly snowfall, rainfall and mean maximum monthly temperatures (1930-97) (Figure 4.16).

December through April exhibited an above average mean monthly snowfall (SWE), with snowfall 2 times the monthly mean in January, March, and April. December, January, and April received above average rainfall. September through April the maximum monthly temperatures were near the mean maximum monthly temperatures, except during February where the maximum monthly temperature was 2.7°C above the mean. Using the moist adiabatic lapse rate (-6.5°C/km), maximum monthly temperatures in the starting zone were near 0°C in March, and above 0°C in April. The above average precipitation and warm spring temperatures likely resulted in a well-recorded wet spring snow avalanche.

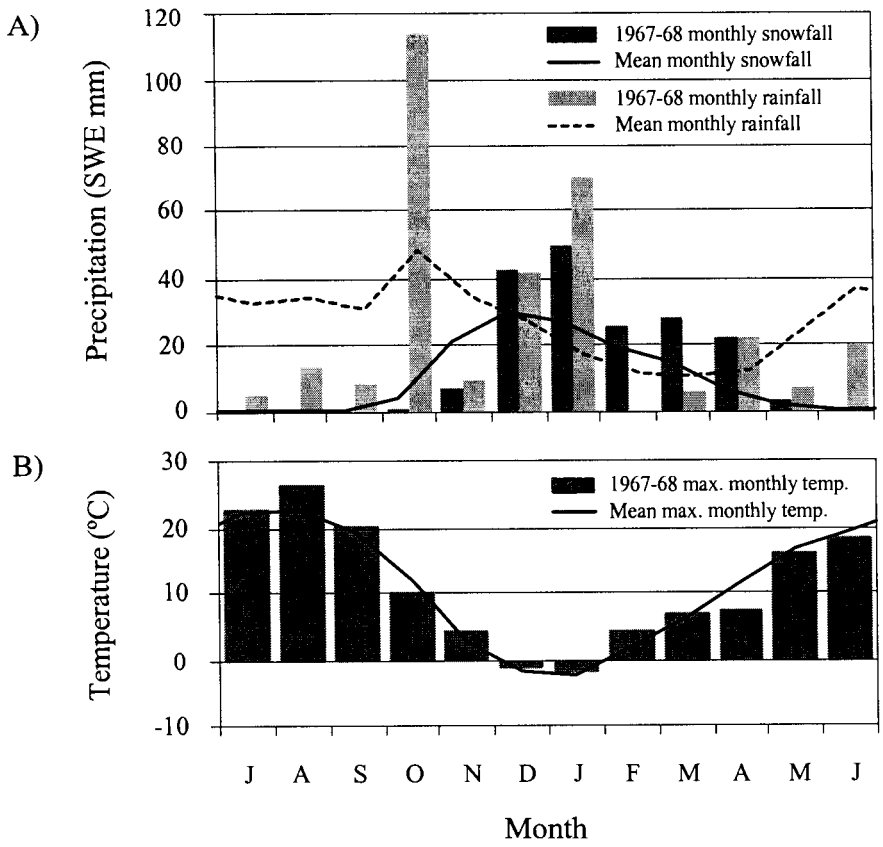

Figure 4.16 (A) monthly snowfall and rainfall (B) maximum monthly temperatures at Tatlayoko Lake, BC.

4.5.2 Historical Activity

Air photographs taken of Blackhorn SAIL before and after the 1967-68 snow avalanche event were compared (Figure 4.17). The SAIL shape and size was maintained between 1965-94. Characteristics of the avalanche track (e.g., zone of accumulation) appear the same, with little difference in treeline along the active avalanche track. Saplings are more apparent on the avalanche track in 1994, although the track remains largely unvegetated. The treeline located 30 m upslope of the lake (opposite side of the valley to the SAIL avalanche track) is similar in both years, suggesting that snow avalanches have continued to cross the frozen lake scarring and killing trees on the upslope side.

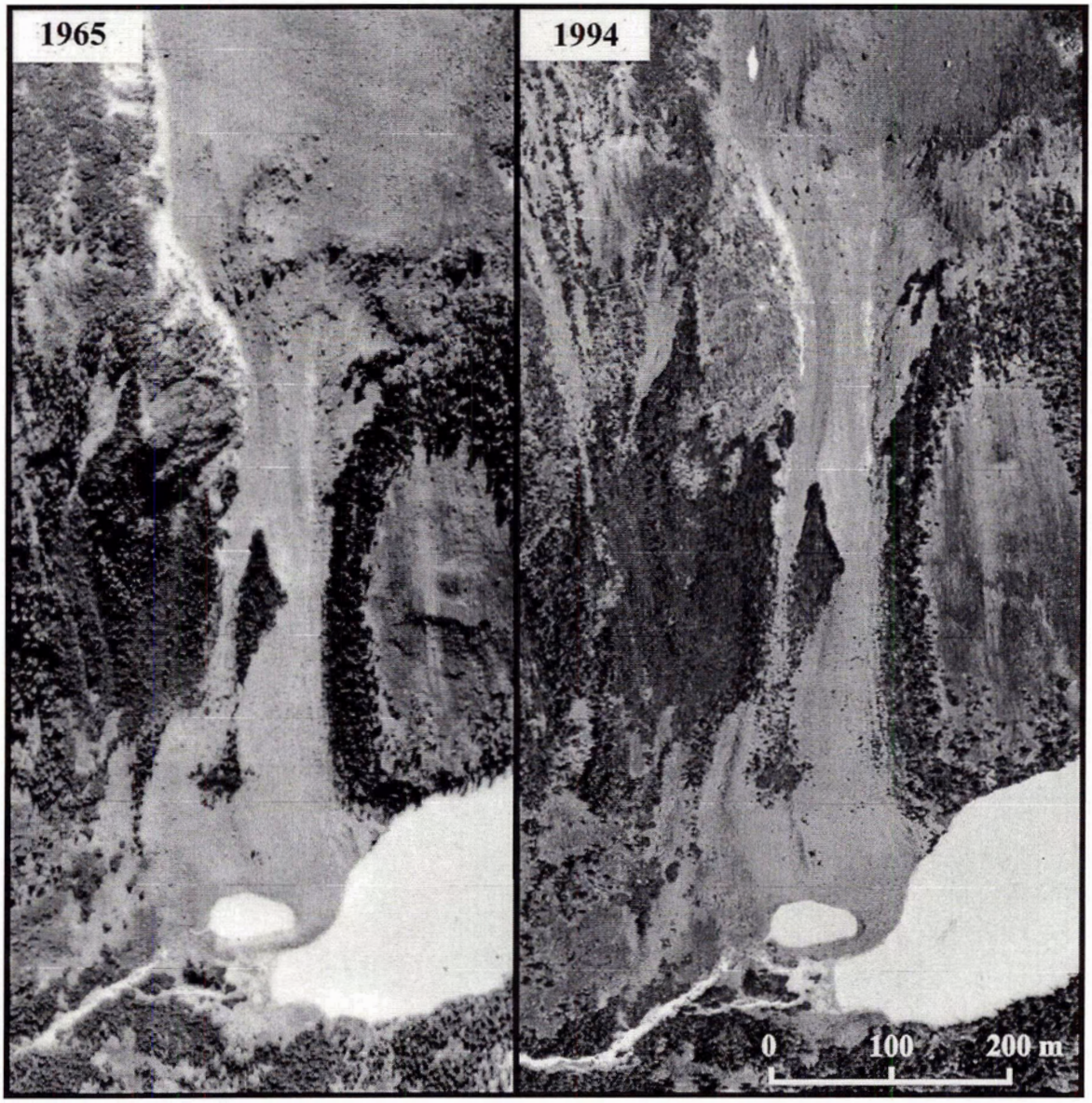

Figure 4.17 (A) Air photograph taken in 1965 (BC5151 No.220), (B) Air photograph taken in 1994 (BCC94067 No.136).

4.5.3 Development of Blackhorn SAIL

Site characteristics suggest wet, full-depth spring snow avalanches starting from the bowl-shaped catchment are responsible for forming and maintaining Blackhorn SAIL. Based on the sparsely vegetated, gentle slope morphology of the track, full-depth snow avalanches at this site remain ground-based. The erosive power necessary to move boulders larger than 1 m^3 with masses greater than 2650 kg are likely a result of wet spring snow avalanches (Gardner 1970), that bulldoze unconsolidated debris in the impact area in the direction of avalanche flow (Smith *et al.* 1994). Snow avalanches are extremely competent at this site to move boulders with estimated masses to be $\leq$4325 kg, and possibly boulders up to 10,971 kg. Based on the shape of the avalanche profile (long and concave) it is possible that an avalanche boulder tongue was the initial supply of available sediment in the impact area before evolving into a SAIL (Luckman 1978). Wet snow avalanches tend to follow track topography (Perla and Martinelli 1976), and the SAIL is not located in direct alignment with the avalanche track (Figure 4.15). Maximum theoretical impact pressures for wet, ground-based avalanches at Blackhorn SAIL range between 0.2 to 0.25 MPa (θ = 15°). It appears that little infill of the pool occurs between high magnitude low-frequency events, likely due to the weight and size of available the debris.

CHAPTER 5: SPOON LAKE SAIL

5.1 SITE DESCRIPTION AND GEOMORPHOLOGY

Spoon Lake SAIL is located 18 km east of Chilliwack and 20 km north of the USA border on Cheam Ridge in the Skagit Range on the windward side of the Northern Cascade Mountains (49°10'25"N latitude and 121°40'45"W longitude; Figure 5.1). The bedrock geology of Cheam Ridge consists of fine-grained volcanic rock with a small quantity of carbonate conglomerates (Monger 1989). The Quaternary history of Cheam Ridge has not been documented. According to Saunders *et al.* (1987) the Chilliwack Valley, located just northwest of Cheam Ridge, was deglaciated approximately 11,000 years ago. Monthly air temperatures at the nearest weather station 10 km to the northwest at Agassiz (20 m asl; Meteorological Service of Canada 2001) average (1896-1998) 9.9 °C (monthly maximum 29.6°C and minimum -12.7°C). The average total annual precipitation was 1,733.2 mm/yr

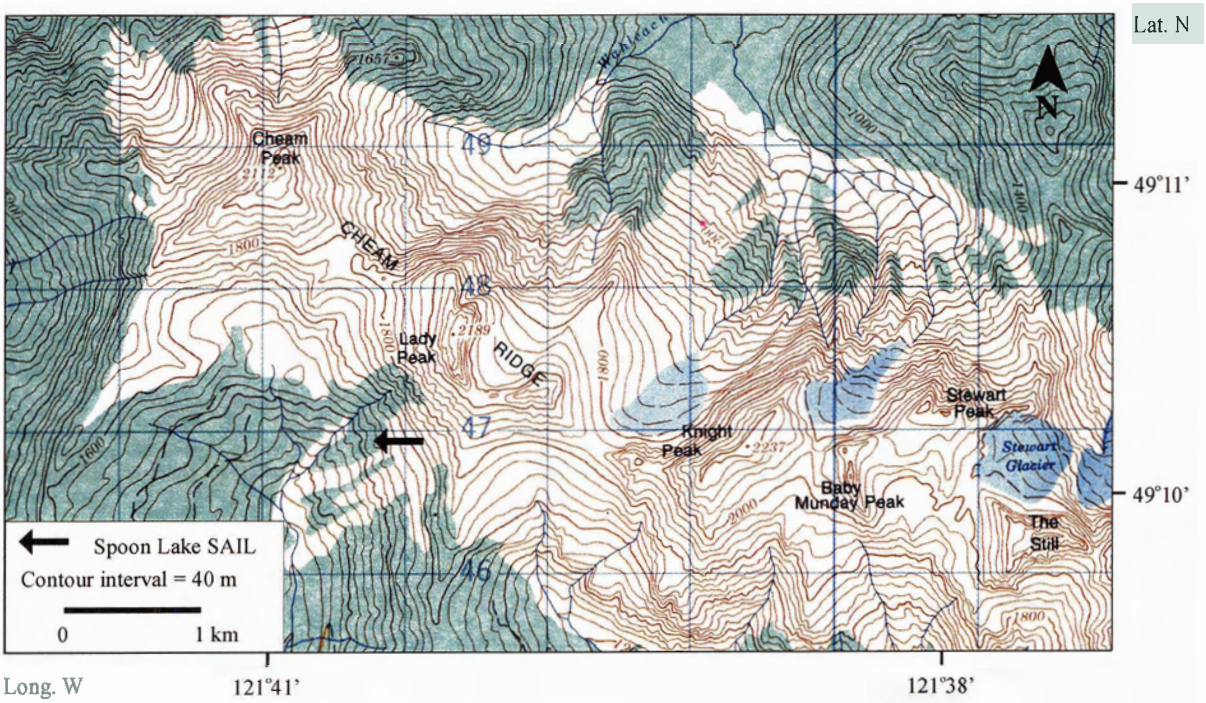

Figure 5.1 Spoon Lake SAIL study site location (NTS map sheet 92H/4, 1:50,000).

(monthly maximum 588.4 mm), and average total annual snowfall SWE was 82.5 mm/yr (monthly maximum 203.6 mm).

Positioned below the west-southwest face of Lady Peak (2190 m asl), the SAIL is identified as Spoon Lake (1470 m asl). The SAIL pool is situated with its long axis perpendicular to the primary avalanche track. The pool is 62 m long and 38 m wide, giving it a width:length of 1:1.6 (Table 5.1, Figure 5.2). The pool has a maximum depth of 5 m (August, 2002; Figure 5.3). The estimated volume of water in the SAIL pool is 4,000 m^3. The water level of the pool is maintained by snowmelt and runoff from upslope and the SAIL.

The SAIL ridge at Spoon Lake rises 10 m above the pool surface and extends distaly approximately 55 m (Table 5.1, Figure 5.4), before terminating in a stand of mature avalanche scarred and/or killed mountain hemlock (*Tsuga mertensia*), subalpine fir (*A. lasiocarpa*), and yellow cedar (*Chamaecyparis nootkatensis*) trees. The highest point on the ridge has a proximal slope angle of 58° (snow free), and a distal slope angle of 8° (Table 5.1, Figure 5.3). Spoon Lake SAIL ridge is composed of unconsolidated fine sediments with a few cobbles (cm) and boulders (m). The estimated volume of the SAIL ridge protruding above the pool is 22,000 m^3. The ridge is vegetated by a mixed assemblage of arctic lupine (*Lupinus arcticus*), cow parsnip (*Heracleum lanatum*), fireweed (*Epilobium angustifolium*), Indian hellebore (*Veratrum viride*), tiger lily (*Lilium columbianum*), western spring-beauty (*Claytonia lanceolata*), and yellow glacier lily (*Erythronium grandiflorum*). Due to thick vegetation cover, few cobbles and boulders are exposed on the ridge surface.

Two concave avalanche paths converge at the Spoon Lake SAIL. The primary track is situated immediately above the SAIL on an unconfined slope below Lady Peak (Table 5.1, Figure 5.5). The track gradient is relatively consistent (30-35°), except at the 20°-sloped bedrock outcrop located 130 vertical m from the pool creating a jump morphology (Figure 5.6). A second track originates from a southwesterly facing slope on Cheam Ridge and is channeled through a deeply incised gully at treeline before terminating at north end of Spoon Lake (Figure 5.7). This track likely plays a secondary role at the site. A snow avalanche in the spring of 2002 arrived with sufficient force to break and displace the seasonal ice in the pool, and left behind a trail of fine-sediments and tree debris on the

partially-snow covered pool (Figure 5.8). The lower portions of both tracks are covered with intermittent patches of mountain hemlock (*T. mertensiana*) and subalpine fir (*A. lasiocarpa*) krumholtz trees, interspersed with grasses and other low-lying vegetation.

Table 5.1 Summary of Spoon Lake SAIL site geomorphology. *Italics* represent estimated measurements.

Track Morphology	
Longitudinal profile	concave
Morphology of track	jump
Confined / unconfined	unconfined
Track Dimensions	
Slope of track (°)	9-45
Length of track (m)	*700*
Maximum fall (m)	*350*
Width of track (m)	*62*
Pool Dimensions	
Length (m)	62
Width (m)	38
Width to length ratio	1.6
Maximum depth (m)	5
Approximate volume (m^3)	*4,000*
Ridge Dimensions	
Maximum proximal slope height (m)	10
Maximum distal slope height (m)	-
Maximum width (m)	55
Mean proximal slope angle (°)	58 (*31*)
Mean distal slope angle (°)	8
Volume above water (m^3)	*22,000*
Entire volume (m^3)	-

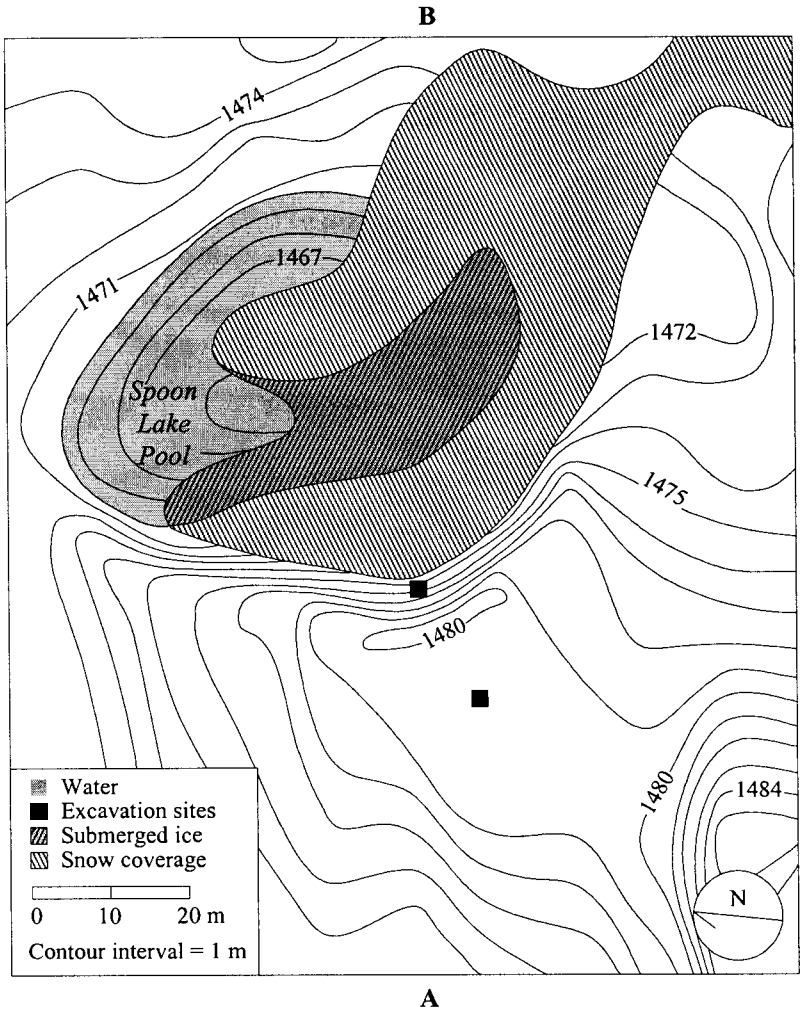

Figure 5.2 Contour map of Spoon Lake SAIL. A-B illustrate transect shown in Figure 5.3.

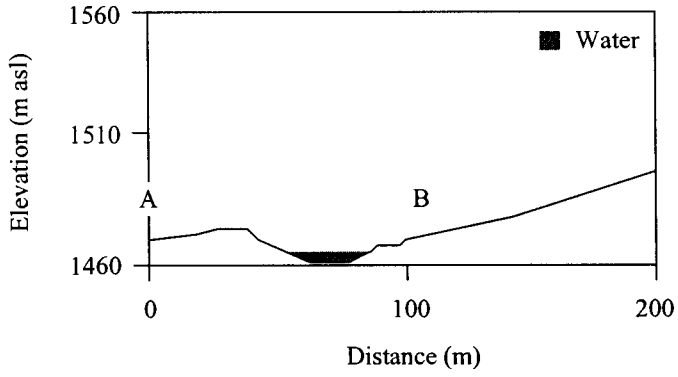

Figure 5.3 Close-up of Spoon Lake SAIL and lower portion of the avalanche track. A-B illustrate transect shown in Figure 5.2.

Figure 5.4 Spoon Lake SAIL partially covered by remnant snow and ice. (Photograph taken July 29, 2002)

Figure 5.5 Primary avalanche track that terminates at Spoon Lake SAIL. (Photograph taken July 29, 2002)

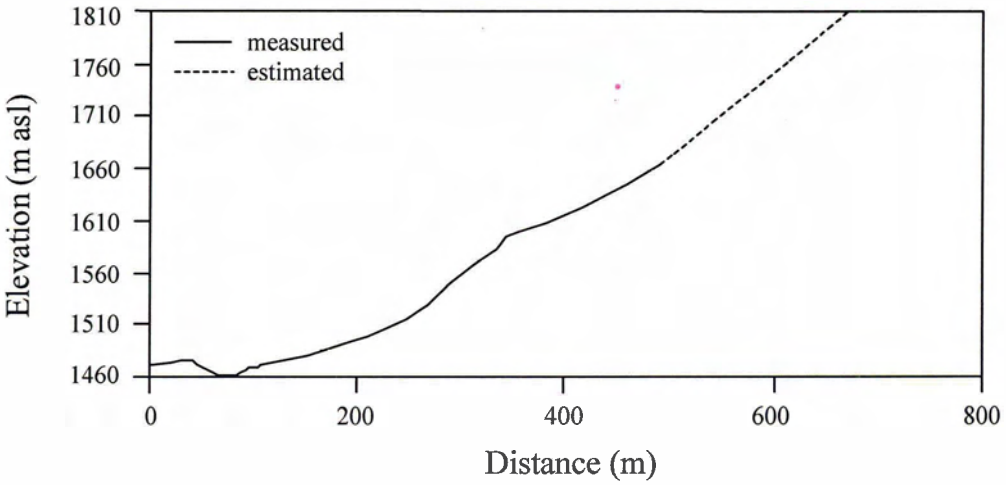

Figure 5.6 Spoon Lake SAIL avalanche track profile.

Figure 5.7 Secondary avalanche track that terminates at Spoon Lake SAIL. (Photograph taken July 29, 2002)

Figure 5.8 Sediment and detrital wood avalanched from secondary track covering remnant snowpack in SAIL. (Photograph taken July 29, 2002)

5.2 DENDROCHRONOLOGY

Wood samples collected from Spoon Lake SAIL were a mixture of mountain hemlock, subalpine fir, and yellow cedar. The samples collected included 53 cross-sections (Table 5.2). Of these samples, 36 were collected from the SAIL pool and ridge, and 17 were collected from the forest behind the SAIL.

Table 5.2 Wood samples collected at Spoon Lake SAIL.

No.	Sample No.	Species	Sample Type	Living	Duration (yrs)	Range
SAIL Pool and Ridge						
1	SL02-801	subalpine fir	cross section	N	32	-
2	SL02-802	mountain hemlock	cross section	N	120	1874-1993
3	SL02-803	subalpine fir	cross section	N	69	1921-1989
4	SL02-804	mountain hemlock	cross section	N	67	-
5	SL02-805	mountain hemlock	cross section	N	119	-
6	SL02-806	subalpine fir	cross section	N	115	-
7	SL02-807	subalpine fir	cross section	N	24	1966-1989
8	SL02-808	mountain hemlock	cross section	N	106	-
9	SL02-809	subalpine fir	cross section	N	82	-
10	SL02-810	subalpine fir	cross section	N	49	1941-1989

Continued...

Table 5.2 Continued...

11	SL02-811	subalpine fir	cross section	N	66	1908-1973
12	SL02-812	mountain hemlock	cross section	N	76	-
13	SL02-813	subalpine fir	cross section	N	77	1913-1989
14	SL02-814	subalpine fir	cross section	N	45	1895-1939
15	SL02-815	subalpine fir	cross section	N	116	-
16	SL02-816	yellow cedar	cross section	N	66	1933-1998
17	SL02-817	subalpine fir	cross section	N	46	1944-1989
18	SL02-818	subalpine fir	cross section	N	104	-
19	SL02-819	mountain hemlock	cross section	N	55	-
20	SL02-820	mountain hemlock	cross section	N	95	-
21	SL02-821	mountain hemlock	cross section	N	42	1954-1995
22	SL02-822	subalpine fir	cross section	N	51	1948-1998
23	SL02-823	subalpine fir	cross section	N	98	-
24	SL02-824	subalpine fir	cross section	N	93	-
25	SL02-825	mountain hemlock	cross section	N	76	1914-1989
26	SL02-826	subalpine fir	cross section	N	31	1968-1998
27	SL02-827	subalpine fir	cross section	N	93	1897-1989
28	SL02-828	mountain hemlock	cross section	N	105	1869-1973
29	SL02-829	mountain hemlock	cross section	N	65	-
30	SL02-830	subalpine fir	cross section	N	41	-
31	SL02-831	subalpine fir	cross section	N	58	1938-1995
32	SL02-832	subalpine fir	cross section	N	100	-
33	SL02-833	subalpine fir	cross section	N	129	-
34	SL02-834	mountain hemlock	cross section	N	85	1887-1971
35	SL02-835	mountain hemlock	cross section	N	109	1881-1989
36	SL02-836	mountain hemlock	cross section	N	92	1842-1934
37	SL02-852	mountain hemlock	cross section	N	56	1946-2001
38	SL02-853	mountain hemlock	cross section	N	83	1919-2001
Forest Behind SAIL						
1	SL02-837	mountain hemlock	cross section	Y	29	1974-2002
2	SL02-838	mountain hemlock	cross section	Y	25	1978-2002
3	SL02-839	mountain hemlock	cross section	N	36	1954-1989
4	SL02-840	mountain hemlock	cross section	N	57	1944-2000
5	SL02-841	mountain hemlock	cross section	Y	57	1946-2002
6	SL02-842	subalpine fir	cross section	Y	79	1924-2002
7	SL02-843	subalpine fir	cross section	Y	99	1904-2002
8	SL02-844	mountain hemlock	cross section	Y	106	1897-2002
9	SL02-845	subalpine fir	cross section	Y	111	1892-2002
10	SL02-846	subalpine fir	cross section	Y	104	1899-2002
11	SL02-847	subalpine fir	cross section	Y	88	1915-2002
12	SL02-848	subalpine fir	cross section	Y	104	1899-2002
13	SL02-849	subalpine fir	cross section	Y	73	1930-2002
14	SL02-850	subalpine fir	cross section	Y	98	1905-2002
15	SL02-851	subalpine fir	cross section	Y	83	1920-2002

Cross-sections were collected from 38 detrital boles and stumps found in the *pool or on the SAIL ridge*. Cross-sections SL02-801 to SL02-808, SL02-852, and SL02-854 were taken from boles situated on the remnant snow covered southwest corner of the pool. Cross-sections SL02-809 to SL02-SL02-836 were collected from boles (some partially buried) located on the south to west side of the SAIL ridge.

Cross-sections SL02-837 to SL02-851 were collected from 13 living, and 2 dead trees found *in situ* within the *forested area behind SAIL* (40 m southwest). Avalanche scars on the trees were aligned with the primary snow avalanche track. Prominent avalanche events recorded by the scars dated to 1990-91 (recorded in 4 trees), and 1946-47 (recorded in 3 trees).

Cross-Dating Avalanche-Killed Trees

Living mountain hemlock, subalpine fir, and yellow cedar tree-ring chronologies (cross-dated by Huisman (1996)) were used to provide perimeter dates for the detrital samples (Table 5.3, 5.4). SL02-815 and SL02-853 were cross-dated using marker years (scar and kill dates). Of the detrital cross-sections (n = 40) collected, 23 (57.5%) cross-dated, and 17 (42.5%) did not.

Table 5.3 Living tree-ring chronologies used to date detritus wood from Spoon Lake SAIL.

Attribute	Chronology 1	Chronology 2	Chronology 3
Source	Huisman (2000)	Huisman (2000)	Huisman (2000)
Species	Mt. Hemlock	Subalpine fir	Yellow cedar
Site Characteristics			
Location	Mt. Cheam	Mt. Cheam	Mt. Cheam
Latitude	49°11'85"N	49°11'85"N	49°11'85"N
Longitude	121°40'85"W	121°40'85"W	121°40'85"W
Elevation	1460	1460	1460
Series Statistics			
Number of Cores	37	41	39
Series Correlation	0.596	0.642	0.482
Mean Sensitivity	0.274	0.235	0.227
Autocorrelation	0.682	0.794	0.814
Length (years)	364	408	469
Range	1637-2000	1592-1999	1531-1999

Table 5.4 Detrital wood cross-dating statistics (MH = mountain hemlock, SF = subalpine fir, YC = yellow cedar).

Sample No.	Sp.	Cross-Dated Interval (yrs)	Bark	Continuous Outer Ring	Cross-Dated with	Correlation of Path			
						Arstan	A	B	C
SL02-802	MH	1874-1993	Y	Y	MH (cofecha)	-	0.404	-	-
SL02-803	SF	1921-1989	N	Y	SF (cofecha)	-	0.496	0.37	0.499
SL02-807	SF	1969-1989	N	Y	SF (arstan)	0.35	0.509	-	0.413
SL02-810	SF	1943-1989	N	Y	SF (arstan)	0.489	0.468	0.387	0.385
SL02-811	SF	1908-1973	N	Y	SF (cofecha)	-	0.596	0.452	-
SL02-813	SF	1914-1989	N	Y	SF (cofecha)	-	0.129	0.27	-
SL02-814	SF	1895-1939	N	N	SF (arstan)	0.642	0.633	0.543	0.584
SL02-816	YC	1933-1998	N	Y	used scar/kill date	-	-	-	-
SL02-817	SF	1944-1989	Y	Y	SF (arstan)	-0.015	0.401	0.399	0.328
SL02-821	MH	1956-1995	Y	Y	MH (cofecha)	-	0.329	0.537	-
SL02-822	SF	1950-1998	Y	Y	SF (cofecha)	-	0.399	0.408	0.573
SL02-825	MH	1916-1989	Y	Y	MH (cofecha)	-	0.372	0.391	0.431
SL02-826	SF	1968-1998	Y	Y	SF (arstan)	0.442	0.285	0.335	0.499
SL02-827	SF	1897-1989	N	Y	SF (cofecha)	-	0.449	0.553	0.615
SL02-828	MH	1871-1973	Y	Y	SF (cofecha)	-	0.392	0.291	0.349
SL02-831	SF	1940-1995	Y	Y	SF (cofecha)	-	0.576	0.318	-
SL02-834	MH	1890-1971	N	N	MH (cofecha)	-	0.484	0.416	0.41
SL02-835	MH	1881-1989	N	Y	MH (cofecha)	-	0.428	0.295	0.337
SL02-836	MH	1842-1934	Y	Y	MH (cofecha)	-	0.407	0.372	0.321
SL02-839	MH	1954-1989	N	Y	MH (cofecha)	-	0.742	0.737	0.509
SL02-840	MH	1944-2000	N	N	MH (cofecha)	-	0.469	0.523	-
SL02-852	MH	1946-2001	Y	Y	MH (cofecha)	-	0.378	0.375	-
SL02-853	MH	1919-2001	Y	Y	used scar/kill date	-	-	-	-

Disturbance Results

High-magnitude snow avalanche events at Spoon Lake SAIL were identified using the ERI of the scars, reaction wood, and narrow rings, along with the age of the trees established in the forest behind the SAIL, and dates of avalanche-killed trees (Figure 5.9). No snow avalanche events had ERI's greater than 10% in all three categories. The three most well-recorded snow avalanche events using the ERI's were 1990-91, 1963-64, and 1946-47. Since scar years are the most accurate record of snow avalanche events, these three event years were not entirely based on the highest sum of ERI percentages. The ERI of reaction wood was underrepresented because it was present throughout half of the cross-sections, as opposed to abrupt rings of reaction wood that typically occur after disturbance events. The kill dates of trees (Figure 5.9) suggested two other winters of well-recorded snow avalanche events, which were 1989-90 (9 trees cross-dated to this kill date) and 1998-99 (3 trees cross-dated to this kill date).

The recurrence interval of high-magnitude events could not be calculated since no events had all ERI's > 10%. The recurrence interval (calculated using data between 1939-2002) of avalanche events having two of three ERI's > 10% at this site is 10.6 years. Using ERI's and kill dates the recurrence interval is 8 years. The ERI's suggest that lower-magnitude avalanche events occur often at this site. The age of the detrital wood and living trees at this site implies some stability of the SAIL and avalanche track.

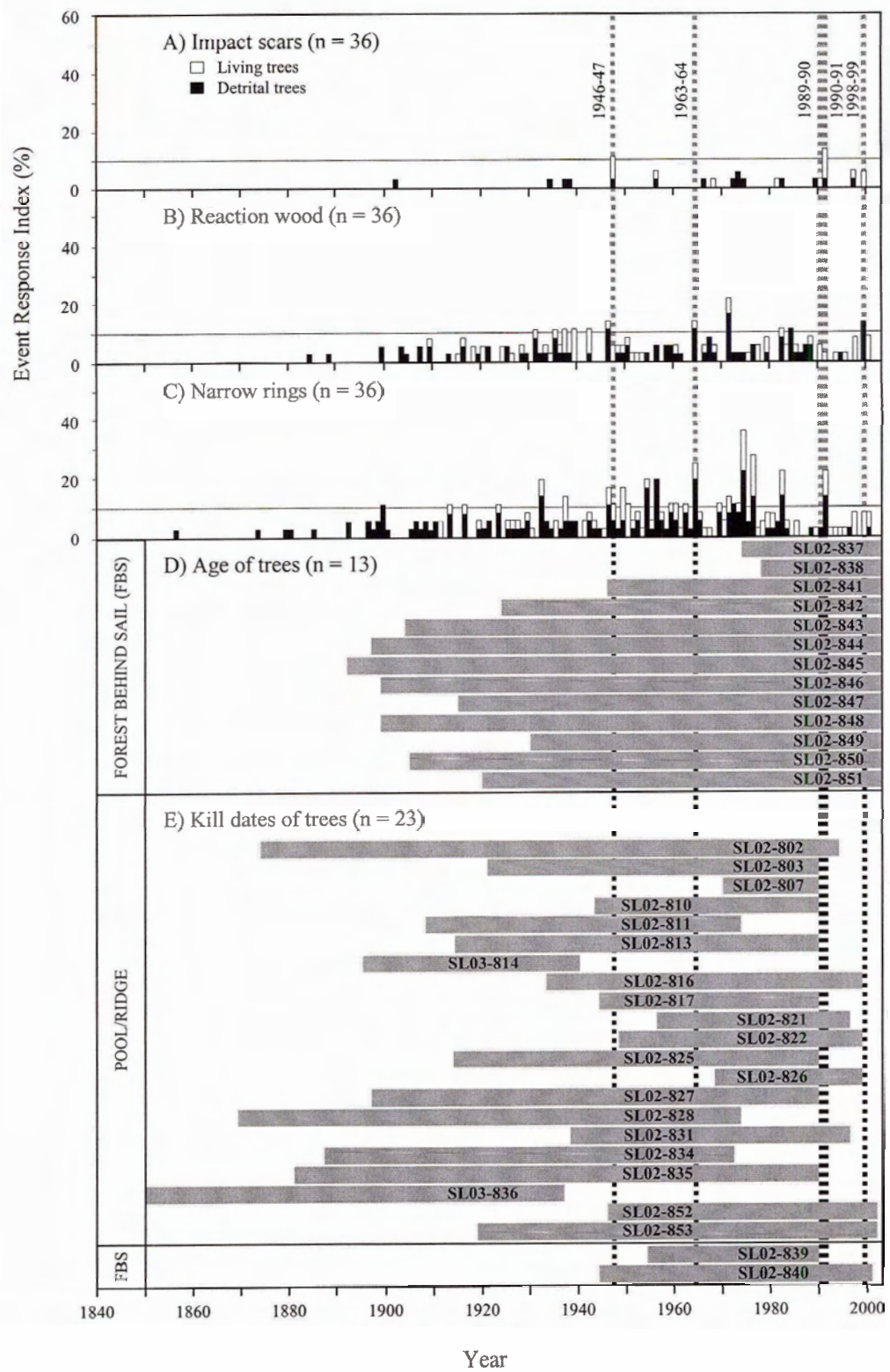

Figure 5.9 Spoon Lake SAIL ERI (A) impact scars, (B) reaction wood and (C) narrow rings. (D) Age of trees and (E) Kill dates of trees. Vertical lines illustrate well-recorded snow avalanche events using dendrochronology.

5.3 LICHENOMETRY

Lichen measurements of 5 *R. geographicum* were taken from one boulder (boulder 1) on the SAIL ridge (Table 5.5). The boulder was located on the proximal slope of the ridge approximately 20 m north of the highest portion of the ridge. Lichen age was assigned using the andesite substrate Mount Rainier *R. geographicum* curve developed by Porter (1981). The maximum age of the lichen measured was 52.5 +/-2 years, indicating that it established in 1968 +/-2 years (Figure 5.10). *R. geographicum* were observed on 6 additional rocks on the SAIL ridge, but were not measured due to their irregular shape. The number of *R. geographicum* measured at this site (n = 5) is a reflection of the number of boulders present and the vegetation cover on the SAIL ridge. Since the lichen at the site were very limited, no trend could be observed from the lichen age-frequency diagram.

Table 5.5 *R. geographicum* measurements from Spoon Lake SAIL ridge (ALD = Age of the Largest Diameter).

Lichen	A-axis (mm)	B-axis (mm)	ALD (yrs): Andesite Substrate
1	27.6	24.3	52.5 +/- 2
2	22.3	25.2	46.3 +/- 2
3	20.1	19.1	36 +/- 2
4	18.8	18.4	34 +/- 2
5	22.9	18.7	42 +/- 2

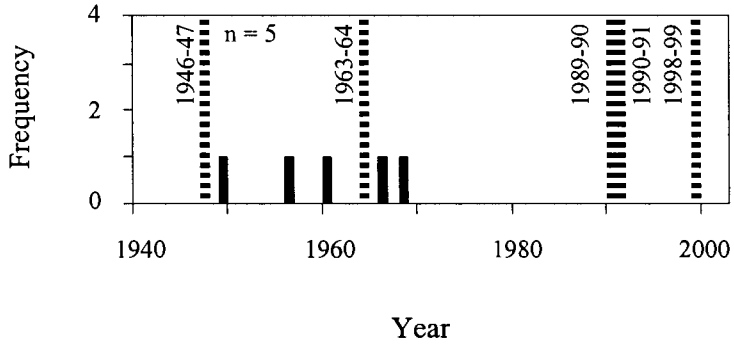

Figure 5.10 Age-frequency diagram of the establishment of *R. geographicum* on Spoon Lake SAIL. Vertical lines illustrate well-recorded snow avalanche events identified using dendrochronology.

5.4 GRAIN-SIZE ANALYSIS

Pits were dug on the distal and proximal slopes of Spoon Lake SAIL ridge (Figure 5.7). The same stratigraphy was observed in both pits, and consisted of horizon 1, which extended from the vegetated surface of the ridge to a depth of 10 cm, a 2 cm thick buried organic layer, and horizon 2, which extended below 12 cm. Since the collected samples (350-550 g) were to be representative of the horizon and the sediment from the pool ice/bottom/bank, sediment sizes greater than 64 mm (cobble size) were not included. Few sediments larger than 64 mm were encountered when digging the excavation pits.

Sediment samples were collected from the horizon 1, organic layer, and horizon 2 on the distal slope of the SAIL ridge (Figure 5.11). Strata 1 consisted of 38% fine sediment and 62% coarse sediment. The organic layer consisted of 73% fine sediment and 27% coarse sediment. Horizon 2 consisted of 53% fine sediment and 47% coarse sediment. Sediment samples were collected from sediment covering the remnant ice on the SAIL pool, from the pool bottom (at the east side of the pool), and from the pool bank (at the north side of the pool) (Figure 5.12). The sediment covering the remnant ice consisted of 80% fine sediment and 20% coarse sediment. Sediment from the pool bottom consisted of 88% fine sediment and 12% coarse sediment. Sediment from the pool bank consisted of 90% fine sediment and 10% coarse sediment.

A total of 18 boulders (size > 256 mm) exposed on the surface of the SAIL were measured (Table 5.6). The largest boulder measured (boulder 2) had an approximate weight of 1,060 kg. It was located on the distal slope of the ridge, 20 m north of the highest part of the SAIL ridge.

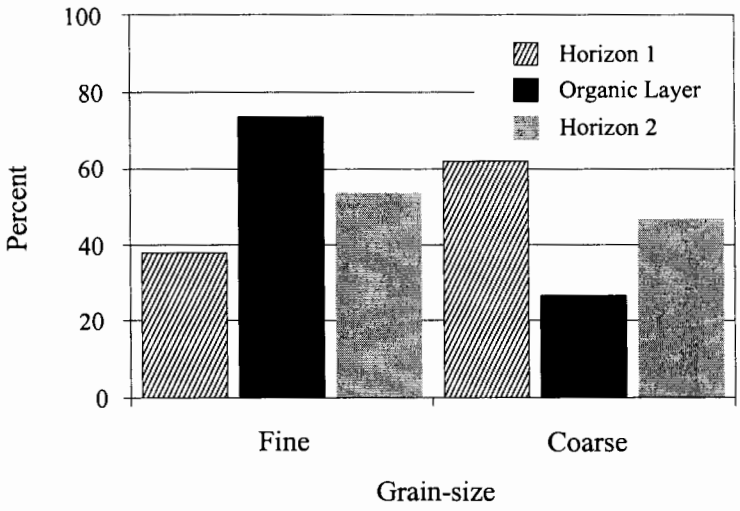

Figure 5.11 Percentage of fine and coarse sediment in strata 1and 2 on the distal slope of Spoon Lake SAIL ridge.

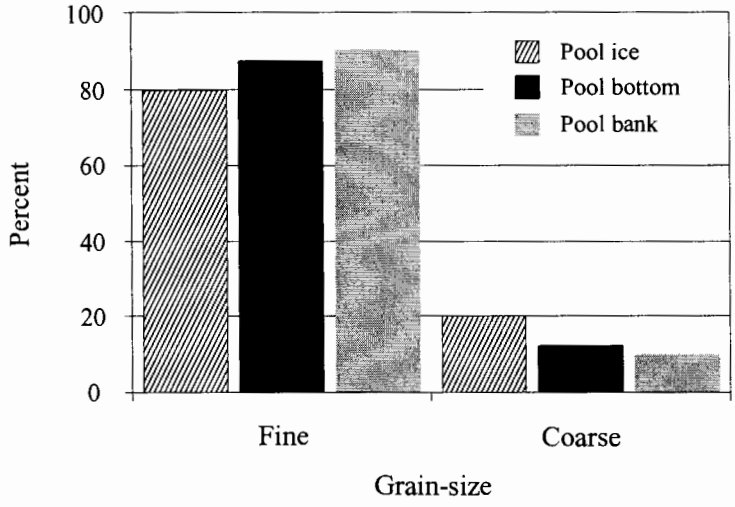

Figure 5.12 Percentage of fine and coarse sediment in sediment on pool ice, sediment from pool bottom, and sediment from pool bank at Spoon Lake SAIL.

Table 5.6 Measurements and locations of boulders situated on the Spoon Lake SAIL ridge (P = proximal, C = crest, D = distal).

No.	A-axis (m)	B-axis (m)	C-axis (m)	Vol. (m^3)	Mass (kg)	Location	No.	A-axis (m)	B-axis (m)	C-axis (m)	Vol. (m^3)	Mass (kg)	Location
1	0.45	0.28	0.12	0.015	40	D	10	0.55	0.33	0.12	0.022	58	D
2	1	1	0.4	0.4	1060	D	11	0.52	0.3	0.2	0.031	83	D
3	0.55	0.55	0.45	0.136	361	D	12	0.45	0.3	0.15	0.02	54	D
4	0.5	0.3	0.2	0.03	80	D	13	0.5	0.42	0.38	0.08	211	D
5	0.55	0.38	0.2	0.042	111	D	14	0.56	0.45	0.21	0.053	140	D
6	0.8	0.35	0.22	0.062	163	D	15	0.3	0.27	0.2	0.016	43	D
7	1.5	0.45	0.35	0.236	626	D	16	0.75	0.3	0.28	0.063	167	D
8	0.7	0.45	0.22	0.069	184	D	17	0.5	0.42	0.15	0.032	83	D
9	0.57	0.38	0.4	0.087	230	D	18	0.55	0.26	0.12	0.017	45	P

5.5 DISCUSSION

Five snow avalanche events were well-recorded at Spoon Lake SAIL, and include 1946-47, 1963-64, 1989-90, 1990-91, and 1998-99. Of these, the weather during the winter of 1989-90 was described because 9 trees in the forest behind the SAIL were killed during this event. The SAIL ridge is well vegetated with low-lying vegetation, which supports the theory of long-term SAIL development.

Late-lying snowpacks at elevations above 1300 m asl (Porter 1981), and the presence of few cobbles and boulders on the SAIL ridge inhibit lichen establishment at this site. The five lichen measurements were taken from one boulder. The largest lichen measured established in 1949 +/- 2 years; therefore, this boulder was likely deposited during the well-recorded 1946-47 snow avalanche. The limited lichenometric evidence supports the dendrochronological evidence at this site.

5.5.1 Weather in Winter of 1989-90

The weather data used to gain an understanding of the temperature and snowfall conditions at Spoon Lake SAIL during the winter of 1989-90 was measured at the Agassiz weather station located 10 km northwest of Spoon Lake SAIL. Although there is a 1450 m asl difference in elevation between the sites, the data are used to illustrate

trends in the local weather conditions. Monthly snowfall (SWE), rainfall and maximum monthly temperature (°C) from July 1989 to June 1990 were graphed with mean monthly snowfall, rainfall and mean maximum monthly temperatures (1896-1998; Figure 5.13).

During December this area received 200 mm more rain than normal (nearly double), and January and February received both above mean monthly snowfall and rainfall. The maximum monthly temperatures were similar to the mean maximum monthly temperatures. Using the moist adiabatic lapse rate (-6.5°C/km), maximum monthly temperatures near the starting zone were above 0°C in March. The above average precipitation in the winter likely resulted in the well-recorded event in the early winter or spring.

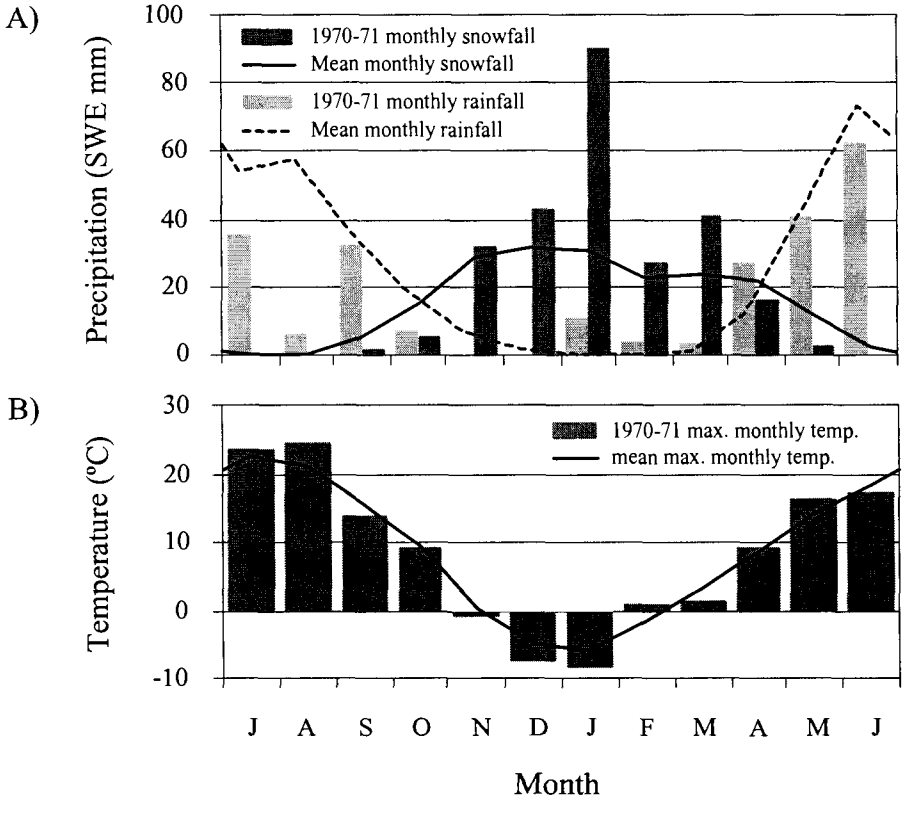

Figure 5.13 (A) Monthly snowfall and rainfall (B) maximum monthly temperatures at Agassiz, BC.

5.5.2 Historical Activity

Air photographs taken of Spoon Lake SAIL before and after the 1989-90 (most well-recorded) snow avalanche event were compared (Figure 5.14). The SAIL shape and size was maintained between 1961-1993. No apparent change in the avalanche track is observed, and vegetation on the track and in the forested area behind the SAIL appear relatively unchanged.

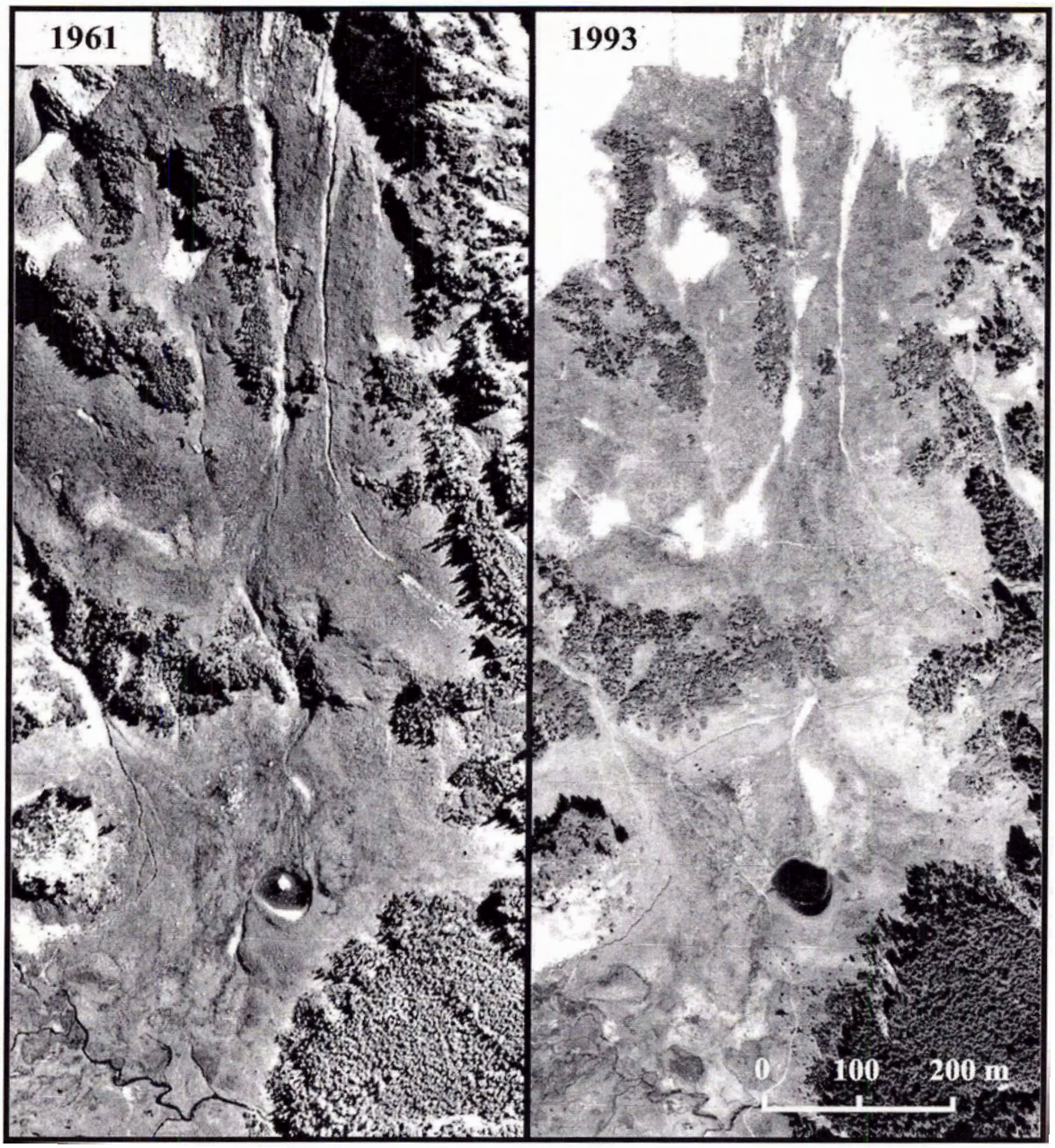

Figure 5.14 (A) Air photograph taken in 1961 (BC4016 No.2), (B) Air photograph taken in 1993 (BCB93032 No. 171).

5.5.3 Development of Spoon Lake SAIL

Site characteristics suggest wet, full-depth avalanches are responsible for forming and maintaining Spoon Lake SAIL. Cheam Ridge is subject to moist maritime air masses typically resulting in wet snow avalanches, and the low-lying vegetation (i.e., the grasses growing the track) creates a smooth sliding surface resulting in full-depth avalanches (Luckman 1977a, Armstrong 1986). Snow avalanches that maintain the SAIL likely occur in the early winter and/or during the spring when the snowpack at the base of the track is not too deep to be excavated. Although the ridge is primarily composed of fine sediments, high-magnitude snow avalanches at this site have the ability to move boulders estimated to be $\leq$ 1060 kg.

The position of the snow avalanche starting zone at Spoon Lake SAIL is not well-defined. A bedrock outcrop on the track creates a jump and suggests that snow avalanches may be airborne for approximately 130 vertical m, before plunging into the SAIL. Upon re-establishing contact, the avalanche impact force moves excavated sediment radially from the impact area (Smith *et al.* 1994). Maximum theoretical impact pressures for wet, airborne avalanches at Spoon Lake SAIL range between 5.9 to 6.9 MPa (assuming $\theta = 60^{\circ}$). A resistant geologic feature (e.g., relic moraine or bedrock ridge) appears to be restricting water drainage and trapping sediments, creating a bog at approximately 1860 m asl (Spoon Lake SAIL elevation). This resistant feature likely initially restricted or trapped snow avalanche flow from both avalanche tracks that converge at the SAIL.

The development of horizon 1, the buried organic layer, and horizon 2 in the SAIL ridge indicates that the SAIL has been stable for some time. Sediment samples collected from the SAIL pool bottom and on the remnant snowpack on the SAIL pool in the summer of 2002, both consisted of approximately 80% fines and 20% coarse sediments, confirming that snow avalanches excavate the pool depositing sediment on the SAIL ridge. The 2002 spring snow avalanche excavated sediment from the SAIL pool and killed 2 trees sampled on the remnant snowpack on the SAIL pool. This 2002 snow avalanche along with the number of well-recorded snow avalanche events in the past 50 years suggests that snow avalanches with impact pressures sufficient to excavate Spoon

Lake SAIL pool occur more frequently than once every 50-150 years as suggested by Smith *et al.* 1994.

CHAPTER 6: PEYTO LAKE SAIL

6.1 SITE DESCRIPTION AND GEOMORPHOLOGY

Peyto Lake SAIL is located in the Waputik Range of the Park Ranges, on the leeside of the southern Canadian Rocky Mountains, in northern Banff National Park. The SAIL (1860 m asl) is situated below the east face of Caldron Peak (3050 m asl), located at the southwest end of Peyto Lake, approximately 1.5 km downvalley of the maximum extent of the LIA moraines at Peyto Glacier (Figure 6.1). Caldron Mountain is composed of fine-grained sedimentary rocks (i.e., siltstone, mudstone, sandstone), thickly-bedded with carbonate rocks (i.e., limestone and dolostone) (AGS 1999). The more resistant carbonate bedrock creates cliffs; whereas, the less resistant siltstones, mudstones, and sandstones produce low gradient slopes abundantly covered with weathered rock debris. The pronounced strike and dip of the bedding is northwest, approximately 30° southwest (AGS 1999). Monthly air temperatures at the nearest long-term weather station 110 km

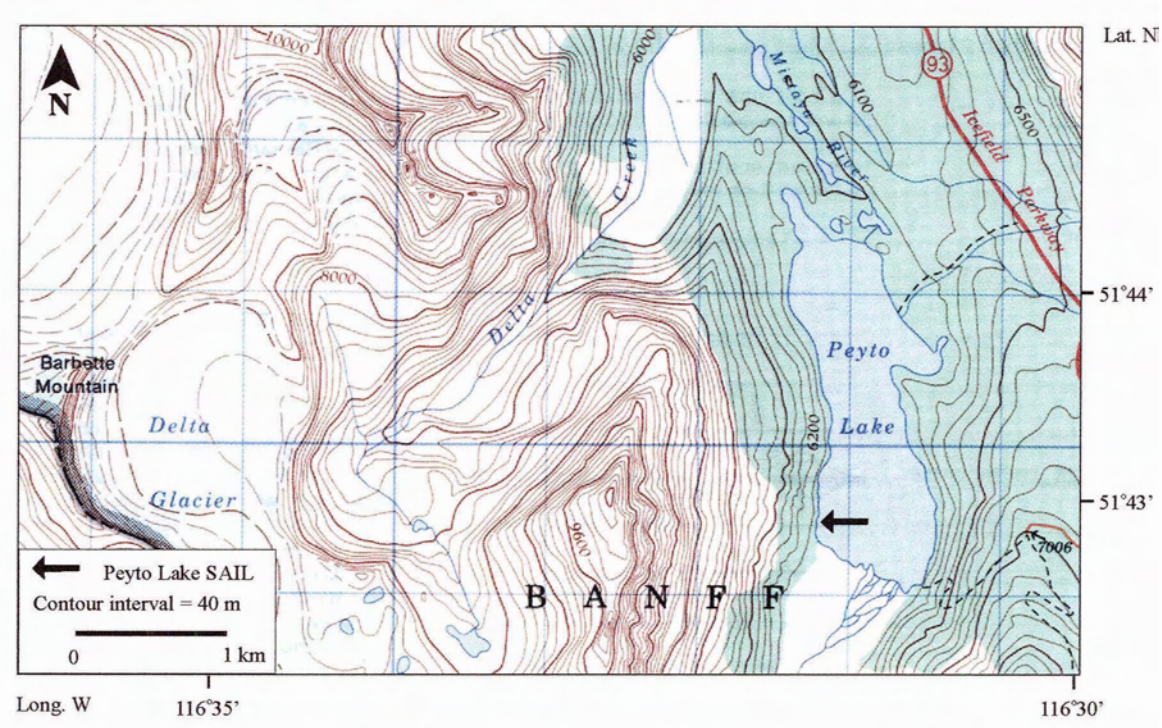

Figure 6.1 Peyto Lake SAIL study site location (NTS map sheet 82N/10, 1:50,000).

southeast at Banff (1380 m asl; Meteorological Service of Canada 2001) average (1896-1995) 2.4°C (monthly maximum 26.6°C and minimum -32.6°C). The average total annual precipitation was 509.8 mm/yr (monthly maximum 195.4 mm), and average total annual snowfall SWE was 196 mm/yr (monthly maximum 143.6 mm).

The Peyto Lake SAIL pool is situated with its long axis perpendicular to the avalanche track. The pool is 50 m long and 32 m wide, giving it a width:length ratio of 1:1.5 (Table 6.1, Figure 6.2). The pool is roughly elliptical-shape as a result of sediment deposition and the establishment of sedges around the perimeter of the pool. The maximum depth of the pool is 2 m, which is located in the centre of the pool. The estimated volume of water in the pool is 1,300 m^3. The water level of the Peyto Lake SAIL pool is maintained by snowmelt and runoff from upslope and the SAIL.

Table 6.1 Summary of Peyto Lake SAIL site geomorphology. *Italics* represent estimated measurements.

Track Morphology	
Longitudinal profile	convex
Morphology of track	chute / fall
Confined / unconfined	both
Track Dimensions	
Slope of track (°)	16-80
Length of track (m)	*630* (430)
Maximum fall (m)	*350* (215)
Width of track (m)	50
Pool Dimensions	
Length (m)	50
Width (m)	32
Width to length ratio	1.5
Maximum depth (m)	2
Approximate volume (m^3)	*1,300*
Ridge Dimensions	
Maximum proximal slope height (m)	1.5
Maximum distal slope height (m)	5.5
Maximum width (m)	34
Mean proximal slope angle (°)	11
Mean distal slope angle (°)	19
Volume above water (m^3)	*6,300*
Entire volume (m^3)	*26,000*

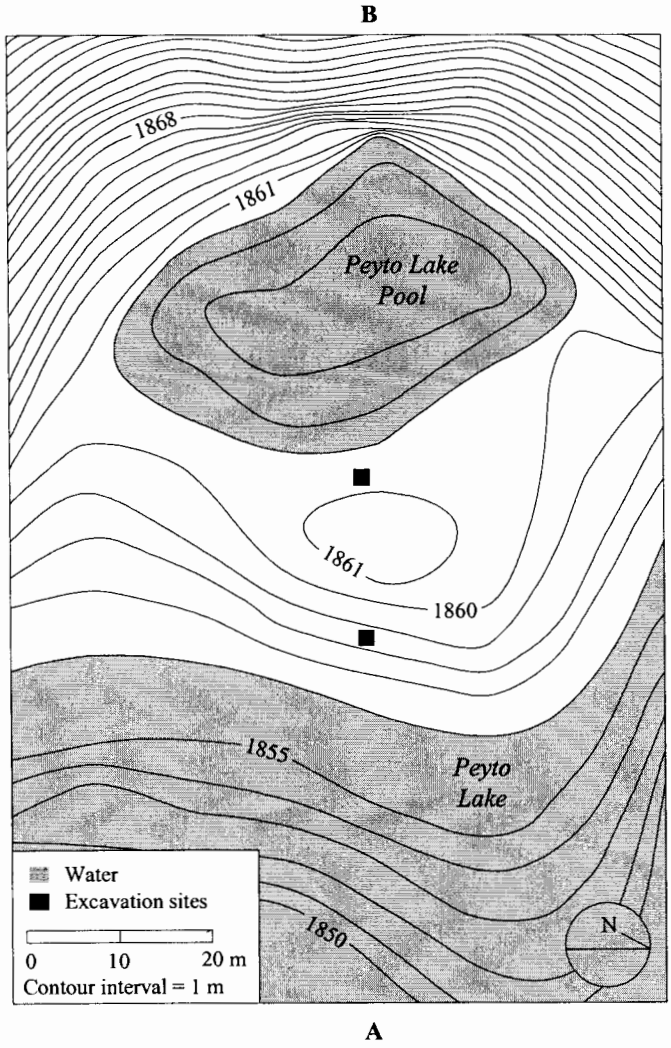

Figure 6.2 Contour map of Peyto Lake SAIL. A-B illustrate transect shown in Figure 6.3.

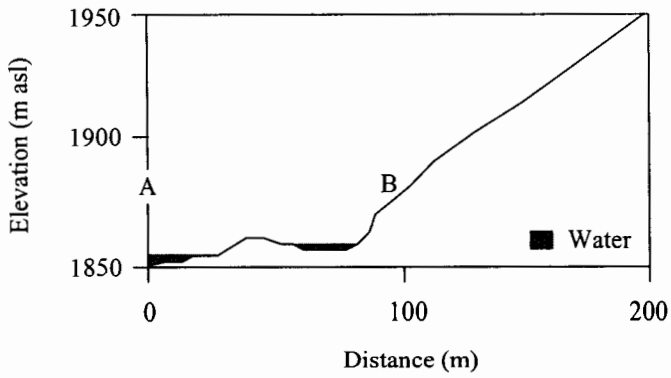

Figure 6.3 Longitudinal profile of Peyto Lake SAIL and lower portion of the avalanche track. A-B illustrate transect shown in Figure 6.2.

The SAIL ridge is 26-34 m wide, rises 1.5 m above the pool water level and 5.5 m above the water level of Peyto Lake (Table 6.1, Figure 6.3). At its highest point, the proximal slope angle is 11° and the distal slope angle is 19°. The SAIL ridge is composed of unconsolidated fine sediments with a few cobbles (cm) and boulders (m). The estimated volume of the SAIL ridge protruding above the pool and lake level is 6,300 m^3; whereas, the estimated volume of the entire SAIL including above and below the water level was 26,000 m^3. The ridge is vegetated by a mixed assemblage of arctic lupine (*L. arcticus*), black swamp gooseberry (*Ribes lacustre*), cinqufoil (*Potentilla sp.*), common red paintbrush (*Castilleja miniata*), cow parsnip (*H. lanatum*), Engelmann spruce saplings (*Picea engelmannii*), fireweed (*E. angustifolium*), juniper (*Juniperus communis*), roses (*Rosa sp.*), soapberries (*Shepherdia canadensis*), subalpine fir saplings (*A. lasiocarpa*), timothy grass (*Phleum pratense*), willow (*Salix sp.*), and vetch (*Vicia sp.*). Due to extensive vegetation cover, few cobbles and boulders are exposed on the ridge surface (Figure 6.4).

Peyto Lake SAIL is located at the base of a convex avalanche track (Table 6.1, Figure 6.5). The upper portion of the track is unconfined and terminates in a triangular-shaped catchment area at 2030-2080 m asl (100 m wide at 2080 m asl), below which the avalanche track is approximately 50 m wide (Figure 6.6). The lower, shallowly confined portion of the track has a chute morphology, except at the immediate base of the track where a 10 m cliff has a fall morphology (Figure 6.3). The latter portion of the track is primarily vegetated by Engelmann spruce (*P. engelmannii*) and subalpine fir (*A. lasiocarpa*) saplings. Scarred mature Engelmann spruce and subalpine fir trees situated on the periphery of the SAIL and the lower portion of the track delineate the boundaries of major avalanche events (Figure 6.7). The avalanche track immediately south of the SAIL track has an abundant sediment supply at the base of the track, and a relatively consistent slope angle of 20° (Figure 6.5, 6.6).

Figure 6.4 Overview of Peyto Lake SAIL. (Photograph taken August 25, 2002)

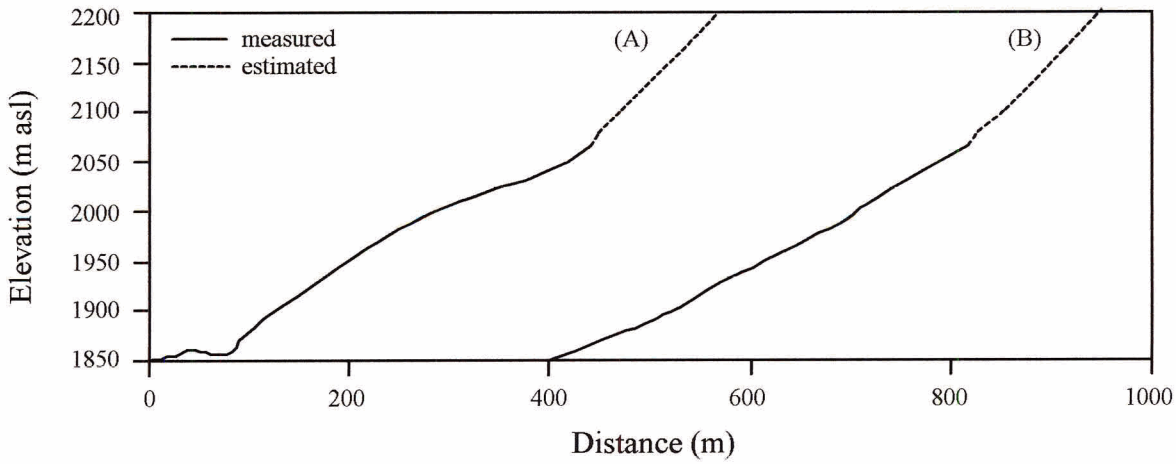

Figure 6.5 Avalanche track profiles of Peyto Lake SAIL (A) and adjacent track (B). See Figure 6.7 for location.

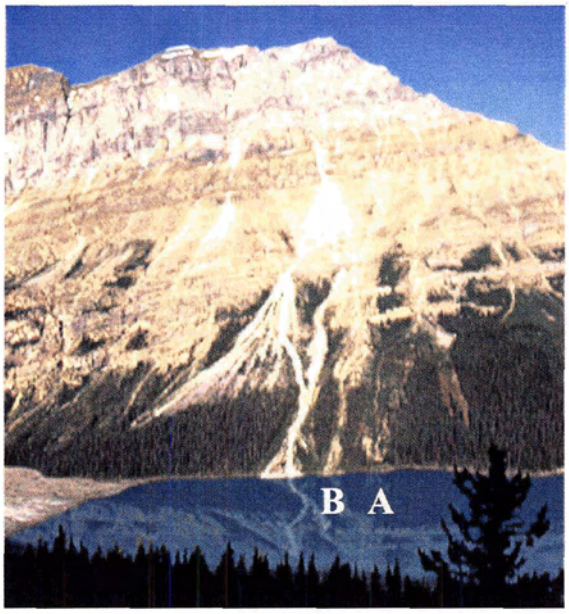

Figure 6.6 East side of Caldron Peak. (A) Peyto Lake SAIL avalanche track, and (B) adjacent track. (Photograph taken August 25, 2002)

Figure 6.7 Peyto Lake SAIL and lower portion of the avalanche track. (Photograph taken August 25, 2002)

6.2 DENDROCHRONOLOGY

Wood samples collected from Peyto Lake SAIL were a mixture of Engelmann spruce, subalpine fir, and willow. The samples collected included 23 cross-sections, 9 cores and 8 wedges, totaling 40 trees (Table 6.2). Of these samples, 18 were collected from the avalanche track, 8 were collected from the SAIL ridge, 10 were collected from the periphery of the SAIL, and 4 were collected from the SAIL pool.

Table 6.2 Wood samples collected from Peyto Lake SAIL.

No.	Sample No.	Species	Sample Type	Living	Duration (yrs)	Range
Avalanche Track						
1	PL02-820	Engelmann spruce	cross section	Y	51	1952-2002
2	PL02-821	Engelmann spruce	cross section	Y	52	1951-2002
3	PL02-822	subalpine fir	cross section	Y	46	1957-2002
4	PL02-823	subalpine fir	cross section	Y	68	1935-2002
5	PL02-824	subalpine fir	cross section	Y	73	1930-2002
6	PL02-825	Engelmann spruce	cross section	Y	34	1969-2002

Continued...

Table 6.2 Continued...

7	PL02-826	subalpine fir	cross section	Y	78	1925-2002
8	PL02-827	subalpine fir	cross section	Y	32	1971-2002
9	PL02-828	subalpine fir	cross section	Y	31	1972-2002
10	PL02-829	Engelmann spruce	cross section	Y	55	1948-2002
11	PL02-830	subalpine fir	cross section	Y	55	1948-2002
12	PL02-831	Engelmann spruce	cross section	Y	63	1940-2002
13	PL02-402	subalpine fir	core	Y	>85	1918-2002
14	PL02-403	subalpine fir	core	Y	>121	1882-2002
15	PL02-404	subalpine fir	core	Y	>39	1964-2002
16	PL02-901	Engelmann spruce	core	Y	51	1952-2002
17	PL02-902	Engelmann spruce	core	Y	>118	1885-2002
18	PL02-903	Engelmann spruce	core	Y	>170	1833-2002
SAIL Ridge						
1	PL02-813	willow	cross section	Y	19	1984-2002
2	PL02-814	willow	cross section	Y	26	1977-2002
3	PL02-815	willow	cross section	Y	18	1985-2002
4	PL02-801	Engelmann spruce	cross section	Y	101	1902-2002
5	PL02-802	Engelmann spruce	cross section	N	43	-
6	PL02-807	subalpine fir	cross section	N	66	1905-1970
7	PL02-808	Engelmann spruce	cross section	N	109	1863-1971
8	PL02-401	subalpine fir	core	Y	26	1977-2002
SAIL Periphery						
1	PL02-904	Engelmann spruce	core	Y	>112	1891-2002
2	PL02-905	Engelmann spruce	core	Y	>121	1882-2002
3	PL02-809	Engelmann spruce	wedge	Y	43	1960-2002
4	PL02-810	Engelmann spruce	wedge	Y	43	1960-2002
5	PL02-811	Engelmann spruce	wedge	Y	43	1960-2002
6	PL02-812	Engelmann spruce	wedge	Y	43	1960-2002
7	PL02-816	Engelmann spruce	wedge	Y	43	1960-2002
8	PL02-817	Engelmann spruce	wedge	Y	43	1960-2002
9	PL02-818	Engelmann spruce	wedge	Y	43	1960-2002
10	PL02-819	Engelmann spruce	wedge	Y	43	1960-2002
SAIL Pool						
1	PL02-803	Engelmann spruce	cross section	N	92	1879-1970
2	PL02-804	Engelmann spruce	cross section	N	63	1908-1970
3	PL02-805	Engelmann spruce	cross section	N	90	1881-1970
4	PL02-806	Engelmann spruce	cross section	N	74	1878-1951

Cross-sections and cores were collected from living trees on the *avalanche track*. The cross-sections (n = 12) were sampled from the base of the avalanche track (1860 m asl) upward to 2000 m asl, where the size of the trees noticeably decreased. These cross-sections were collected from the largest sapling trees within the delineated avalanche

track to determine age of establishment. The saplings sampled ranged in age from 31 to 78 years, and in height from 1.5 to 3.5 m. The trees cored (n = 6) ranged in age from >39 to >170 years, and in height from 3 to 11 m. Of these trees, 5 were heavily masticated on the upslope side, and 2 had multiple leaders. Trees PL02-902 and PL02-903 were the largest trees (11 m and 9 m in height), and were located mid-track at an approximate elevation of 1950 m asl (90 vertical m above the SAIL).

Cross-sections were collected from living and avalanche-killed trees *on and along the periphery of the SAIL*. Cross-sections PL02-803 to PL02-806 were sampled from detrital trees floating in the SAIL pool (Figure 6.8). Since most of the detrital wood on the ridge was rotten, only 3 cross-sections (PL02-802, PL02-807, and PL02-808) were collected from avalanche-killed trees. Cross-sections (PL02-813, PL02-814, and PL02-815) were sampled from the living willow shrub; the oldest sample was 26 years old. The age of the largest sapling cored on the ridge (PL02-401) and was 26 years old. Cross-section PL02-801 was sampled from a 101 years old Engelmann spruce tree, and showed evidence of abrupt reaction wood in 1971 and a severe scar in 1975-76.

Cores and wedges were collected from mature Engelmann spruce trees on the periphery of the SAIL. The cores were >112 and >121 years old since the samples did not include the pith. The wedges were sampled from 7 trees situated on the periphery of the SAIL ridge, and 1 tree (PL02-819) situated on the periphery at the immediate base of the avalanche track. All eight wedges had an obvious scar in 1970-71. Wedge PL02-819 also had a second scar in 1985-86. Approximately 30 rotten avalanche-killed trees were located within a 10 m radius on the avalanche trackside of PL02-819 (Figure 6.9). These detrital boles were pointed in the direction of avalanche flow, and were likely killed in the 1970-71 event.

Figure 6.8 Avalanche-killed trees in Peyto Lake SAIL pool. (Photograph taken August 25, 2002)

Figure 6.9 Approximately 30 avalanche-killed trees pointing downslope in the direction of avalanche flow. (Photograph taken August 25, 2002)

Cross-Dating Avalanche-Killed Trees

Two Engelmann spruce chronologies collected near Peyto Lake by Schweingruber (1983) obtained from the International Tree-Ring Data Bank (ITRDB) (Grissino-Mayer and Fritts 1997) and Carter *et al.* (1999), were used to cross-date the avalanche-killed trees (Table 6.3). The avalanche-killed trees PL02-803 to PL02-808 cross-dated using COFECHA (Table 6.4). Of the 7 cross-sections collected, 1 did not cross date.

Table 6.3 Living tree-ring chronologies used to date detritus wood from Peyto Lake SAIL.

Attribute	Chronology 1	Chronology 2
Source	Schweingruber (1983)	Carter *et al.* (1999)
Species	Engelmann spruce	Engelmann spruce
Site Characteristics		
Location	Peyto Lake	Hilda Creek
Latitude	51°45'N	52°11'30"N
Longitude	116°13'W	117°08'30"W
Elevation	2050	2075
Series Statistics		
Number of Cores	26	16
Series Correlation	0.721	0.514
Mean Sensitivity	0.187	0.184
Autocorrelation	0.814	0.816
Length (years)	350	413
Range	1634-1983	1586-1998

Table 6.4 Detrital wood cross-dating statistics (ES = Engelmann spruce, SF = subalpine fir).

Sample No.	Sp.	Cross-Dated Interval (yrs)	Bark	Continuous Outer Ring	Cross-Dated with	Correlation of Path			
						A	B	C	D
PL02-805	ES	1881-1970	N	N	Schweingruber (1983)	0.424	0.466	-	-
					PL02-801	0.491	0.532	-	-
PL02-808	ES	1863-1971	Y	Y	PL02-801/805	0.744	0.641	0.656	0.639
PL02-803	ES	1879-1970	N	N	PL02-801/805/808	0.521	0.504	0.502	0.536
PL02-806	ES	1878-1951	N	N	PL02-801/803/805/808	0.640	0.651	0.516	0.650
PL02-804	ES	1908-1970	Y	Y	PL02-805	0.416	0.496	0.481	-
PL02-807	SF	1905-1970	N	Y	Carter *et al.* (1999)	0.553	0.405	0.465	-

Note: PL02-805 cross-dated to Schweingruber's (1983) living Engelmann spruce chronology and PL02-801. PL02-808 cross-dated to the PL02-801/805 chronology. PL02-803 cross-dated to the PL02-801/805/808 chronology. PL02-806 cross-dated to the PL02-801/803/805/808 chronology. PL02-804 only cross-dated to PL02-805, and PL02-807 cross-dated to Carter *et al.*'s (1999) living Engelmann spruce chronology.

Dendrochronology Disturbance Results

High-magnitude snow avalanche events at Peyto Lake SAIL were determined using the ERI of the scars, reaction wood, and abrupt ring changes, along with the age of the trees established on the track and ridge, and dates of the avalanche-killed trees (Figure 6.10). Since most detrital wood was rotten, and episodic snow avalanches remove evidence of previous events, only the most recent (approximately the last 30 years) could be reconstructed. The most well-recorded snow avalanche event in the samples collected was in 1970-71, having ERI's ≥30% for impact scars, reaction wood, and narrow rings. The age of the oldest trees (PL02-814 and PL02-401) growing on the ridge were 26 years. An ecesis of 6 years would date these trees to the 1970-71 avalanche event, with 4 of 7 avalanche-killed trees date to this event.

Snow avalanche events in 1985-86 and 1990-91 had ERI's greater than 20% for both reaction wood and narrow rings, but no evidence of impact scars, establishment of trees on the track or ridge, or tree kill dates. Other events recorded in the ERI were 1946-47, 1964-65, and 1975-76. Reaction wood and narrow ring ERI's were ≥10% in these years. Based on the establishment age of 6 trees (PL02-403, 902, 905, 803, 805, and 806), there appears to have been large avalanche event prior to the late-1870's.

The recurrence interval of high-magnitude events could not be calculated since there is only one record of this type of event (1970-71). The recurrence interval (calculated using data between 1970-2002) of avalanche events having two of three ERI's > 10% at this site is 8.2 years. The ERI's post-dating the 1970-71 event suggest that lower-magnitude avalanche events occur often at this site. The age of the detrital wood and living trees at this site implies some stability of the SAIL and avalanche track.

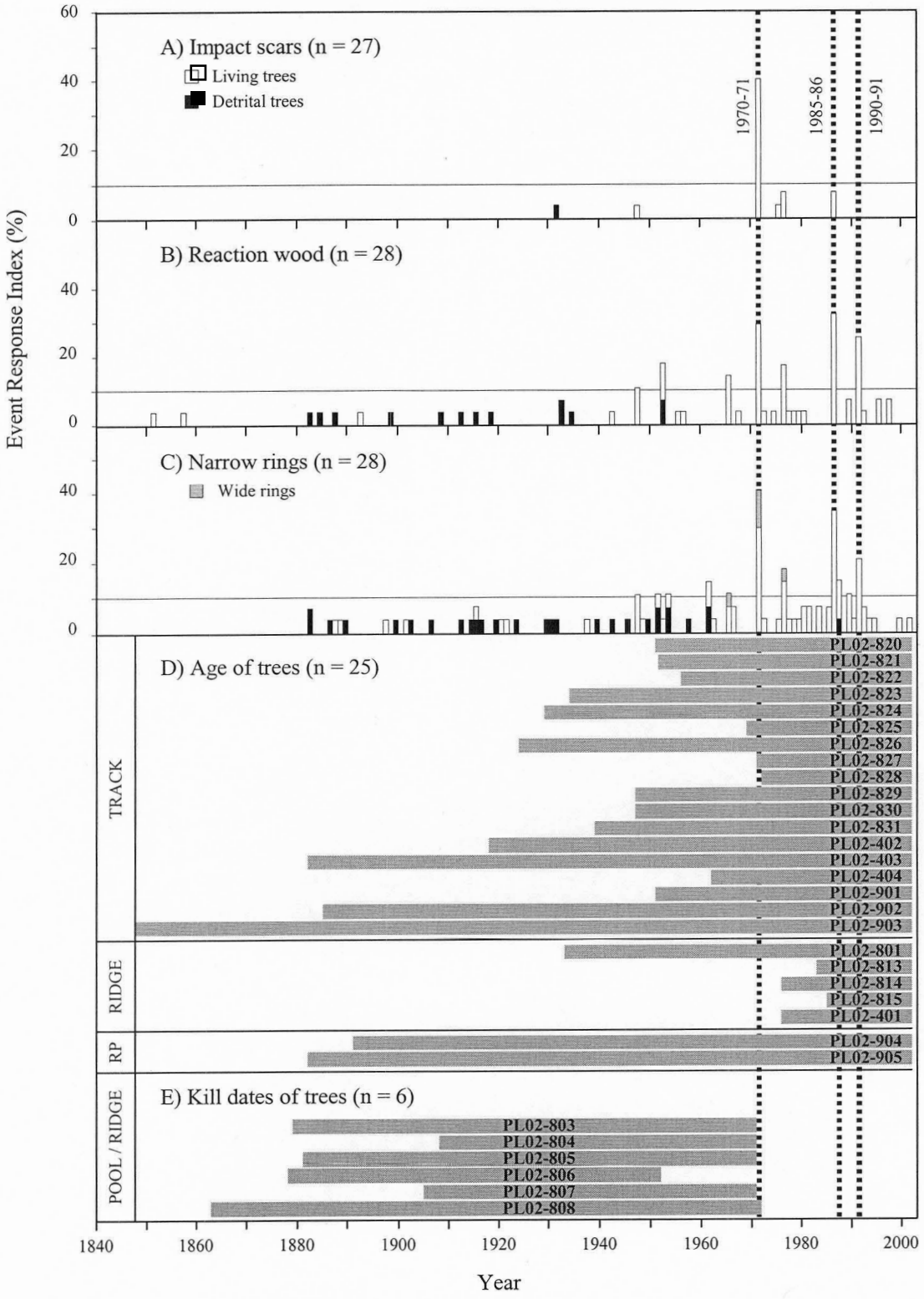

Figure 6.10 Tree event response index of (A) scars, (B) reaction wood and (C) narrow rings. (D) Age of trees and (E) kill dates of trees. Vertical lines illustrate well-recorded snow avalanche events using dendrochronology.

6.3 LICHENOMETRY

Lichen measurements of 14 *R. geographicum* were taken from two boulders on the SAIL ridge (Table 6.5). Lichen 1 to 4 were measured on a boulder situated on the crest of the ridge approximately 15 m north of the highest portion of the ridge; lichen 5 to 14 were measured on a boulder located on the distal slope of the ridge approximately 5 m south of the highest portion of the ridge. Lichen age was determined using the Cavell-Tonquin *R. geographicum* curve developed by Luckman (1977b). The lichen measured at Peyto Lake SAIL was estimated to range in age between 12 and 24 years, indicating establishment from 1978 to 1990 (Figure 6.11). The number of *R. geographicum* measured at this site (n = 14) is a reflection of the calcareous substrate and the limited number of boulders present on the SAIL ridge. Although the number of lichen at the site was limited, the lichen age-frequency diagram peaked at 1981.

Table 6.5 *R. geographicum* measurements from Peyto Lake SAIL ridge.

Lichen	A-axis (mm)	B-axis (mm)	Age of Largest Diameter (yrs)
1	8.2	5.4	19.5
2	5.1	4	12.1
3	5.9	4.7	14
4	5.9	5.6	14
5	8.7	8.2	20.7
6	10.2	9	24.3
7	8.9	7.5	21.2
8	8.6	7.6	20.5
9	7.3	6.1	17.4
10	8.1	6.6	19.3
11	9.1	7.8	21.7
12	8.9	7.8	21.2
13	8.6	7	20.5
14	7.5	7.5	17.9

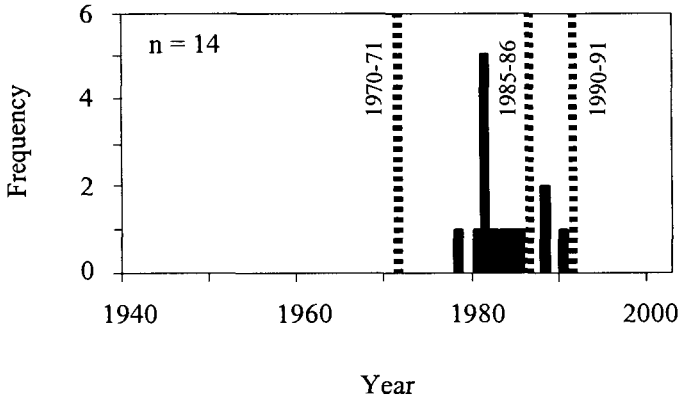

Figure 6.11 Age-frequency diagram of the establishment of *R. geographicum* on Peyto Lake SAIL. Vertical lines illustrate well-recorded snow avalanche events using dendrochronology.

6.4 GRAIN-SIZE ANALYSIS

Pits were dug on the distal and proximal slopes of Peyto Lake SAIL ridge (Figure 6.7). The same stratigraphy was observed in both pits, and consisted of horizon 1 which extended from the vegetated surface of the ridge to a depth of 60 cm, and horizon 2 which extended below 60 cm (Figure 6.12). A distinct thin organic layer, approximately 1 cm width, separated horizon 1 and 2.

Samples were collected from horizon 1 and 2 on the distal slope of the SAIL ridge. Horizon 1 consisted of 46% fine sediment and 54% coarse sediment; and the horizon 2 consists of 56% fine sediment and 44% coarse sediment (Figure 6.13). The sediment samples collected were to be representative of the ridge stratigraphy, but since the sample size was small (between 350-500 g), sediment sizes greater than 64 mm (cobble size) were not included. However, few sediments larger than 64 mm were encountered when digging the excavation pits.

A total of 9 boulders (size > 256 mm) exposed on the surface of the SAIL were measured (Table 6.6). The largest boulder measured (boulder 7) had an approximate weight of 1,007 kg. It was located on the distal slope of the ridge, approximately 10 m south of the highest part of the ridge, and 5 m from Peyto Lake.

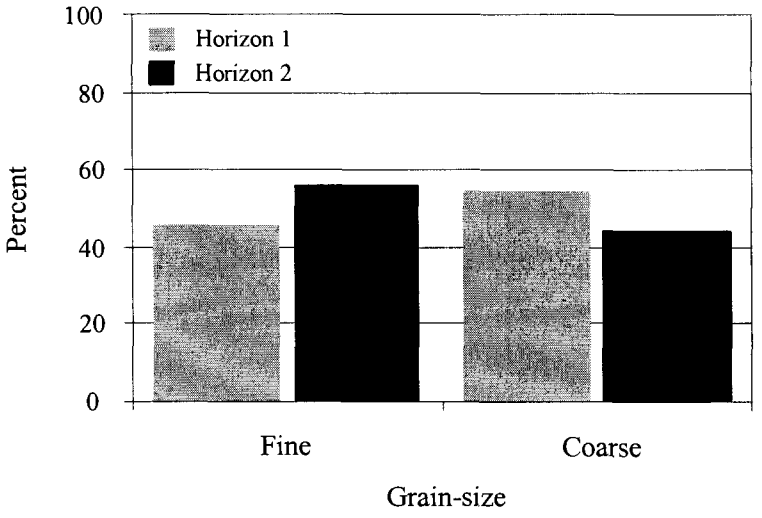

Figure 6.12 Percentage of fine and coarse sediment in horizon 1 and 2 on the distal slope of Peyto Lake SAIL ridge.

Table 6.6 Measurements, mass, and locations of boulders situated on Peyto Lake SAIL ridge (C = crest, D = distal, * = partially buried boulders).

No.	A-axis (m)	B-axis (m)	C-axis (m)	Volume (m^3)	Mass (kg)	Location
1	1.0	0.5	0.5	0.250	663	C
2	0.4	0.3	0.2	0.024	64	C*
3	0.7	0.4	0.2	0.056	148	D
4	0.4	0.2	0.4	0.028	74	D*
5	0.4	0.4	0.2	0.021	56	D*
6	0.5	0.2	0.4	0.030	80	D
7	1.0	1.0	0.4	0.380	1007	D
8	0.7	0.7	0.73	0.358	948	D*
9	1.0	0.6	0.35	0.210	557	D

6.5 DISCUSSION

The most well-recorded snow avalanche occurred in the winter of 1970-71, when many of the mature trees on the SAIL periphery were scarred. Based on the age and size of the vegetation present on the track, this avalanche was most likely not full-depth. Explanations for the persistence of a well-vegetated avalanche track at this site include: a) no full-depth avalanches occur and trees >10 cm in diameter break during high-

magnitude avalanches, b) the track has not been denuded since the last full-depth avalanche, or c) a combination of a and b.

The calcareous rock type and the presence of few cobbles and boulders on the SAIL ridge inhibit lichen establishment at this site. The lichen age-frequency distribution suggests an avalanche event in the late-1970's. Due to the way in which the Cavell-Tonquin *R. geographicum* curve was constructed, it likely underestimates the age of young lichen (e.g., those measured). If the boulders, colonized by lichen measured, were deposited during the 1970-71 event, lichenometry supports the dendrochronologic evidence.

6.5.1 Weather in Winter of 1970-71

The weather data used to gain an understanding of the temperature and snowfall conditions at Peyto Lake SAIL during the winter of 1970-71 was measured at the Banff weather station located 110 km southeast of Peyto Lake SAIL. Although there is a 480 m difference in elevation between the sites, the data is used to illustrate trends in the local weather conditions. Monthly snowfall SWE, rainfall and maximum monthly temperature (°C) from July 1970 to June 1971 was graphed with mean monthly snowfall, rainfall and mean maximum monthly temperatures (1896-1995) (Figure 6.14).

January exhibited 3 times the mean monthly snowfall (January mean is 31.1 SWE mm), and March exhibited nearly 2 times the monthly snowfall (March monthly mean is 23.9 SWE mm). The other months exhibited near normal mean monthly snowfall. January, February and April received above average rainfall. September through April the maximum monthly temperatures were below the mean maximum monthly temperature, except during February where the maximum monthly temperature was 0.7°C (2.1°C above the mean February temperature). Using the moist adiabatic lapse rate (-6.5°C/km), maximum monthly temperatures in the starting zone were likely well below 0°C until April. Theories of weather conditions to produce the well-recorded avalanche event in the winter of 1970-71 include: a) the well above average mid-winter snowfall and cold temperature resulting in a dry mid-winter surface snow avalanche, and b) the

above average March snowfall and warm April temperatures resulting in a wet, spring surface snow avalanche.

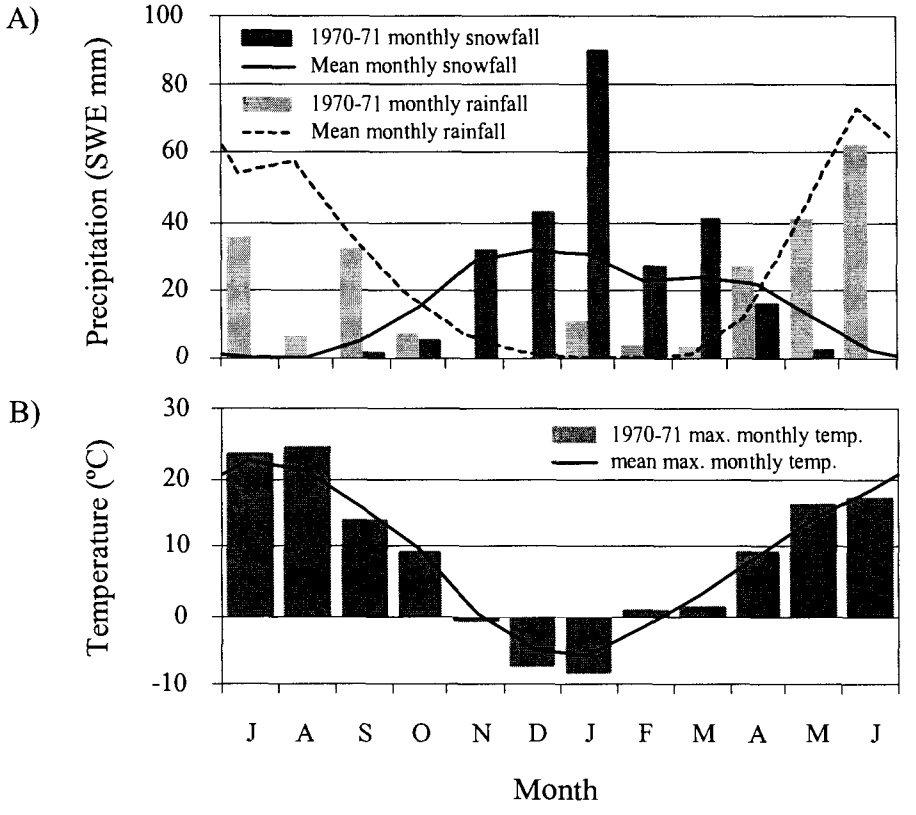

Figure 6.13 (A) monthly snowfall (B) maximum monthly temperatures at Peyto Lake SAIL.

6.5.2 Historical Activity

Air photographs taken of Peyto Lake SAIL before and after the 1970-71 (most well-recorded) snow avalanche event were compared (Figure 6.15). Due to the poor resolution of the 1952 air photograph a detailed examination of the site cannot be made. However, it is evident that the SAIL existed in 1952. In both photographs mature trees delineate the avalanche track and SAIL, and seedlings vegetate the active avalanche track. Also, the track located south of the SAIL track appears to be relatively unchanged.

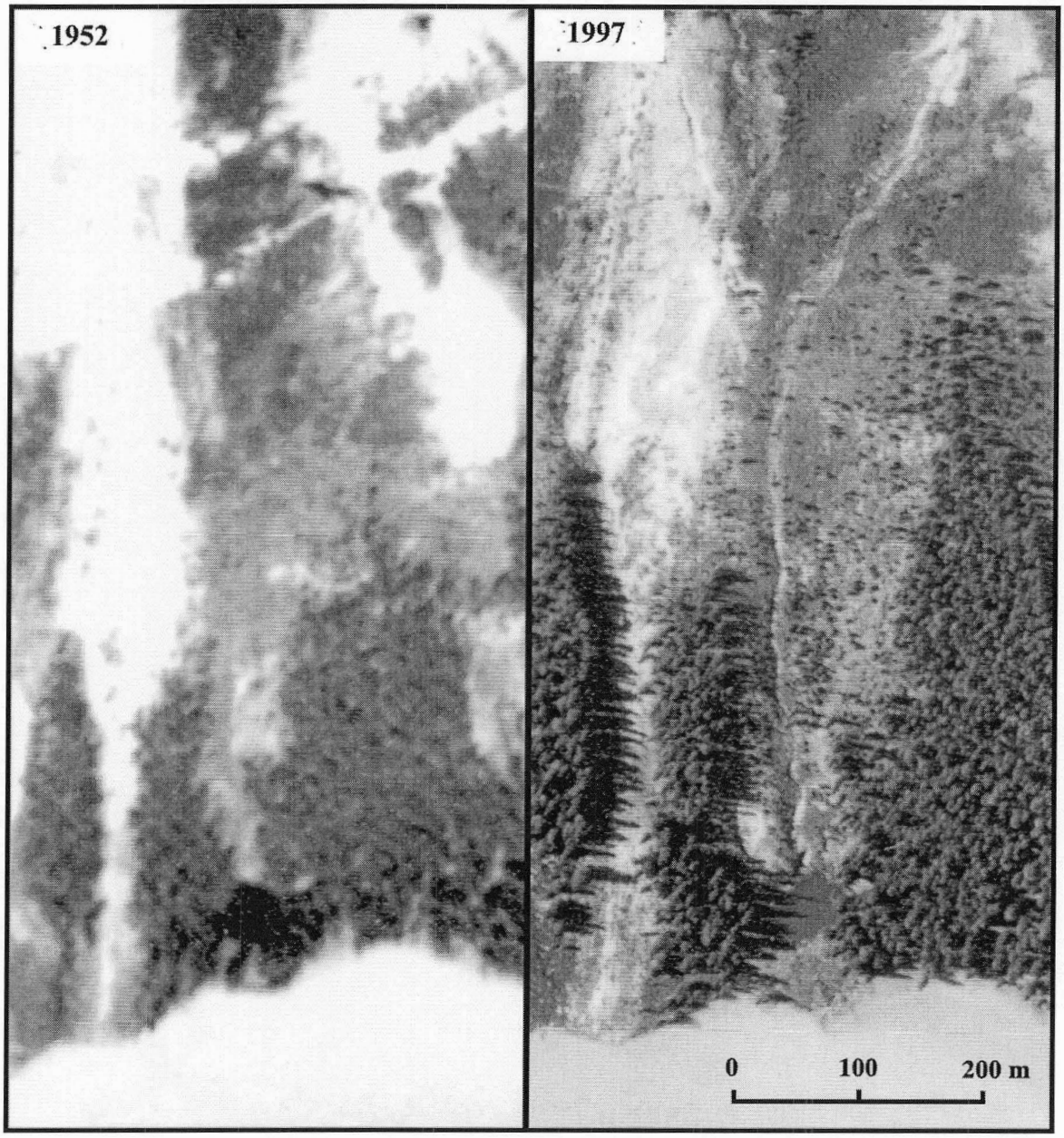

Figure 6.14 (A) Air photograph taken in 1952 (BC1534 No.18), (B) Air photograph taken in 1997 (BCB97053 No.246). Small-scale air photograph taken in 1952 has resulted in poor resolution.

6.5.3 Development of Peyto Lake SAIL

The position of the avalanche starting zone at Peyto Lake SAIL is not known. However, it is likely that snow collects in the triangular-shaped catchment zone (at 2080

m asl) is released, accelerating as it moves down the convex track. Vegetation on the lower track indicates that the 1970-71 snow avalanche was not full-depth on this part of the track. The avalanche likely became airborne as it descended over the cliff at the base of the track, plunging into the SAIL upon re-establishing contact with the ground. Upon re-establishing contact, the explosive avalanche impact force excavated sediment radially from the impact area (Smith *et al.* 1994). Although the ridge is primarily composed of small sediments, high-magnitude snow avalanches at this site have the ability to move boulders estimated to be ≤ 1007 kg. The maximum theoretical impact pressures for dry airborne avalanches at Peyto Lake SAIL range between 2.3 to 3.0 MPa, and for wet, airborne avalanches at range between 6.7 to 7.9 MPa (assuming $\theta = 80°$). The adjacent track (B) likely does not promote SAIL formation because of a smaller snow catchment area (not enough snow to create high impact pressure) and a relatively constant slope gradient.

Based on the site characteristics, Peyto Lake SAIL formed when there was a sufficient sediment accumulation at the base of the avalanche track to enable SAIL formation. The development of the SAIL ridge stratigraphy (including a buried organic layer), and the vegetated surface indicates that the SAIL has been stable for some time.

Fitzharris (1987) identified 1971-72 as a major snow avalanche winter in western Canada. Little evidence of snow avalanching, except for one avalanche-killed tree on the SAIL ridge, was recorded at Peyto Lake SAIL during this winter. The Banff weather station received 65% more snowfall in the winter of 1971-72 than the winter of 1970-71. Based on this one observation, snow avalanches that maintain the SAIL form do not correlate with major regional snow avalanche winters. It is likely that a large amount of snow was present at the base of the track, impeding the excavation of the SAIL pool by airborne snow avalanches. Also, snow drifting at the base of the cliff may have decreased the plunging distance.

CHAPTER 7: SUMMARY AND CONCLUSIONS

7.1 SUMMARY

The three SAIL sites examined share common morphologies: a water-filled bowl-shaped depression distally bounded by an arcuate crescent-shaped ridge, situated obliquely to the avalanche track. The SAIL's were formed in regions having very different climates (maritime, continental), in turn creating different types of snow avalanches. As the recent high-magnitude avalanche occurrences recorded at these sites differ from the sourced avalanche chronology of Fitzharris (1987), it seems likely that the events that maintain SAIL's are related to local weather conditions.

SAIL pool and ridge dimensions were variable between sites. The maximum SAIL ridge width formed opposite the deepest part of the SAIL pool at Peyto Lake SAIL, and likely at Spoon Lake SAIL. The distal slope angle of SAIL ridge is steeper than the proximal angle at Blackhorn and Spoon Lake SAIL's. The water levels of the SAIL pools are all different. The water level of Blackhorn SAIL pool is below the surrounding lake level, Peyto Lake SAIL pool is well above the surrounding lake level, and Spoon Lake SAIL has no adjacent lake.

The SAIL site characteristics support the theoretical SAIL formula, where SAIL formation is a function of the variation in snow avalanche path topography, availability of unconsolidated debris in the impact area, and snow avalanche impact pressures with the ability to physically move the available debris. Snow avalanche path topography determines whether avalanches remain ground-based or become airborne. Ground-based snow avalanches excavate by bulldozing (e.g., Blackhorn SAIL), and airborne snow avalanches excavate by "exploding" upon impact (e.g., Spoon Lake and Peyto Lake SAIL's). The available unconsolidated debris in the impact area ranged in size from fine sediments mixed with pebbles and occasional cobbles and boulders at Spoon Lake and Peyto Lake SAIL's, to a rocky matrix with lots of boulders at Blackhorn SAIL.

Corrected maximum theoretical impact pressures for high-magnitude snow avalanche events that maintain the three SAIL sites ranged from 0.2 to 7.9 MPa. The

high (maximum) values suggest that the corrected impact pressure equation may overestimate impact pressures, since they far exceed destructive impact pressures cited in the literature. The low values imply that impact pressures < 1 MPa may be responsible for SAIL formation and maintenance, which do not support Smith *et al.*'s (1994) hypothesis that impact pressures > 1 MPa maintain SAIL geomorphology.

Evidence of SAIL excavation from the summer of 2002 at Spoon Lake SAIL supports SAIL's development through episodic events, and suggests that excavation occurs more frequently at this site than once every 50-150 years. At Blackhorn and Peyto Lake SAIL's excavation may occur once every 50-150 years. Snow avalanches that supply sediment to the impact area may be different from those that excavate sediment in the impact area. High-magnitude snow avalanches at these SAIL's have the ability to move boulders that have a mass of at least 1000 kg. Although the presence of water at the base on the avalanche track is not an essential ingredient for SAIL formation, two of the sites (Blackhorn and Peyto Lake SAIL) were formed along lakeshores.

Even though the formation of the three distinct SAIL's under study all tell a different story, they all have evidence of long-term development and appear to be, at present, stable features. The distal slope of Blackhorn SAIL ridge is abundantly covered with lichen, and Spoon Lake and Peyto Lake SAIL ridges are well-vegetated and underlain by well-developed strata including a buried organic layer. Evidence of lichen-free cobbles and boulders on SAIL ridges suggests that snow avalanches continue to excavate and maintain SAIL form. Also, the air photographs revealed that the SAIL's remained relatively unchanged after the most well-recorded snow avalanche event.

Using Corner's (1980) SAIL morphology classification, which included tongues, pits, and pools, the sites under study are pits. The three other SAIL's previously studied by Smith *et al.* (1994) in the Canadian Cordillera are pits and share the same common morphology with those in this study (e.g., similar shape and volumetric estimates of sediment in mound). Of the SAIL's studied globally, 17 are tongues, 29 are pits, and 20 are pools. Of the 6 SAIL's studied in the Canadian Cordillera, 4 were located in the Canadian Rockies. The 6 sites in the Canadian Cordillera have all been deglaciated since the retreat of the Wisconsinan glaciation, approximately 10,000 years ago in that they occupy elevations below documented LIA and Holocene glacial moraines. Evidence of

long-term SAIL development and stability suggests that these features have been developing for some time.

7.2 CONCLUSIONS

The goals this study were: 1) to describe the geomorphology at each snow avalanche impact landform site; 2) to document recent high-magnitude snow avalanches at each site and, 3) to explain the development of the snow avalanche impact landforms studied. The geomorphology was successfully described at each site. Dendrochronology and lichenometry proved to be effective techniques in determining recent (approximately 50-100 years) snow avalanche history and landform stability. The most well-recorded avalanche events using dendrochronology was in 1967-68 at Blackhorn SAIL, 1989-90 at Spoon Lake SAIL, and 1970-71 at Peyto Lake SAIL.

The high-magnitude events that maintain the three SAILs are brought about by local weather conditions. Nevertheless, each SAIL is unique and tells a different story. Blackhorn SAIL was interpreted to be an avalanche boulder tongue before evolving into a SAIL. Spoon Lake SAIL was formed as a result of a resistant geologic feature restricting snow avalanche flow in the impact area resulting in excavation. Peyto Lake SAIL formed when there was a sufficient sediment accumulation in the avalanche impact area to enable SAIL formation. Due to limited research conducted in the past, particularly in North America, the findings of this study will provide further insight in to the formation of snow avalanche impact landforms.

The SAIL formula was developed using site characteristics of SAIL's previously studied, and supported by the sites under study. SAIL formation is most likely a function of the variation in topography of the avalanche track, the availability of unconsolidated debris in the impact area, and avalanche impact pressure with the ability to physically move the available debris in the trajectory path of avalanche flow. Track topography influences whether snow avalanches remain ground-based or become airborne. It appears, based on this study, that excavation by ground-based snow avalanches is done by bulldozing debris, and excavation by airborne snow avalanches is done by exploding upon impact. The gentle slope of Blackhorn SAIL track results in ground-based snow

avalanches, and the jump morphology of Spoon Lake SAIL track and fall morphology of Peyto Lake SAIL track result in airborne snow avalanches. Evidence of new material being excavated from the pool and deposited on the SAIL ridge confirms that these features are formed and maintained through episodic high-magnitude snow avalanche events. Excavation involves both erosional and depositional processes. The frequency of snow avalanche events that excavate the SAIL is site specific, and at some sites likely has more frequent avalanches than the 50-150 years suggested by Smith *et al.* (1994). The following evidence suggests long-term SAIL development of the sites under study: dendrogeomorphic dating, lichen coverage, vegetated SAIL ridge, SAIL ridge stratification, and historical air photographs. This evidence supports previous research suggesting development throughout the past few thousand years, and possibly throughout the Holocene.

Limitations of Study:

The main limitations of this study are:

- *Small sample size studied.* The study provided a detailed description of only three SAIL's in the southern Canadian Cordillera. By examining a larger number of SAIL's (e.g., 100) in the Canadian Cordillera, a more systematic analysis of SAIL morphology could be performed. For example, Lee *et al.* (2002) plotted many relationships, such as pool depth vs. pool diameter, pool depth vs. pool diameter ratio, break in slope vs. plunge pool depth, and break in slope vs. diameter ratio, to determine gain a better understanding of submarine plunge pool morphology.
- *Small-scale air photograph limitation.* In looking for of a second study site in the Coast Mountains, the area between Pemberton and Tatla Lake, British Columbia was searched using air photographs and topographic maps. This search was unsuccessful, and was likely a result of the small-scale air photographs making it difficult to identify SAIL's.
- *Geobotanical dating tools were not always successful.* Lichenometry and dendrochronology proved to be useful only for documenting recent snow avalanche events. Due to the lack of lichen at Spoon Lake and Peyto Lake SAIL's,

lichenometry could not be employed. Similarly the lack of dateable organic buried within the SAIL ridges precluded an assessment of long-term SAIL dynamics (e.g., Smith et al. 1994).

- *Difficult to document older snow avalanche events using ERI's.* The limitation of using ERI's as indicators of snow avalanche activity is that more recent snow avalanches can remove evidence of older high-magnitude snow avalanche events, and scarred living trees can heal over showing no obvious signs of damage. Therefore, older high-magnitude snow avalanche events are less likely to be well-recorded, and in turn not identified by the 10% cut-off.

Future Research Considerations:

Further research on SAIL's should focus on:

- *Studying a larger sample size.* Examine a larger number of SAIL's and associated avalanche tracks (e.g., 100) in the Canadian Cordillera to perform a systematic analysis of SAIL morphology. In doing so, trends and relationship in the SAIL's may be revealed. For example, do snow avalanches that move sediment by bulldozing move larger sediments (i.e., boulders) than snow avalanches that move sediment by explosion on impact? Explore past climate vs. present climate to determine site dynamics during the SAIL life.
- *Using large-scale air photographs.* Examine large-scale (e.g., 1:10,000) air photographs and topographic maps when searching for SAIL sites to increase the likelihood of identifying potential sites.
- *Focusing attention of collecting submerged woody detritus* visible on the samples on the bottom of the SAIL pools. Cross-dating of this subfossil material may provide a way to extend the dendrochronological record of snow avalanche activity at the SAIL sites.
- *Thematically grouping SAIL's.* Provided a sufficiently large number of SAIL's can be identified, to determine whether their geomorphology is related to variables such as climate and geology.

- *Using Ground Penetrating Radar (GPR).* Use GPR to determine the composition, stratigraphy, and distribution of sediment on the SAIL ridge. GPR would also likely explain the perched water table observed at some sites.

REFERENCES

Aarseth, I., Lønne, Ø., and O. Giskeødegaard. 1989. Submarine slides in glaciomarine sediments in some western Norwegian fjords. *Marine Geology* **88**: 1-21.

Ahrens, C.D. 1994. *Meteorology Today: An Introduction to Weather, Climate, and the Environment.* West Publishing Company, St. Paul.

Alberta Geologic Survey (AGS). 1999. Geological Map of Alberta; Alberta Geological Survey, Map 236, Scale 1:1,000,000.

Aplin, P.S., and D.J. Hill. 1979. Growth analysis of circular lichen thalli. *Journal of Theoretical Biology* **78**: 347-363.

Armstrong, B.R. 1986. *The Avalanche Book.* Golden, Colorado: Fulcrum Incorporated.

Armstrong, R.L., and B.R. Armstrong. 1987. Snow and avalanche climates of the western United States: a comparison of maritime, intermountain and continental conditions. In *Avalanche Formation, Movement and Effects (proceedings of the Davos Symposium), IAHS Publication* 162, Wallingford: IAHS 281-293.

Ballantyne, C.K. 1989. Avalanche impact landforms on Ben Nevis, Scotland. *Scottish Geographical Magazine* **105**: 38-42.

Benedict, J.B. 1967. Recent glacial history of an alpine area in the Colorado Front Range, USA. 1: Establishing a lichen growth curve. *Journal of Glaciology* **6**: 817-832.

Benedict, J.B. 1985. Arapaho Pass. Glacial geology and archeology at the crest of the Colorado Front Range. *Center for Mountain Archeology Research Report,* 3, Ward, Colorado, 197 p.

Benedict, J.B. 1990. Experiments on lichen growth. I. Seasonal patterns and environmental controls. *Arctic and Alpine Research* **22**: 244-254.

Bernhardt, T. N.D. The Canadian Biodiversity Web Site: Canada's Ecozones. Accessed December 2002. http://www.canadianbiodiversity.mcgill.ca/english/index.htm.

Beschel, R.E. 1973. Lichens as a measure of the age of recent moraines. *Arctic and Alpine Research* **5**: 303-309.

Beschel, R.E., and A. Weidick 1973. Geobotanical and geomorphological reconnaissance in West Greenland, 1961. *Arctic and Alpine Research* **5**: 311-319.

Blikra, L.H., Hole, P.A., and N. Rye. 1989. Skred i Norge. Hurtige massebevegelser og avsetningstyper i alpine områder, Indre Nordfjord. *Norges Geologiske Undersøkelse, Skrifter* **92**: 1-17.

Bone, R.M. 2002. Canada's physical base. *The Regional Geography of Canada* **2**: 42-92.

Bull, W.B., Schlyter, P., and S. Brogaard. 1995. Lichenometric analysis of the Kärkerieppe slush-avalanche fan, Kärkevagge, Sweden. *Geografiska Annaler* **77A**: 231-240.

Bull, W.B., and M.T. Brandon. 1998. Lichen dating of earthquake-generated regional rockfall events, Southern Alps, New Zealand. *GSA Bulletin* **110**: 60-84.

Burrows, C.J., and V.L. Burrows. 1976. Procedures for the study of snow avalanche chronology using growth layers of woody plants. *University of Colorado, Institute of Arctic and Alpine Research, Occasional Paper 23*, 54 p.

Butler, D.R., and Malanson, G.P. 1985. A history of high-magnitude sow avalanches, southern Glacier National Park, Montana, U.S.A. *Mountain Research and Development* **5**: 175-182.

Butler, D.R., and Malanson, G.P., and J.G. Oelfke. 1987. Tree-ring analysis and natural hazard chronologies: minimum sample sizes and index values. *Professional Geographer* **39**: 41-47.

Butler, D.R. 1989. Canadian Landform Examples 11. Subalpine snow avalanche slopes. *Canadian Geographer* **33**: 269-273.

Calkin, P.E., Kaufman, D.S., Przybyl, B.J., Whitford, W.B., and B.J. Peck. 1998. Glacial regimes, periglacial, landforms, and Holocene climate change in the Kigluaik Mountains, Seward Peninsula, Alaska, USA. *Arctic and Alpine Research* **30**: 154-165.

Calkin, P.E., and J.M. Ellis. 1980. A lichenometric dating curve and its application to Holocene glacial studies in the Central Brooks Range, Alaska. *Arctic and Alpine Research* **12**: 245-265.

Calkin, P.E., and J.M. Ellis. 1984. Development and application of a lichenometric dating curve, Brooks Range, Alaska. In *Quaternary Dating Methods*, ed. W.C. Mahaney, Amsterdam: Elsevier, 227-246.

Cameron, W. N.D. Chinooks-Warm West Winds. Accessed November 2002. http://www.mountainnature.com/Climate/Chinook.htm.

Canadian Council on Ecological Areas (CCEA). N.D. Terrestrial Ecozones of Canada. Accessed December 2002. http://www.ccea.org/ecozones/index.html.

Carlson, A.B., Sollid, J.L., and B. Torp. 1983. *Valldal, Kvartaergeologi og geomorfologi* [1:50,000 map sheet 1319IV]. Oslo: Geografisk Institutt, Universitetet i Oslo.

Carrara, P.E. 1979. The determination of snow avalanche frequency through tree-ring analysis and historical records at Ophir, Colorado. *Geological Society of America Bulletin* **90**: 773-780.

Carter, R., LeRoy, S., Nelson, T., Laroque, C.P., and Smith, D.J. 1999. Dendroglaciological investigations at Hilda Creek rock glacier, Banff National Park, Canadian Rocky Mountains. *Géographie physique et Quaternaire* **53**: 365-371.

Cook, E.R. 1985. Program ARSTAN (Version 6.04P).

Cook-Talbot, J.D. 1991. Sorted circles, relative-age dating and palaeoenvironmental reconstruction in an alpine periglacial environment, eastern Jotunheimen, Norway: lichenometric and weathering-based approaches. *The Holocene* **1**: 128-141.

Corner, G.D. 1973. Meteorittkrater i Tromsø. *Ottar* **76**: 13-14.

Corner, G.D. 1975. Rundvatnet-avalanche plunge pool or meteorite impact crater? *Norsk Geografisk Tidsskrift* **29**: 75-76.

Corner, G.D. 1980. Avalanche impact landforms in Troms, North Norway. *Geografiska Annaler* **60**: 1-10.

Daffern, T. 1983. *Avalanche Safety for Skiers and Climbers*. Calgary: Rocky Mountain Books.

Davis, G.H. 1962. Erosional features of snow avalanches, Middle Fork Kings River, California. *U.S. Geological Survey. Professional Paper, 450-D*: D122-D225.

De Quervain, M., and R. Meister. 1987. 50 years of snow profiles on the Weissfluhjoch and relations to the surrounding avalanche activity (1936/37-1985/86). In *Avalanche Formation, Movement and Effects (proceedings of the Davos Symposium)*, ed. B. Salm, and H. Gubler. *IAHS Publication* 162, Wallingford: IAHS 161-181.

De Scally, F.A., and J.S. Gardner. 1989. Evaluation of avalanche-mass determinination approaches: an example from the Himalaya, Pakistan. *Journal of Glaciology* **35**: 248-252.

Elverhøi, A., Norem, H., Anderson, E.S., Dowdeswell, J.A., Fossen, I., Haflidason, H., Kenyon, N.H., Laberg, J.S., King, E.L., Serjrup, H.P., Solheim, A., and T. Vorren. 1997. On the origin and flow behaviour of submarine slides on deep-sea fans along the Norwegian-Barents Sea continental margin. *Geomarine Letters* **17**: 119-125.

Farrar, J.F. 1974. A method for investigating lichen growth rates and succession. *Lichenologist* **6**: 151-155.

Farre, J.A., and W.B.F. Ryan. 1985. 3-D view of erosional scars on U.S. Mid-Atlantic continental margin. *The American Association of Petroleum Geologists Bulletin* **69**: 923-932.

Fitzharris, B.B. 1987. A climatology of major avalanche winters in western Canada. *Atmosphere-Ocean* **25**: 115-136.

Fitzharris, B.B., and I.F. Owens. 1984. Avalanche tarns. *Journal of Glaciology* **30**: 308-312.

Fraser, C. 1978. *Avalanches and Snow Safety.* London: John Murray Publishers Ltd.

Fritts, H.C. 1976. *Tree-Rings and Climate.* London: Academic Press.

Gardner, J. 1970. Geomorphic significance of avalanches in the Lake Louise area, Alberta, Canada. *Arctic and Alpine Research* **2**: 135-144.

Gardner, J. 1983. Observations on erosion by wet snow avalanche, Mount Rae area, Alberta, Canada. *Arctic and Alpine Research* **15**: 271-274.

Gault, D.E., Quaide, W.L., and V.R. Oberbeck. 1968. Impact cratering mechanics and structures. In *Shock Metamorphism of Natural Materials*, ed. B.M. French and N.M. Short, Baltimore: Mono Book Corp. 87-99.

Gellatly, A.F. 1982. Lichenometry as a relative-age dating method in Mount Cook National Park, New Zealand. *New Zealand Journal of Botany* **20**: 343-353.

Glen, D.M. 1974. Tree-ring dating of snow avalanches. *Journal of the Colorado-Wyoming Academy of Sciences* **12**: 46.

Gordon, J.E., and M.J. Sharp. 1983. Lichenometry in dating recent glacial landforms and deposits, southeast Iceland. *Boreas* **12**: 191-200.

Gray, J.T. 1973. Geomorphic effects of avalanches and rockfall on steep mountain slopes in central Yukon Territory. In *Research In Polar And Alpine Geomorphology: Proceedings of the 3rd Guelph Symposium on Geomorphology*, ed. B.D. Fahey, and Thompson, R.D. Norwich: Geo-Abstracts, 107-117.

Grissino-Mayer, H.D., and Fritts, H.C. 1997. The International Tree-Ring Data Bank: and enhanced global database serving the global scientific community. *The Holocene* **7**: 235-238.

Hill, D.J. 1981. The growth of lichens with special reference to the modelling of circular thalli. *Lichenologist* **13**: 265-287.

Hodgson, D.M. 1978. Lichenometric studies of three glaciers in the Yukon Territory of Canada. Unpublished B.Sc. thesis, University of Edinburgh.

Hole, J. 1981. Groper danna av snøskred i Sunnylven og tilgrensande områder på Sunnmøre. Førbels resultat. *Norsk Geografisk Tidsskrift* **35**: 167-172.

Holmes, R.L. 1983. Computer-assisted quality control in tree-ring dating and measurement. *Tree-Ring Bulletin* **43**: 69-78.

Holmes, R.L. 1999. Users Manual for Program COFECHA. *Laboratory of Tree-Ring Research*, University of Arizona, Tucson, 8 p.

Hopfinger, E.J. 1983. Snow avalanche motion and related phenomena. *Annual Reivews Fluid Mechanics* **15**: 47-76.

Huisman, L. 1996. The growth response of a mixed conifer forest to climate at Mt. Cheam, Chilliwack, British Columbia. Unpublished B.Sc. thesis, University of Victoria.

Innes, J.L. 1983. Lichenometric dating of debris flow activity in the Scottish Highlands. *Earth Surface Processes and Landforms* **8**: 579-588.

Innes, J.L. 1985. Lichenometry. *Progress in Physical Geography* **9**: 187-254.

Karlén, W. 1973. Holocene glacier and climatic variations in the Kebnekaise Mountains, Swedish Lapland. *Geografiska Annaler* **55A**: 29-63.

Keylock, C. 1997. Snow avalanches. *Progress in Physical Geography* **21**: 481-500.

Kotyakov, V.M. 1974. Recent work in the U.S.S.R. *Ice* **46**: 2-8.

Kotyakov, V.M., Rzhevskii, B.N., and V.A. Samoilov. 1977. The dynamics of avalanches in the Khibins. *Journal of Glaciology* **19**: 431-439.

Kuriowa, D. 1974. Recent work in Japan. *Ice* **45**: 4-6.

LaChapelle, E. 1966. Avalanche forecasting – a modern synthesis. *International Association of Science Hydrology Publication* **69**: 350-356.

Lands Directorate. 1986. *Terrestrial Ecozones of Canada*, Ecological Land Classification No. 19, 26.

Larocque, S.J., Bernard, H., and L. Filion. 2001. Geomorphic and dendrochronological impacts of slushflows in central Gaspé Peninsula (Québec, Canada). *Geografiska Annaler*: **83A**: 191-201.

Larocque, S.J., and D.J. Smith. *submitted.* Calibrated *Rhizocarpon geographicum* growth curve for the Mount Waddington area, British Columbia Coast Mountains, Canada.

Larocque, S.J., and D.J. Smith. 2003. Little Ice Age glacial activity in the Mt. Waddington area, British Columbia Coast Mountains, Canada. Canadian Journal of Earth Sciences **40**: 1413-1436.

Lang, T.E., and Brown, R.L. 1980. Numerical simulation of snow avalanche impact on structures. *U.S. Department of Agriculture, Forest Service, Research Paper RM-216.*

Lee, S.E, Talling, P.J., Ernst, G.G.J., and A.J. Hogg. 2002. Occurrence and origin of submarine plunge pools at the base of the US continental slope. *Marine Geology* **185**: 363-377.

Liestøl, O. 1974. Avalanche plunge-pool effect. *Norsk Polarinstitutt Arbok1972* 179-181.

Liestøl, O. 1975. Reply. *Norsk Geografisk Tidsskrift* **29**: 76.

Lock, W.W., Andrews, J.T., and P.J. Webber. 1979. A Manual for Lichenometry. *British Geomorphological Research Group, Technical Bulletin no.26 London.*

Luckman, B.H. 1971. The role of snow avalanches in the evolution of alpine talus slopes. In *Slopes, Forms and Process*, Instituted of British Geographers Special Publication **3**: 93-100.

Luckman, B.H. 1977a. The geomorphic activity of snow avalanches. *Geografiska Annaler* **59A**: 31-48.

Luckman, B.H. 1977b. Lichenometric dating of Holocene moraines at Mount Edith Cavell, Jasper, Alberta. *Canadian Journal of Earth Sciences* **14**: 1809-1822.

Luckman, B.H. 1978. Geomorphic work of snow avalanches in the Canadian Rocky Mountains. *Arctic and Alpine Research* **10**: 261-276.

Luckman, B.H. 1996. Dendroglaciology at Peyto Glacier, Alberta, Canada. In *Tree-Rings, Environment, and Humanity*, ed. J.S. Dean, D.M. Meko, and T.W. Swetnam. *Radiocarbon*, Tuscon, 679-688.

Luckman, B.H. 1998. Holocene glacier history of the North American Cordillera. *AMQUA 1998: American Quaternary Association Program and Abstracts of the 15th Biennial Meeting,* Puerto Vellarta, Mexico, 5-7 September 1998, 35p.

Luckman, B.H. 2000. The Little Ice Age in the Canadian Rockies. *Geomorphology* **32**: 357-384.

Luckman, B.H., Matthews, J.A., Smith, D.J., McCarroll, D., and D.P. McCarthy. 1994. Snow-avalanche impact landforms: a brief discussion of terminology. *Arctic and Alpine Research* **26**: 128-129.

Marion, J., Filion, L., and B. Hétu. 1995. The Holocene development of a debris slope in subarctic Québec, Canada. *The Holocene* **5**: 409-419.

Martinelli, M. 1974. *Snow Avalanche Sites: Their Identification and Evaluation.* U.S. Department of Agriculture Information Bulletin 360, 27p.

Martinelli, M. 1986. A test of the avalanche runout equations developed by the Norwegian Geotechnical Institute. *Cold Regions Science and Technology* **13**: 19-33.

Matthews, J.A. 1974. Families of lichenometric dating curves from the Storbreen gletschervorfeld, Jotunheimen, Norway. *Norsk geografisk Tidsskrift* **28**: 215-235.

Matthews, J.A., and D. McCarroll. 1994. Snow-avalanche impact landforms in Breheimen, Southern Norway: origin, age, and paleoclimatic implications. *Arctic and Alpine Research* **26**: 103-115.

McCarroll, D. 1993. Modelling late-Holocene snow-avalanche activity: incorporating a new approach to lichenometry. *Earth Surface Processes and Landforms* **18**: 527-539.

McCaroll, D. 1994. A new approach to lichenometry: dating single-age and diachronous surfaces. *The Holocene* **4**: 382-398.

McCarthy, D.P. 1985. Dating Holocene geomorphic activity of selected landforms in the Geikie Creek Valley, Mount Robson Provincial Park, British Columbia. Unpublished M.Sc. thesis, University of Western Ontario, 304.

McCarthy, D.P. 1999. A biological basis for lichenometry? *Journal of Biogeography* **26**: 379-386.

Mears, A.I. 1992. Snow avalanche hazard analysis for land-use planning and engineering, *Colorado Geological Survey Bulletin 49.*

Mellor, M. 1978. Dynamics of snow avalanches. In *Rockslides and Avalanches. I. Natural Phenomena*, ed. B. Voight, Amsterdam: Elsevier, 753-792.

Melosh, H.J. 1989. *Impact Cratering: A Geologic Process*. New York: Oxford University Press.

Meteorological Service of Canada. 2001. Historical Canadian Climate Database Version 2. Accessed November 2002. http://www.cccma.bc.ec.gc.ca/hccd/data/access_data.html.

Monger, J.W.H. 1989. Geology, Hope, British Columbia; Geological Survey of Canada, Map 41-1989. sheet 1, scale 1:250,00.

Nyberg, R. 1985. Debris flows and slush avalanches in northern Swedish Lapland. Distribution and Geomorphological significance. *Meddelanden Från Lunds Univerdsitets Geografiska Institution Avhandlinger*, 97. 222.

Natural Resources Canada (NRC). 2000. Introduction to the Geology of the Canadian Cordillera. Accessed November 2002. http://www.nrcan.gc.ca/gsc/pacific/vancouver/earthsci/index_e.htm.

Nyberg, R. 1989. Observations of slushflows and their geomorphological effects in the Swedish Mountain area. *Geografiska Annaler* **71A**: 185-198.

Orombelli, G., and S.C. Porter. 1981. Lichen growth curves for the southern flank of the Mont Blanc Massif, western Italian Alps. *Arctic and Alpine Research* **15**: 193-200.

Pattern, R.S., and D.H. Knight. 1994. Snow avalanches and vegetation pattern in Cascade Canyon, Grand Teton National Park, Wyoming, USA. *Arctic and Alpine Research* **26**: 35-41.

Peev, C.D. 1966. Geomorphic activity of snow avalanches. In *International Symposium on the Scientific Aspects of Snow and Ice Avalanche, 5-10 April, 1965, Davos, Switzerland.* IAHS Publication No. **69**: 357-368.

Perla, R.I., and M. Martinelli. 1976. *Avalanche Handbook.* U.S. Department of Agriculture Handbook 489, 238p.

Pettersen, B.R. 1973. Meteorittkrater oppdaget i Nord-Norge. *Astr. Tidsskr.* **6**: 89-91.

Piper, D.J.W., Shor, A.N., and J.E. Hughes-Clarke. 1988. The 1929 Grand Banks earthquake slump and turbidity current. *Geological Society of America Special Paper* **229**: 77-92.

Pitman, G.T.K. 1973. A lichenometrical study of snowpatch variation in the Frederikshåb district, southwest Greenland and its implication for the study of climatic and glacial fluctuations. *Bulletin Grønlands geoliske Undersøkelse* **104**: 1-31.

Potter, N., Jr. 1969. Tree-ring dating of snow avalanche tracks and the geomorphic activity of avalanches, Northern Absaroka Mountains, Wyoming. *Geological Society of America, Special Paper* **123**: 141-165.

Porter, S.C. 1981. Lichenometric studies in the Cascade Range of Washington: establishment of *Rhizocarpon geographicum* growth curves at Mount Rainier. *Arctic and Alpine Research* **13**: 11-23.

Proctor, M.C.F. 1977. The growth of the crustose lichen *Buellia canescens*. *New Phytologist* **79**: 659-653.

Proctor, M.C.F. 1983. Sizes and growth rates of the lichen *Rhizocarpon geographicum* on the moraines of the Glacier de Valsorey, Valais, Switzerland. *Lichenologist* **15**: 249-262.

Rapp, A. 1959. Avalanche boulder tongues in Lappland. *Geografiska Annaler* **41**: 34-48.

Rapp, A., and R. Nyberg. 1981. Alpine debris flows in northern Scandinavia. *Geografiska Annaler* **63A**: 183-196.

Reite, A.J. 1976. Stormdalen. In: Sveian, H., Kvartærgeologisk kartegging på Saltfjellet i 1976. *Norg. Geol. Undres. Rapport* **1502B**: 27-35.

Reynolds, N.D. 2001. Dating the Bonneville landslide with lichenometry. *Washington Geology* **29**:11-16.

Roberts, W.A. 1968. Impact cratering mechanics and structures. In *Shock Metamorphism of Natural Materials*, ed. B.M. French and N.M. Short. Baltimore: Mono Book Corp., 101-114.

Saunders, I.R., Clague, J.J., and M.C. Roberts. 1987. Deglaciation of Chilliwack River valley, British Columbia. *Canadian Journal of Earth Sciences* **24**: 915-923.

Schaerer, P.A., and A.A. Salway. 1980. Seismic and impact-pressure monitoring of flowing avalanches. *Journal of Glaciology* **26**: 179-186.

Schaerer, P.A. 1967. The amount of snow deposited at avalanche sites. *In: Physics of Snow and Ice. Proceedings of the Conference on Low Temperature Science, Sapporo, August 14-19, 1966.* Institute of Low Temperature Science, Hokkaido University, Sapporo, **1**: 1255-1260.

Schaerer, P.A. 1981. Avalanches. In *Avalanches, Handbook of Snow, Principles, Processes, Management and Use*, ed. Gray, D.M., and D.H. Male, 475-518. Toronto: Pergamon Press.

Schwiengruber, F.H. 1983. Peyto Lake Engelmann spruce chronologies. The International Tree-Ring Data Bank, IGBP PAGES/World Data Center for Paleoclimatology, NOAA/NGDC Paleoclimatology Program, Boulder, Colorado, USA.

Schweingruber, F.H. 1988. *Tree Rings: Basics and Applications of Dendrochronology.* Holland: Kluwer Acadmic Publishsers.

Schytt, V. 1965. Notes on glaciological activities in Kebnekaise, Sweden during 1965. *Geografiska Annaler* **42A**: 65-72.

Serbenko, V.I. 1954. Snezbnie obvali v verhovyah dolini reki. Tomi [Snow avalanches in the upper reaches of the Tomi river]. *Trudi transportno-energeticheskovo instituta AN SSSR, Zapadno-sibirski filial* **4**: 127-142.

Shimizu, H., Huzioka, T., Akitaya, E., Narita, H., Nakagawa, M., and K. Kawada. 1980. A study on high speed avalanches in the Kurobe canyon. *Journal of Glaciology* **26**: 141-151.

Shroder, J. F. 1978. Dendrogeomorphological analysis of mass movement on Table Cliffs Plateau, Utah. *Quaternary Research* **9**: 168-185.

Shroder, J.F. 1980. Dendrogeomorphology: review and new techniques of tree ring dating. *Progress in Physical Geography* **4**: 161-188.

Shroder, J.F., and D.R. Butler. 1987. Tree-ring analysis in the earth sciences. *Proceedings, International Symposium on Ecological Aspects of Tree-Ring Analysis*, US Department of Energy Conference 8608144, 186-212.

Smith, H.W. 1947. Avalanches. *New Zealand Engineering* **2**: 491-496.

Smith, L. 1973. Indication of snow avalanche periodicity through interpretation of vegetation patterns in the North Cascades, Washington. In *Methods of avalanche control on Washington mountain highways: Washington State Highway Department Research Program Report 8.4*, 55-101.

Smith, D.J., and J.R. Desloges. 2000. Little Ice Age history of Tzeetsaytsul glacier, Tweedsmuir Provincial Park, British Columbia. *Géographie physique et Quaternaire* **54**: 135-141.

Smith, D.J., McCarthy, D.P., and B.H. Luckman. 1994. Snow-avalanche impact pools in the Canadian Rocky Mountains. *Arctic and Alpine Research* **26**: 116-127.

Smith, D.J., Wood, C., Luckman, B.H., and B.J. Robinson. 2000. Dendroglaciology at Saskatchewan Glacier, Banff National Park, Canada. International Conference on Dendrochronology for the Third Millennium, Mendoza, Argentina, 2-7 April.

Stethem, C., Jamieson, B., Schaerer, P., Liverman, D., Germain, D., and S. Walker. 2003. Snow avalanche hazard in Canada – a review. *Natural Hazards* **28**: 487-515.

Varem-Sanders, T.M.L. 1996. Program ITRviewer (Version 2.0).

Ward, R.G.W. 1985. Geomorphological evidence of avalanche activity in Scotland. *Geografiska Annaler* **67A**: 247-256.

Webber, P.J., and J.T. Andrews. 1973. Lichenometry: a commentary. *Arctic and Alpine Research* **5**: 295-302.

Wentworth, C.K. 1922. A scale of grade and class terms for clastic sediments. *Journal of Geology* **30**: 377-392.

Wilber, R.J., Milliman, J.D., and Halley, R.B. 1990. Accumulation of bank-top sediment on the western slope of Great Bahama Bamk: rapid progradation of a carbonate megabank. *Geology* **18**: 970-974.

Wiles, G.C., Jacoby, G.C., Davi, N.K., and R.P. McAllister. 2002. Late Holocene glacier fluctuations in the Wrangell Mountains, Alaska. *Geological Society of America Bulletin* **114**: 896-908.